Antivirals Acting on Viral Envelopes with a Biophysical Mechanism of Action

by

Sietske Speerstra

A thesis submitted in partial fulfillment of the requirements for the degree of

Master of Science

Department of Biochemistry

University of Alberta

ABSTRACT

Most antivirals target viral proteins and are specific for only one virus, or even one viral genotype. Whereas viral proteins are encoded in the plastic viral genome, virion lipids are not and their rearrangements during fusion of the virion envelope to cellular membranes are conserved among otherwise unrelated enveloped viruses. Antivirals that inhibit these lipid rearrangements could thus pose a high barrier to resistance and have broad-spectrum activities. Fusion occurs through a hemifusion stalk in which only the outer leaflets are fused, bent with their polar heads forming a smaller radius than their hydrophobic tails (negative curvature). Outer leaflets enriched in phospholipids with head groups of larger cross sections than their lipid tails ("inverted cone") disfavor this negative curvature, inhibiting fusion. The rigid amphipathic fusion inhibitors (RAFIs) are synthetic compounds of inverted cone molecular geometry. They inhibit the infectivity of otherwise unrelated enveloped viruses. The leading RAFI aUY11 has an ethynyl-perylene hydrophobic and an uracil-arabinose polar moiety. aUY11 intercalates in viral envelopes to directly inhibit virion-to-cell fusion. Previous studies showed that amphipathicity, rigidity, and inverted cone molecular geometry are required.

My hypothesis is that the inverted cone molecular geometry of the RAFIs increases the energy barrier for the hemifusion stalk, inhibiting fusion. Then, chemically distinct compounds with similar amphipathicity, rigidity, and inverted cone shape would have similar antiviral potencies, regardless of specific chemical groups. Alternatively, the perylene group exposed to visible light may induce viral lipid peroxidation. Then, the perylene group and absorbance at visible spectrum would be required. I evaluated the activities of twenty-five chemically distinct RAFIs with similar amphipathicity, rigidity, and inverted cone shape. The perylene moiety and absorption at visible spectrum were not required, but a minimum length of the hydrophobic

moiety of 10.3 Å was. The arabino moiety could be modified or replaced by other groups. Cytidine replacement for uracil was not tolerated, indicating the O_8 carbonyl group is required. Bilayer intercalation was required but not sufficient. The vast majority of RAFIs had no overt cytotoxicity (CC_{50} > 20 μM; TI > 250−1200). Carbonyl or butylamide substitutions for arabino or cytidine replacement for uracil, increased cytotoxicity. Cytotoxicity was mainly determined by the polar moiety and there was no correlation between antiviral and cytostatic activities. The definition of the effects of shape and chemical groups on the activity of the RAFIs opens the possibility for rational design of lipid-acting antivirals active against a broad spectrum of enveloped viruses.

PREFACE

This thesis is an original work by Sietske Speerstra. The research conducted for this thesis forms part of an international research collaboration, led by Professor Luis M. Schang at the University of Alberta, with Dr. Vladimir A. Korshun being the lead collaborator at the Institute of Physico-Organic Chemistry, Minsk, Russia. The analyses of the results (Chapter 3) and the discussion (Chapter 4) are my original work, as well as the literature review in Chapter 1.

The research described in this thesis has been submitted for publication as Speerstra, S; Alexey A. Chistov; Gleb V. Proskurin; Andrey V. Aralov; Egor A. Ulashchik; Philipp P. Streshnev; Vadim V. Shmanai; Vladimir A. Korshun; Schang, LM (2017) Antivirals Acting on Viral Envelopes with a Biophysical Mechanism of Action. I was responsible for data collection and analysis as well as the manuscript composition. Dr. Luis M. Schang was the supervisory author and was involved in concept formation, assisted with the data analysis, and contributed to manuscript edits.

DEDICATION

To Beppe Sietske

ACKNOWLEDGEMENTS

First and foremost, I would like to express my deepest gratitude to my supervisor, Dr. Luis Schang, for his academic guidance and encouragement. Working on this project with Luis' mentorship has been a very rewarding and invaluable experience.

I would also like to thank the other members of my committee, Drs. Maya Shmulevitz and Nicolas Touret, for their insightful suggestions and interest in my work.

I am grateful to the members of the Schang laboratory; Abdullah, Bizhan, Che, Consuelo, Esteban, Furkat, Kristen, Matthew F., Matthew B., Michael, MiYao, Rachael, Rory, and Rebecca, for their productive working relationship as well as their friendship.

This research would not have been possible without the collaborators under the lead of Dr. Vlademir Korshun, who synthesized the compounds described in this thesis. The absorbance spectra, fluorescence spectra, and MTT readings were produced using the respective equipment of Drs. Maya Shmulevitz, Gary Eitzen, and Lorne Tyrrell. This research was supported by grants from the Canadian Institutes for Health Research and the Burroughs Wellcome Fund. Support for my graduate studies has come from the Faculty of Graduate Studies and Research (FGSR) and Alberta Health Services for the Graduate Recruitment Studentship and the Department of Biochemistry for the Biochemistry Graduate Assistantship in Teaching and Learning Skills Award. Travel awards granted by the International Society for Antiviral Research, the FGSR, and the Graduate Student Association have allowed me to present my work at the International Conference for Antiviral Research.

I thank Drs. Jo Parrish and Adrienne Wright for providing me with the opportunities that allowed me to explore my teaching interests, and for their respective mentorship in the Graduate

Teaching and Learning- and Biochemistry Graduate Assistantship in Teaching and Learning Skills programs.

Finally, I would like to thank my family for their encouragements, my partner Eric for displaying his love and pride, and for my friends across campus for making my time in graduate school some of the most enjoyable to date!

TABLE OF CONTENTS

LIST OF TABLES

LIST OF FIGURES

LIST OF ABBREVIATIONS

25HC	25-hydroxycholesterol
AAPH	and 2,2′-azobis (2-amidinopropane)
AdV	Adeno virus
AMVN	2,2'-azobis (2,4-dimethylvaleronitrile)
AP2	Adaptor protein 2
ATP	Adenosine triphosphate
BSA	Bovine albumin serum
C-	Carboxy-
CC_{50}	Cytotoxic concentration 50%
CCR5	C-C Chemokine receptor 5
CD4	Cluster of differentiation 4
DAA	Direct acting antiviral
DEPE	Deilaidoylphosphatidylethanolamine
DMEM	Dulbecco Modified Eagle's Medium
DMSO	Dimethyl sulphoxide
DOPC	1,2-dioleoyl-*sn*-glycero-3-phosphocholine
DPPC	1,2-dipalmitoyl-*sn*-glycero-3-phosphocholine
EC_{50}	Effective concentration 50%
EGCG	Epigallocatechin gallate
FBS	Fetal Bovine Serum
FDA	Food and Drug Administration
GAG	Glycosaminoglycan
gB	Glycoprotein B
gC	Glycoprotein C
GFP	Green fluorescent protein
gH	Glycoprotein H
gL	Glycoprotein L
gp120	Glycoprotein 120
gp41	Glycoprotein 41
HA	Hemagglutinin
HBV	Hepatitis B virus
HCV	Hepatitis C virus
HR	Heptad repeat
HS	Heparan sulphate
HSV-1	Herpes simplex virus 1
HSV-2	Herpes simplex virus 2
HVEM	Herpes virus entry mediator
IAV	Influenza A virus
IFITM	Interferon-inducible transmembrane protein
IFN	Interferon
MTT	3-(4,5-dimethylthiazol-2-yl)-2,5-diphenyltetrazolium

N-	Amino-
NA	Neuraminidase
NTP	Nucleotide triphosphate
PBS	Phosphate buffered saline
PE	Phosphatidyl ethanol amine
pfu	Plaque-forming unit
POPC	β-oleoyl-γ-palmitoyl-L-α-phosphatidylcholine
PS	Phosphatidyl serine
PV	Poliovirus
RAFI	Rigid amphipathic fusion inhibitor
RSV	Respiratory syncytial virus
SA	Sialic acid (N-acetylneuramic acid)
SIN	Sindbis virus
SNARE	Soluable N-ethylmaleimide-sensitive factor (NSF)-attachment protein receptor
TI	Therauetic index
TMD	Transmembrane domain
VACV	Vaccinia virus
VSV	Vesicular stomatitis virus
COP	Coat protein
LPC	Lysophosphatidyl choline

CHAPTER 1: INTRODUCTION

1.1 Viral entry

Inhibition of viral entry is an attractive antiviral target (De Clercq and Li, 2016; Colpitts and Baumert, 2016; Mitchell et al., 2017; Pietschmann, 2017; Xiao et al., 2014; Yamauchi and Helenius, 2013). Entry inhibitors prevent infection altogether, before any damage to the cells can occur. Moreover, such drugs need not to be transported across membranes to reach intracellular targets. Only three entry inhibitors are approved by the FDA, however (De Clercq and Li, 2016); enfuvirtide, which acts on the HIV envelope gp41 to inhibit the conformational change required for fusion (Kilby et al., 1998), maravivoc, which binds to the HIV-1 C-C Chemokine receptor (CCR) 5 on the surface of $CD4^+$ cells (Dorr et al., 2005; Fätkenheuer et al., 2005), and palivizumab, a monoclonal antibody against respiratory syncytial virus (RSV) fusion protein F. These entry inhibitors act on viral proteins and are thus specific for only one virus, or even just a subset of one (mariviroc, Raymond et al., 2015). They are also prone to select for antiviral resistance (Adams et al., 2010; Greenberg and Cammack, 2004; Ratcliff et al., 2013; Waters et al., 2008).

Several entry steps are conserved across multiple viruses. Most viruses attach to heparan sulphate- or sialic acid- containing glycans on the cell surface, for example, and envelope-to-cell membrane fusion is conserved among all enveloped viruses. Compounds that target such steps could thus be expected to have broad spectrum antiviral activities (Badani et al., 2014; Bobardt et al., 2008; Chamoun et al., 2012; Cheng et al., 2008; Edinger et al., 2014). Such compounds have the potential to be active against even only partially characterized emerging viruses. Lipids

in the virion envelopes are not encoded in the viral genomes, which can mutate under selective pressures. Antivirals targeting envelope lipids are thus likely to present a higher barrier to selection for resistance.

Many important pathogenic human viruses, such as influenza A virus (IAV), human immunodeficiency virus (HIV), herpes simplex virus (HSV) -1 and -2, Zika virus, and Ebola virus, have lipid envelopes. The viral envelopes must fuse with cellular membranes for infection to occur (**Figure 1.1**) (Harrison, 2008). During membrane fusion, two lipid bilayers merge. It is generally accepted that lipid bilayer fusion occurs through an intermediate structure, the hemifusion stalk (Aeffner et al., 2012; Chernomordik and Kozlov, 2005; Chlanda et al., 2016; Markosyan et al., 2000; Melikyan et al., 1995; Xu et al., 2005). In this stalk, the outer leaflets of the lipid bilayers are already fused while the inner leaflets are still separated (**Figure 1.2**) (Chernomordik and Kozlov, 2005; Chernomordik et al., 1998). The outer leaflets are thus bent in a negative curvature, in which the radius of the polar head groups is smaller than that of the hydrophobic lipid tails. (Aeffner et al., 2012; Campelo et al., 2008; Chang and Jackson, 2015; Cohen and Melikyan, 2004; McMahon and Gallop, 2005; Stachowiak et al., 2013). As bending membranes requires energy, the lipid rearrangements required for bending the fusing leaflets pose one of the energy barriers to fusion.

Lipids have different molecular geometries (**Figure 1.3**). Lipids with head groups of larger cross sections than those of their lipid tails are said to have an inverted cone shape. Outer leaflets enriched in inverted cone shape phospholipids tend to adopt spontaneous positive curvatures. Inverted cone shaped phospholipids consequently inhibit the formation of the negative curvature required for the hemifusion stalk (Chernomordik and Kozlov, 2005; Chernomordik et al., 1995a, 1985; Gaudin, 2000a; Gunther Ausborn et al., 1995; Vogel et al., 1993; Yeagle et al., 1994).

Although such phospholipids have antiviral properties (Chernomordik et al., 1997; Gaudin, 2000a), they are not suitable as antivirals. Phospholipids are rapidly metabolized and often toxic.

1.2 The Rigid Amphipathic Fusion Inhibitors (RAFIs)

1.2.1 The RAFIs inhibit the infectivity of otherwise unrelated envelope viruses

The rigid amphipathic fusion inhibitors (RAFIs) are a family of synthetic amphipathic small molecules with polar moieties of larger cross sections than those of the rigid hydrophobic moiety. Such molecular geometry gives the RAFIs a general inverted cone molecular shape. The first described RAFIs, aUY11 and dUY11, have polar moieties derived from arabinose- or deoxyribose uridine and rigid hydrophobic moieties composed of ethynylperylene (**Figure 1.4**) (Colpitts et al., 2013; St Vincent et al., 2010). They inhibit the infectivity of unrelated enveloped viruses, including IAV, HSV-1 and -2, hepatitis C virus (HCV), vesicular stomatitis virus (VSV), and Sindbis virus, among others, at nanomolar concentrations. The RAFIs have no effects on the infectivity of the non-enveloped poliovirus, reovirus or adenovirus (Colpitts et al., 2013; St Vincent et al., 2010).

The RAFIs are active when virions or cells are treated before infection, although they are more active when virions are pre-treated (Colpitts et al., 2013; St Vincent et al., 2010). The RAFIs intercalate in the hydrophobic environment of various unrelated enveloped virions or protein-free liposomes (Colpitts et al., 2013; St Vincent et al., 2010), without affecting membrane fluidity (Colpitts et al., 2013; St Vincent et al., 2010). They directly inhibit lipid mixing between enveloped viruses and cells at concentrations similar to those that inhibit viral infectivity (Colpitts et al., 2013; St Vincent et al., 2010). The RAFIs also inhibit lipid mixing between cells and liposomes, indicating that they act independently of viral proteins. They

inhibit the transition from the lamellar to the inverted hexagonal phase in bilayer stacks (Colpitts et al., 2013), a transition which proceeds through negative curvature intermediates. We thus proposed a model in which the RAFIs act directly on lipids to inhibit the formation of the negative curvature required for the hemifusion stalk (Colpitts et al., 2013; St Vincent et al., 2010). Other models have also been proposed. The RAFIs may intercalate in membranes to induce peroxidation of membrane phospholipids when excited by light (Vigant et al., 2014). In this model, the perylene moiety was proposed to be required for the generation of singlet oxygen species (Vigant et al., 2014), which then would peroxidise envelope lipids, which would in turn increase the rigidity of the membrane (Vigant et al., 2014). A similar mechanism has been proposed for hypericin and LJ001 (Lenard et al., 1993; Vigant et al., 2014).

Membrane fusion and fissions are also required for many cellular processes, such as exocytosis, endocytosis, vesicular transport, mitosis, meiosis, and fertilization (Martens and McMahon, 2008). Intracellular fusions are mediated by N-ethylmaleimide-sensitive factor (NSF)-attachment protein receptor (SNARE) (Chen and Scheller, 2001). SNAREs have C-terminal transmembrane anchors in each of the two fusing bilayers. During fusion, the SNAREs join at the N-termini and zipper progressively towards the membrane-anchored C-termini. The SNARE rearrangements bring the membranes in close apposition and eventually result in fusion. Post-fusion SNARE complexes are disassembled by NSF for subsequent fusions. This latter disassembly is an energy-dependent process driven by ATP consumption (Söllner, 2003). Many other steps in cellular membrane fusion are driven by NTP consumption. Rab GTPases use GTP to enhance the efficiency of the fusion between SNAREs (Lommer et al., 2009; Murray et al., 2016). GTP provides the energy required for the fusions between the membranes of the endoplastic reticulum mediated by the fusion protein atlastin (Winsor et al., 2017). Dynamin uses

GTP to exert mechanical force on membranes resulting in membrane rearrangements. Cellular proteins, including clathrin cages and COP coats, modulate membrane curvatures, which bind membranes through their curved protein interfaces (Chernomordik and Kozlov, 2003; Zimmerberg and Kozlov, 2006).

1.2.2 The RAFIs are specific for virion-to-cell fusions

Whereas the RAFIs intercalate in cellular membranes too, they have no major effects on cell viability or replication (therapeutic index (TI) > 935 and > 3,000 for aUY11 and dUY11, respectively) (Colpitts et al., 2013; St Vincent et al., 2010). Although the mechanisms of this specificity for virus-to-cell fusion over physiological cellular fusions are yet not understood, two models have been proposed (Colpitts et al., 2013; St Vincent et al., 2010; Vigant et al., 2014), both are based on the virions being metabolically inactive (Colpitts et al., 2013; St Vincent et al., 2010; Vigant et al., 2014). In one model, the RAFIs inhibit the fusion of enveloped viruses by increasing the energy required for the formation of the hemifusion stalk (Colpitts et al., 2013; St Vincent et al., 2010). Cells would not be equally affected as a result of their ability to remodel lipids and change membrane curvatures via many energy-dependent mechanisms. The RAFIs would then specifically inhibit virus-to-cell fusion based on their physical properties such as shape, rigidity and amphipathicity, rather than on chemical properties, such as reactive functional groups. Then, chemically distinct molecules with similar shape, rigidity, and amphipathicity should also specifically inhibit enveloped virus infectivity with similar potency and regardless of specific chemical groups.

RAFIs have no obvious major effects on cellular fusions or fissions. Firstly, aUY11 and dUY11 have little effects on mitosis, even at high concentrations (therapeutic index > 3,000) (St Vincent et al., 2010). Secondly, aUY11 does not inhibit the infectivity of non-enveloped viruses

such as poliovirus and reovirus that enter via endocytosis, which requires fusions between endocytic compartments (Colpitts et al., 2013; Rauma et al., 1999; Schulz et al., 2012). Thirdly, the RAFIs do not inhibit exocytosis (Colpitts, Eitzen, and Schang, 2013, unpublished results). Viruses that egress though pathways that require cellular fusion pathways, such as IAV, still egressed from cells (Bruce et al., 2010). The mechanisms of this specificity for virus-to-cell fusion over cellular fusions are not yet understood. Cells treated with RAFIs after infection produce virions containing RAFIs in their envelopes, which are not infectious (Colpitts et al., 2013; St Vincent et al., 2010).

1.2.3 Previous RAFI structure activity relationship studies

Limited structure activity relationship (SAR) studies on the RAFIs had been performed before (**Figure 1.5**) (St Vincent et al., 2010). Compounds with deoxyribose uridine polar moieties and shorter hydrophobic moieties were less potent (EC_{50} 40 and 51 μM for compounds with 1-ethynylpyrene [dUY2] or 4-ethynylpyrene [dUY3] hydrophobic moieties, respectively) (St Vincent et al., 2010). Compounds with non-planar (EC_{50} 37 μM [dUY5]) or rotationally flexible (EC_{50} 7.4 μM [dUY4]; 35 μM [dUY6]; 6.2 μM [dUY8]) hydrophobic moieties also had decreased potency. Additions of polar oxygen atoms in the linker, resulting in rotational flexibility, decreased potency as well (EC_{50} 14 μM [aUY12]; > 200 μM [dUY7]; or 6.2 μM [dUY8]). Addition of polar oxygen atoms to the hydrophobic moiety, disrupting the amphipathicity, decreased potency even more (EC_{50} > 200 μM [dUY1]; 60 μM [aUY1]; > 200 μM [dUY9]).

Modifications to the polar arabinose moieties did not have obvious effects. Sugar moieties with three, two, or one hydroxyl groups had activities within three-fold from each other (EC_{50} 0.131 μM [arabinose, aUY11]; 0.048 μM [deoxyribose, dUY11]; 0.087 μM [dideoxyribose;

ddUY11]). Larger pivalomethyl additions to the polar moiety did not affect activity either (EC_{50} 0.190 [PvddUY11]). However, larger 3',5'-O-(tetraisopropyldisiloxane-1,3-diyl) groups, disrupting the overall molecular shape and amphipathicity, had 30,000-fold decreased activity (EC_{50} 165 μM [Mk-dUY11]).

Overall, it was concluded that the antiviral mechanism of the RAFIs depends on amphipathicity, rigidity of the hydrophobic moiety, and an overall inverted cone shape (St Vincent et al., 2010). In these SAR series, all compounds without perylene moiety had low potencies.

1.3 Viral entry mechanisms

In order to replicate, viruses must deliver their genomes to cells. The global mechanisms of viral entry are generally conserved among different viral families. For example, the majority of viruses bind to cellular glycans expressed on the cell surface. These primary interactions confine and concentrate virions onto the cell surface for subsequent interactions. Whereas some viruses enter cells at the plasma membrane, most are internalized by cellular pathways such as clathrin-mediated endocytosis or macropinocytosis. Most human pathogenic viruses, including HSV-1, -2, HIV, HCV, IAV, Ebola virus, are enveloped. All enveloped viruses must also fuse with cellular membranes to enter cells. Whereas the viral proteins mediating viral fusion differ, the lipid rearrangements during membrane fusion are fairly well conserved.

1.3.1 Primary and secondary attachment

Most enveloped and non-enveloped viruses attach to cells by first binding to cellular glycans exposed on the surface of the plasma membrane, such as glycosaminoglycans or sialoglycans. These carbohydrates are ubiquitous and many microbes, including most viruses, have evolved to

use them to attach to target cells (Chen et al., 2008; Stencel-Baerenwald et al., 2014). Viruses bind to cellular glycans with low affinity, but this low affinity binding serves to concentrate the virions at the cell surface.

Glycosaminoglycans are long unbranched polysaccharides of repeating disaccharides of uronic acid and hexosamine, which are linked to cell surface proteins (Raman et al., 2005). Glycosaminoglycans are highly diverse. They can be comprised of one of four disaccherides classes (heparin/heparan sulphate, chondroitin/dermatan sulfate, keratan sulfate or hyaluronic acid), which all can be further modified with variable sulphation patterns (Raman et al., 2005).

Of the glycosaminoglycans classes, heparan sulphate is the most common as viral attachment receptor, used by HSV-1, -2 (Spear, 2004), HCV (Morikawa et al., 2007), HIV (Crublet et al., 2008), Sindbis virus (Byrnes and Griffin, 1998), RSV (Levine et al., 1987), adenovirus (Asokan et al., 2006), among others.

A smaller number of other viruses, including influenza-, reo-, adeno-, and rotaviruses bind glycoproteins or glycolipids containing terminal sialic acid moieties (N-acetyl neuraminic acid, Neu5Ac) (Stencel-Baerenwald et al., 2014). Sialic acid is a nine-carbon monosaccharide derived from neuraminic acid, in which the fifth carbon is often acetylated.

The sialic acid binding site of IAV HA is a depression lined with the conserved residues Tyr 98, Trp 153, Glu 190, Leu 194, His 183, and Thr 155. The pyranose moiety of the sialic acid sits on top of the aromatic residues Tyr 98 and Trp 153. The sialic acid is mainly stabilized with hydrogen bonds with Glu 190 Leu 194 His 183, and Thr 155, as well as Van der Waals interactions between the methyl of the N-acetyl group and Trp 153 (Sauter et al., 1992). Attachment proteins from other viruses that bind sialic acid have similar binding pockets. The binding pocket in reovirus σ1 binds sialic acid via hydrogen bonds from backbone groups, and

has a similar small hydrophobic binding pocket for the sialic acid methyl group (Reiss et al., 2012; Stencel-Baerenwald et al., 2014).

Following the primary interactions, virion glycoproteins bind to specific cellular receptors or other proteins with high affinity. Such secondary interactions are more specific than the primary ones, and often determine the tropism of the virus. For example, HIV binds CD4 on helper T cells and macrophages, and HCV binds to receptors involved in lipid metabolism expressed in hepatocytes. Secondary attachment may also induce conformational changes in the viral fusion proteins, resulting in fusion. Not all viruses use secondary attachment steps in their entry process, however. For example, IAV binds solely to sialo-glycans and has no secondary receptor.

1.3.2 Internalization

Many viruses use cellular transport pathways for their internalization (White and Whittaker, 2016; Wisskirchen et al., 2014). For example, HCV hijacks the cholesterol uptake pathway in order to enter hepatocytes (Miao et al., 2017), whereas others such as influenza, reo- and Ebola virus employ different modes of internalization, depending on which ones are available at the time of infection (Bhattacharyya et al., 2010; Rossman et al., 2012; Schulz et al., 2012; Sieczkarski and Whittaker, 2002; de Vries et al., 2011). For example, influenza can enter cells either via clatherin mediated endocytosis or macropinocytosis, depending on which pathway is operational at the time of infection (Rossman et al., 2012; Sieczkarski and Whittaker, 2002; de Vries et al., 2011).

Clatherin-mediated endocytosis is a major route for virus internalization and as such it has been particularly well characterized. The process is initiated by receptor binding at the cell surface, after which the proteins clathrin and adaptor protein 2 (AP2) are recruited to the cargo-

bearing receptors to promote the assembly of clathrin-coated pits. In this process, clathrin modulates the curvature of the membrane, resulting in the budding (fission) of a vesicle, typically of 100 nm in diameter from the plasma membrane.

Internalization by clathrin-mediated endocytosis is used by envelope viruses, including IAV (Chen and Zhuang, 2008), Semliki Forest virus (Kielian and Helenius, 1984; Nieva et al., 1994), HCV (Blanchard et al., 2006), Ebola virus (Bhattacharyya et al., 2010) and VSV (Sun et al., 2005), as well as non-enveloped viruses such as reovirus (Schulz et al., 2012), human papilloma virus (HPV) (Raff et al., 2013), and adenovirus (Nemerow, 2000). Clatherin-mediated endocytosis is inhibited by chlorpromazine. Correspondingly, chlorpromazine inhibits the entry of the broad-spectrum viruses that enter via this pathway (*e.g.* EC_{50} 9.4 μM against HCV (Blanchard et al., 2006), 157 μM against VSV (Sun et al., 2005)).

Although less common, viruses can also use cavelolar-mediated endocytosis pathways. Caveolae are formed in cholesterol and sphingolipid rich domains, at which caveolin proteins are recruited to form 50-80 nm vesicles. The small non-enveloped viruses simian virus 40 (SV40) (Engel et al., 2011; Pelkmans et al., 2002) and enterovirus 71 (Lin et al., 2013), as well as the enveloped hepatitis B virus (HBV) (Macovei et al., 2010) use this entry pathway for entry.

Macropinocytosis is used by cells for the uptake of non-specific fluids, membrane and ligands, and is generally used by viruses that are too large to be internalized by other cellular uptake pathways (Mercer and Helenius, 2012). Such viruses include Ebola virus (Saeed et al., 2010), filamentous IAV (Rossman et al., 2012), or vaccinia virus (VACV) (Mercer and Helenius, 2008). However, smaller viruses such as HPV16 may also use this pathway (Raff et al., 2013).

Regardless of the mode of internalization, most viruses pass through the endocytic pathway, entering into the cytoplasm via either early endosomes, late endosomes, or endo-

lysosomes (White and Whittaker, 2016). The fusion component of entry depends on the particular environmental cues. For many enveloped viruses, acidification is the trigger for fusion with the endosomal membrane. VSV and SFV fuse at the early endosome, triggered by the mildly acidic pH of 5.5 (Helenius, 2013; Sieczkarski et al., 2003). As early endosomes or macropinosomes mature to late endosomes, the pH falls. Influenza and Dengue viruses fuse with late endosomes at ~pH 5.

1.3.3 Virus-to-cell fusion

For most viruses, low pH results in glycoprotein conformational change. However, endosomes present other cues such as receptor binding (*e.g.* Ebola virus and HCV) or the proteolytic cleavage of fusion proteins that trigger entry of some corona viruses.

From the early endosomes, cargo can be directed in various directions. The cargo can return to the plasma membrane, it can move to the Golgi, or it can proceed down to lysosomes in which the contents of the endosome are ultimately degraded.

Not all viruses are internalized, however. Paramyoxoviruses fuse at the plasma membrane at neutral pH, triggered by receptor binding. Herpes- and retroviruses generally fuse at the plasma membrane, but fuse with endosomal membranes in some cell types (St Vincent et al., 2010)

1.3.4 Triggers for fusion

Four events activate viral fusion proteins: receptor binding (HSV-1, -2, HIV, some paramyxoviruses), low pH (IAV, alpha- flavi-, rhabdoviruses), receptor binding and low pH (HCV and EBOV), low pH and proteolytic cleavage (some coronaviruses (SARS CoV),

pneumoviruses (RSV)) (White and Whittaker, 2016). For some viruses, the triggers differ depending on the cell type (retroviruses, herpesviruses).

Several triggers can result in the conformational change to the active fusion state. Some fusion proteins are activated by receptor binding at the plasma membrane. For example, the fusion protein of HIV, gp41, is triggered by binding CD4 and CXC4 or CCR5. Some viruses require the concerted effort of several viral receptor binding proteins to induce the conformational change in the fusion protein. For example, the conformational change of HSV-1, -2 fusion protein gB is triggered by the binding of gD to its cellular receptors, including herpes virus entry mediator (HVEM) or nectin-1 (Akhtar and Shukla, 2009; Rey, 2006). Parainfluenzavirus 5 (PIV5) fusion protein F is activated by the receptor-binding protein hemaglutinin-neuraminidase (HN) (Adu-Gyamfi et al., 2016). Most viruses travel to internal acidic compartments, where proton binding results in the conformational change in the fusion protein (White and Whittaker, 2016).

1.4 Mechanisms of viral fusion

1.4.1 Viral fusion proteins

Whereas cellular fusion proteins have transmembrane anchors in both fusing membranes, viral fusion proteins must mediate fusion with only one transmembrane domain. Viral fusion proteins have a C-terminal transmembrane domain that anchors them to the viral envelope. However, a hydrophobic fusion peptide or 'loop' eventually establishes contact with the cellular membrane during fusion.

Viral fusion proteins differ from virus to virus, but their general mechanisms are similar (**Figure 1.6**). Prior to fusion, they exist in metastable conformations, with the hydrophobic

fusion peptides or loops tucked in hydrophobic pockets within the fusion protein. Fusion proteins undergo a conformational change into a fusion-active extended conformation that involves the insertion of the fusion peptide into the cellular membrane. Immediately following the extension, the fusion protein collapses into a conformation in which the C-terminal transmembrane domain, anchored in the viral membrane, and the fusion peptide, inserted in the cellular membrane, come in close apposition, triggering fusion.

Viral fusion proteins are classified based on their structural similarities. Class I fusion proteins are trimeric and composed primarily of alpha-helices. These proteins are encoded by orthomyxoviruses (Skehel and Wiley, 2000), paramyxoviruses (Lamb and Jardetzky, 2007), retroviruses (Chan et al., 1997), filoviruses (Weissenhorn et al., 1998), and coronaviruses (Xu et al., 2004). Most class I fusion proteins are synthesized as single chain precursors proteolytically cleaved by cellular proteases to generate two polypeptide chains, one of them containing an N-terminal fusion peptide. Some class I fusion proteins contain internal fusion loops rather than fusion peptide, including avian sarcoma leucosis virus (ASLV) and filoviruses. The best studied class I fusion protein is IAV hemagglutinin (HA) (Skehel and Wiley, 2000). HA is synthesized as a single chain (HA_0) (Chen et al., 1998), which forms trimers. HA_0 then is cleaved into two chains linked by disulphide bonds: an N-terminal chain HA_1, responsible for receptor binding, and a C-terminal chain HA_2, required for fusion and infectivity. HA_2 contains the transmembrane anchor and a coiled-coil stalk of three alpha helices protruding from the viral envelope. The hydrophobic fusion peptide is at the N-terminal 20-25 HA_2 residues, buried between the cavities of the coiled coil (Wiley et al., 1981; Wilson et al., 1981). HA_1 is a globular subunit sitting on top of the HA_2, which contains two conserved sialic acid binding domains, and basic residues that trigger the structural fusion rearrangement. Fusion is triggered by low pH, which causes the

HA_1 subunit to move to the side of the HA_2 stalk, while the fusion peptide on HA_2 relocates to the end of the coiled-coil rod toward the target membrane (Carr and Kim, 1993). In the post fusion conformation (Bullough et al., 1994), the coiled coil breaks close to the C-terminal transmembrane domain, resulting in a folded conformation in which the transmembrane domain is on the same side of the N-terminal fusion peptide (Bullough et al., 1994).

The fusion proteins of alphaviruses (E1) (Kielian et al., 2010), bunyaviruses (G_C) (Dessau and Modis, 2013) and most flaviviruses (E) (Modis et al., 2004) are classified as class II fusion proteins. Class II fusion proteins are predominantly composed of beta sheets, lie flat on the virion surface as dimers, and have a fusion loop rather than an N-terminal fusion peptide. Class II fusion proteins are divided into three domains: a beta-barrel shaped domain I, an elongated finger-like domain II, which contains the fusion loop, and a C-terminal domain III that has an immunoglobulin-like fold involved in receptor binding. To prevent untimely conformational changes, they interact with a second viral protein (pE2, G_N and prM for alphaviruses, bunyaviruses and flaviviruses, respectively). During fusion, class II fusion proteins rearrange into trimers that extend from the virion surface.

Class III fusion proteins include the fusion proteins of herpesviruses (glycoprotein B; gB) (Heldwein et al., 2006; Maurer et al., 2013) and rhabdoviruses (G) (Roche et al., 2007). They share features with class I (three stranded coiled-coil, trimeric oligomeric state) and class II fusion proteins (beta-sheet secondary structures, internal loops as fusion peptides). Class III fusion proteins have a relatively complex domain organization. Unlike class I and II fusion proteins, however, the conformational rearrangements during fusion of some class III fusion proteins can be reversible (Gaudin, 2000b).

Based on secondary structure and disulphide bond predictions, the HCV fusion protein E2 was until recently predicted to be a class II fusion protein (Krey et al., 2010). The resolution of the crystal structure of E2 revealed instead a compact globular structure. E2 does not undergo large structural rearrangements during fusion either, unlike the class II fusion proteins (Khan et al., 2014). HCV E2 has a Ig fold, but no other features common to the class II fusion proteins, such as the central beta-barrel in domain I or the hydrophobic loops. Hydrophobic fusion loops, have not been identified in HCV E2. HCV E2 is therefore not a class II fusion protein (Khan et al., 2014; Kong et al., 2013). The fusion protein of bovine viral diarrhea virus, a pestivirus in the *flaviviridae* family, does not resemble other class II viruses either (Li et al., 2013b). There may therefore be several many classes of viral fusion proteins.

The RAFIs inhibit the infectivity of viruses with class I (IAV), class II (Sindbis virus, tick-borne encephalitis virus), class III (VSV, HSV-1 and -2), and class IV fusion proteins (HCV) viruses, at similar concentrations (Colpitts et al., 2013; Orlov et al., 2016; St Vincent et al., 2010), indicating their mechanism of action is independent of the viral fusion proteins.

1.4.2 Bilayer destabilization

The pre- and post fusion structures hint that the refolding of viral (and cellular) fusion proteins mediates fusion by bringing the fusion bilayers in close. Nonetheless, the fusion peptides and transmembrane domains (TMD) of viral fusion proteins also contribute to fusion by destabilizing the fusing membranes (Harrison, 2008).

Fusion peptides or loops are generally conserved segments in fusion proteins, which are critical for fusion and contain hydrophobic as well as some polar residues. The fusion peptides and loops of various fusion proteins have been studied extensively. Nonetheless, the best studied

one is that of influenza HA. This peptide is amphipathic, alpha helical and has a kinked hairpin structure (Han et al., 2001). It inserts in the target membrane roughly parallel to the polar-hydrophobic interface of the outer leaflet with its hydrophobic residues inserted into the hydrophobic region of the bilayer, and the polar residues pointing away from it (Lorieau et al., 2010). The HA fusion peptide is highly conserved. Any number of mutations to the HA fusion peptide result in hemifusion without pore opening (Cross et al., 2001; Melikyan et al., 2000; Qiao et al., 1999), indicating the fusion peptide contributes to the lipid rearrangements in fusion.

The transmembrane domains (TMD) of the viral fusion proteins also contribute to fusion, although their mechanisms also remain unclear. Like the fusion peptides, their sequences are highly conserved, and cannot be mutated without losing fusion. The wild type TMD of HA increases lipid order (Schroth-Diez et al., 2000). It interacts with the fusion peptide (Lai and Freed, 2015), an interaction which should rupture the hemifusion stalk.

1.4.3 Cellular fusion proteins

The cellular fusion proteins SNAREs (soluble NSF attachment receptor) mediate fusion in various intracellular trafficking pathways, including exocytosis, membrane trafficking, protein trafficking, neurotransmitter release, and hormone secretion (Söllner, 2003; Zhou et al., 2015). The SNAREs are anchored in the opposite fusing membranes. The vesicle SNAREs are anchored by C-terminal transmembrane domains (syntaxin and synaptobrevin) or palmitylation of four cysteine residues (synaptosomal-associated protein 25; SNAP-25). The SNARE on the vesicle membrane synaptobrevin first docks at the target membrane containing SNAP25 and syntaxin. To mediate fusion, the SNAREs in the vesicle and target membrane then form a 4-helix coiled-coil (one each of syntaxin and synaptobrevin, two coils of SNAP-25) via heptad repeats.

The similarities between the cellular fusion proteins SNAREs and some viral fusion proteins include the formation of a coiled-coil helix bundle (Skehel and Wiley, 1998) and the large conformational changes that occur during fusion. Fusions stimulated by HA (Kemble et al., 1994; Melikyan et al., 1995) or SNAREs (Grote et al., 2000; McNew, 2000) are arrested in the hemifusion stalk or non-expandable fusion pores (Markosyan et al., 2000) when a transmembrane domain in the proteins is replaced by a lipid anchor. This arrest indicates that the hemifusion stalk is an intermediate stage of both viral and cellular fusions (Kweon et al., 2017; Xu et al., 2005).

Like class I fusion proteins, the SNAREs use the energy of the formation of coiled coil structures to facilitate fusion. Differing from the class I viral fusion proteins, the coiled coil SNARE structure is formed between three different molecules, anchored into each membrane., The interactions between the two membrane anchoring domains in the post fusion conformations are critical for complete fusion mediated by IAV HA (Park et al., 2003), HIV gp41 and SNAREs. Fusion proteins that do not depend on the formation of coiled coils also exist. The cell-to-cell fusion protein EFF-1 (epithelial fusion failure-1), involved in *C. elegans* development is not predicted to contain coiled coils (Mohler et al., 2002). EFF-1 is homologous to the viral class II fusion proteins. Fusion mediated by EFF-1 also proceeds through the hemifusion stalk intermediate, in which one of the membranes is bent into a more curved structure than the other (Zeev-Ben-Mordehai et al., 2014). Viral class II fusion proteins are thus considered functional homologous to the cellular EFF-1 (Pérez-Vargas et al., 2014).

1.4.4 Lipid rearrangements during membrane fusion

Lipid bilayers are mechanically stable, held together as an elastic medium mostly by hydrophobic effects (Tanford, 1978). The lipid polar head groups interact with the surrounding aqueous environment, secluding the lipid tails from the aqueous environment.

The lipid rearrangements during membrane fusion are conserved. Membrane fusions, including viral, intracellular, embryonic development, fertilization, and protein-free liposome fusions all occur through hemifusion intermediates (**Figure 1.2**) (Chernomordik et al., 1993, 2006; Efrat et al., 2007; Floyd et al., 2008; Lee and Lentz, 1997; Lentz, 2006; Xu et al., 2005; Zampighi et al., 2006). Two unfused bilayers must first come in close apposition (2-3 nm) of each other. Bringing the two bilayers in such close apposition costs energy (Helfrich, 1973; Rand and Parsegian, 1989). The electrostatic repulsion between bilayers and the steric hindrance by membrane proteins oppose such close contact between the fusing bilayers. Moreover, the lipids polar head groups interact with water molecules which must also be removed from the intermembrane space first for close contact (Helfrich, 1973). The resulting surface tension that builds up during the removal of water molecules eventually relaxes during the formation of the hemifusion stalk. The fusing bilayers may come in such close apposition only locally, at highly curved point-like membrane protrusions (Chernomordik and Kozlov, 2003; Efrat et al., 2007; Kozlovsky and Kozlov, 2002; Kuzmin et al., 2001), a mechanism that would minimize the area of the fusing bilayers that needs to come into close contact and consequently the activation energy requirement. The formation of such local protrusions also stresses the membrane, making easier the transition to the higher energy hemifusion intermediate.

When the two bilayers come sufficiently close, then the outer leaflets fuse to form a hemifusion stalk (Kozlovsky and Kozlov, 2002). In the hemifusion stalk, the outer leaflets of the

bilayer have already fused, whereas the inner leaflets are still intact. Numerous observations support the hemifusion stalk model. The hemifusion can be detected in lipid mixing studies, in which the transfer of lipophilic and hydrophilic fluorescent dyes are tracked during fusion. The hemifusion stalk has formed when outer leaflet lipid mixing occurs without content mixing. The differential mixing indicates that the outer leaflets have merged before the vesicular content is released. Lipid mixing prior to content mixing has been observed for model membranes with (Lu et al., 2005; Xu et al., 2005) or without (Chanturiya et al., 1997; Lee and Lentz, 1997; Meers et al., 2000) reconstituted SNAREs, in Ca^{2+}-triggered exocytosis (Wong et al., 2007), in yeast vacuole fusion (Jun and Wickner, 2007), in virion-to-cell fusion (Floyd et al., 2008), and in many fusions mediated by viral proteins (Chernomordik et al., 1997; Gaudin, 2000a; Kemble et al., 1994). The hemifusion stalk has also been observed by other approaches such as atomic force microscopy (Oelkers et al., 2016) and electron tomography (Zampighi et al., 2006).

Under the hemifusion stalk model, the outer leaflets must adopt negative curvatures. Enrichment of exogenous lipids that hinder the formation of such curvatures consequently inhibit fusion, as further discussed in **section 1.4.5**. Enrichment in lipids of inverted cone geometries in the outer leaflet block both viral and cellular fusions, including cortical exocytosis, mast cell degranulation, microsome-microsome fusion, and syncytium formation by baculovirus infected cells (Chernomordik and Kozlov, 2008; Chernomordik et al., 1995a, 1995b, 1995c, 1993; McMahon et al., 2010; Pécheur, 2007). The observations that lipid geometry affect membrane fusion also support the models for membrane fusion proceeding through curved intermediates.

Fusion mediated by some modified defective fusion proteins results in a long-life hemifusion stalk, indicating that the unstable hemifusion stalk is an intermediate in the fusion pathway (Kemble et al., 1994; Melikyan et al., 1995; Oelkers et al., 2016). The hemifusion stalk

has also been observed in model membranes (Yang and Huang, 2002), indicating that the formation of these stalks is physically possible. Computational models of fusion through the hemifusion stalks have predicted requirements for energies that are biologically feasible (Kozlovsky and Kozlov, 2002).

In the subsequent fusion steps, the inner leaflets form contact as a single bilayer. This structure is called the hemifusion diaphragm. Eventually the inner leaflets also fuse, resulting in the formation of a fusion pore. This pore formation and pore opening steps require energy as well (Katsov et al., 2006; Risselada et al., 2014). Fusion pore expansion depends on the lipid composition of the inner leaflets; lipids of inverted cone shape promote pore formation (Chanturiya et al., 1997).

Although now less accepted, alternate models proposing different fusion intermediates have been presented (Mayer, 2002), including proteinacious pore intermediates (Chang and Jackson, 2015; Lindau and Almers, 1995; Mayer, 2002). In such models, integral membrane proteins span both fusing bilayers and form an aqueous channel across the two fusing bilayers. Unlike the hemifusion stalk model, the proteinaceous pore model does not require drastic changes in curvature and content mixing generally precedes lipid mixing (Jackson and Chapman, 2008; Lindau and Almers, 1995; Tse et al., 1993). Proteins are not required for fusion, however. Various experimental conditions, for example the addition of polyethylene glycol, which dehydrates bilayers, induce fusion between protein-free bilayers (Chanturiya et al., 1997; Lee and Lentz, 1997; Lentz and Lee, 1999). Dehydration of lipid bilayers also results in spontaneous formation of stalk-like structures (Yang and Huang, 2002).

In biological contexts, membrane fusions are mediated by proteins. However, bilayer fusion can also occur spontaneously under certain experimental conditions. For example,

dehydration of the bilayers (Kozlovsky et al., 2004), promotes fusion. Polyethylene glycol (PEG) also depletes water molecules from the fusion site, and thus results in spontaneous fusion in absence of proteins (Lentz and Lee, 1999). Calcium ions also promote the fusion between protein-free liposomes. While the mechanism of the latter effect is still unclear, the positively charged ions may stabilize the electrostatic interactions with the negatively charged phospholipids in opposing bilayers, bringing them together (Pannuzzo et al., 2014). Bilayers in low pH environments can also fuse spontaneously, possibly by neutralization of the repulsive negative charge of phospholipids (Diizgiineg et al., 1985).

Although viral and cellular fusions differ in their source of energy, membrane composition, and vesicle size, both proceed through the same hemifusion stalk intermediate, as is described in **section 1.4.1**.

1.4.5 Lipids and membrane fusion

Fusion requires the initially near-flat membrane leaflets to adopt positive (radius of the polar head groups larger than that of the lipid tails) and negative (radius of the polar head groups smaller than that of the lipid tails) curvatures. For example, the formation of the hemifusion stalk requires the outer leaflets to adopt negative curvatures and pore expansion requires the inner leaflets to adopt positive curvatures.

The energy required for the formation of the hemifusion stalk is dependent the membrane lipid compositions (Fuller and Rand, 2001; Szule et al., 2002). Membranes adopt spontaneous curvatures based on their lipid composition. Lipids have different molecular shapes, depending on the relative cross sections of the polar head group and the number of hydrophobic acyl chains. Lipids with polar head groups of smaller cross sections than those of their lipids tails, such as phosphatidylethanolamine, are said to have cone shaped geometries, whereas lipids with polar

head groups of larger cross sections than those of their lipids tails, such as lysophosphatidylcholine, are said to have inverted cone shaped geometries. Most lipids in biological membranes have polar head groups of similar cross sections to those of their lipid tails. Such lipids are said to be cylindrical.

Bilayers composed of cylindrical lipids are practically flat. Bending membranes away from their spontaneous curvatures requires energy. In the hemifusion stalk, the outer leaflets have to adopt a curvature comparable to the membrane thickness (Chernomordik et al., 1995a). The energy required for this bending is estimated to be 40 k_BT, where k_B is the Boltzman constant and T is the absolute temperature (Katsov et al., 2006; Kozlov and Chernomordik, 2015; Kozlovsky et al., 2002).

The molecular shape of the lipids determines whether they preferentially form certain mesophases, such as micelles, flat lamellar phases, or inverted hexagonal H_{II} phases. Cone shaped lipids preferentially form micellar structures, inverted cone shaped lipids form inverted hexagonal H_{II} phases, and cylindrical lipids form bilayers.

Outer leaflets enriched in lipids with head groups of smaller cross sections than that of the lipid tails (*i.e.* cone shaped lipids, such as lysophosphatidyl choline) tend to form monolayers with negative curvatures (**Figure 1.3**). Lipids with head groups of larger cross sections than those of the lipid tails (*i.e.* inverted cone shaped lipids, such as phosphatididylethanolamine) tend to form monolayers with positive curvatures in model membranes (**Figure 1.3**) (Fuller and Rand, 2001; Rand et al., 1990; Szule et al., 2002).

Enrichment of inverted cone-shaped lipids in the outer leaflets of bilayers inhibits, at non-lytic concentrations, fusion between microsomes (Vogel et al., 1993), cellular membranes containing baculovirus gp64 fusion protein (Chernomordik et al., 1995b), rabies virus-to-

liposome fusion (Gaudin, 2000a), Sendai virus-to-LUV fusion (Yeagle et al., 1994) and fusion between protein free liposomes (Chernomordik et al., 1995a). Enrichment in cone shaped lipids in the outer leaflets promote fusion. The fatty acid oleic acid, for example, enhances fusion between baculovirus gp64 expressing cells (Chernomordik et al., 1995b).

The effect of inverted cone shape lipids is dependent on the length of the hydrophobic tails. Lipids with shorter chain length have a more pronounced inverted cone shape than lipids with longer chain lengths, but partition less to membranes than lipids with longer chain lengths. Fusion inhibition by short-chain lysolipids is decreased compared to that by short-chain lysolipids (Gaudin, 2000a; Vogel et al., 1993). Inhibition of membrane fusion by long-chain inverted cone shape lipids (*e.g.* stearoyl, 18:0, EC_{50} ~7 mole%) requires higher membrane concentrations of short-chain inverted cone shaped lipids tails (*e.g.* lauroyl, 12:0, EC_{50} ~2 mole%) (Chernomordik et al., 1997; Gaudin, 2000a).

Inhibition of membrane fusion by inverted cone shape lipids is reversible. Lysolipids with short acyl chains can be washed away from the membrane with bovine serum albumin. Addition of lipids with opposite cone shape geometries also neutralizes inhibition (Chernomordik et al., 1997).

1.4.6 Amphipathic inverted cone shaped molecules and viral fusion

In addition to the RAFIs, other small amphipathic inverted cone shaped molecules have been proposed to affect fusion by modulating membrane curvature (**Figure 1.7**). Chlorpromazine is a charged, amphipathic phenothiazine derivative that has been proposed to traverse the membrane to intercalate in the inner leaflet (Fang and Iwasa, 2007; Karunakaran and Fratti, 2013). Once there, it would destabilize the inner leaflet, which must adopt positive curvatures in the hemifusion intermediate. Consistent with this model, chlorpromazine promotes progression to

full fusion from the hemifusion stalk intermediate. Fusion mediated by lipid anchored (Markosyan et al., 2000) or mutated HA (Melikyan et al., 2000), which induces the formation of only the hemifusion stalk without further progression, is rescued by chlorpromazine.

An amphipathic alpha-helical peptide derived from the membrane-anchor domain of HCV protein NS5A, C5a, is active against HCV, Dengue virus, West Nile virus, respiratory synsytial virus (RSV), HBV, VACV, VSV and HIV (Apellániz et al., 2011; Bobardt et al., 2008; Cheng et al., 2008). C5a is proposed to intercalate between the lipid head groups to destabilize and lyse virion envelopes (Apellániz et al., 2011; Bobardt et al., 2008; Cheng et al., 2008). The possibility that C5a also acts by membrane curvature modulating mechanisms has not been excluded.

1.4.7 Differences between viral and cellular fusions

Virions are metabolically inert. The only energy available for virion-to-cell fusion is that stored in the fusion proteins, which is released by attachment, binding and the protein rearrangements. In contrast, cellular fusion proteins use energy provided by metabolism to mediate fusion (Bombardier and Munson, 2015; McMahon et al., 2010), remodel membrane curvatures (Prinz and Hinshaw, 2009; Salzer et al., 2017), or regulate lipid compositions.

In addition to differences in energy availability, virions and most cellular vesicles also differ in size. Virion envelopes are approximately 100 nm in diameter, and rarely larger than ~200 nm, whereas the diameters of endosomes, lysosomes and phagosomes are typically larger (500 to 1000 nm). Nonetheless, there is significant overlap in sizes. Large trafficking vesicles are amost as small as virions (~250 nm), whereas small trafficking vesicles, and clathrin-coated or pinocytic vesicles are approximately the same size as virions (40 to 70 nm).

Whereas virion envelopes are derived from host membranes, their lipid compositions differ from cellular membranes (Brügger et al., 2006; van Genderen et al., 1994; Gerl et al., 2012; Liu

et al., 2011; Scheiffele et al., 1999). Compared to most cellular membranes, including plasma and endosomal membranes, the outer leaflets of virion envelopes are enriched in cholesterol and lipids that promote positive curvatures. For example, the outer leaflets of virion envelope are often enriched in cone shaped sphingolipids (Brügger et al., 2006; van Genderen et al., 1994; Gerl et al., 2012). Virion envelopes are also more enriched in proteins compared to cellular membranes (Aloia et al., 1993). Consequently, virion envelopes are less fluid than most cellular membranes.

1.5 HSV-1 entry

HSV-1, an alphaherpesvirus in the *herpesviridae* family, is an enveloped virus that causes life-long latent infections in the majority of the word population. Reactivations of the virus can result in mucocutanous lesions, such as cold sores, genital lesions, or keratitis, and can cause severe outcomes in immunocompromised individuals.

HSV-1 is nuclear replicating double stranded DNA virus. Its genome is enclosed in a protein capsid, which in turn is surrounded by a protein tegument layer. The lipid envelope surrounds the protein tegument layer and contains the glycoproteins.

HSV-1 entry is more complex than that of most other viruses and, consequently, is not so well understood. HSV-1 and -2 glycoproteins interact with multiple receptors in the broad range of cells these viruses infect. Four glycoproteins are required in the entry to host cells, gB, gD, gH, and gL. A fifth glycoprotein, gC, is involved in low affinity interactions with heparin sulphate, but it is not essential (Turner et al., 1998).

gB and gC mediate primary interactions to heparan sulphate. gC, which is not essential for entry, increases attachment efficiency. gD then mediates the secondary interactions with the

cellular receptors nectin-1, HVEM (used by HSV-1 and -2), or 3-O sulphated heparin sulphate (used by HSV-1 but not HSV-2) (Akhtar and Shukla, 2009; Rey, 2006). Following receptor binding, gD changes conformation, triggering the recruitment of the fusion complex composed by the gH/gL heterodimer and the actual fusogen, gB (Gianni et al., 2006). The role of the gH/gL complex is ambiguous, possibly regulating fusion by gB (Chowdary et al., 2010). gB, the most conserved among HSV entry glycoproteins (Heldwein et al., 2006), interacts with the paired immunoglobin like-type 2 receptor (PILR2) to mediate fusion (Maurer et al., 2013).

It is still unknown how HSV-1 fusion is triggered. HSV-1 generally fuses with the plasma membrane, but also fuses with endosomal membranes, depending on cell type. Fusion to neurons and Vero cells occurs at the plasma membrane at neutral pH (Wittels and Spear, 1991). In Chinese hamster overy or Hela cells, HSV-1 is internalized by endocytosis before fusing with the endosomal membrane in a pH dependent manner (Nicola, 2016). For fusion at the plasma membrane, a model has been suggested in which gB punctures the membrane (Clarke, 2016) due to close contact to the cellular membranes when gD binds cellular receptors (Eisenberg et al., 2012). The release of the membrane potential across the plasma membrane would then create an electric field that could lead to the transition to the postfusion conformation of gB (Clarke, 2016). In endosomes, the low pH could break the hydrogen bonds that hold the fusion loops in place (Stampfer et al., 2010).

Like other class III fusion proteins, gB has five ectodomains. In the post-fusion conformation, these domains are arranged in a hairpin above a TMD (Heldwein et al., 2006). Domain I, which is located close to the virion envelope, contains two fusion loops, which are exposed and face away from the virion envelope in the pre-fusion conformation. Domain III forms the central coiled-coil domain (Heldwein et al., 2006). The structure of the pre-fusion

conformation or the protein rearrangements during fusion remain elusive (Cooper and Heldwein, 2015). Any structural information is based on homology modeling with VSV G, another class III fusion protein. However, since VSV G rearrangements triggered by acidic pH are reversible (Gaudin, 2000b), and those by HSV-1 gB are not (Weed et al., 2016), the accuracy of such models remains unclear.

1.6 Inhibitors of viral fusion

Viral entry inhibitors have some advantages. Firstly, they prevent infection altogether before the virus can damage cells or establish persistent genome reservoirs, such as genome integration (retroviruses), covalently closed circular DNA (HBV), or latent genomes (herpes viruses). Entry inhibitors act outside cells, avoiding the need to cross cell membranes. Entry inhibitors may also prevent potentially pernicious host immune responses. For example, influenza can induce hyperinduction of pro-inflammatory cytokines, which can determine the severity of the infection (Liu et al., 2016). Entry inhibitors can also complement existing therapies.

Most current antiviral strategies focus on inhibition of replication (De Clercq and Li, 2016). Viral strains that are resistant to inhibitors acting on intracellular targets involved in replication are most likely to still be sensitive to entry inhibitors (Lee et al., 2017).

Several viral entry steps are conserved. Most viruses attach to either heparan sulfate or sialic acid, for example, and the lipid bilayer of enveloped viruses must fuse with cellular membranes to enter cells. Such conserved steps have the potential to be useful as targets for broad spectrum antivirals.

1.6.1 Approved entry inhibitors

Three antivirals that block viral entry are approved for clinical use. They act by different mechanism of actions. Entry is inhibited by blocking of the transition from pre- to post-fusion conformations of viral fusion proteins. Some peptides that mimic the heptad repeat of the viral fusion proteins prevent the structural rearrangements that occur during fusion. Enfuvirtide (Fuzeon, approved in 2003), is a 36-amino acid such peptide. It mimics the HR-2 region of the HIV fusion protein gp41 to compete with the interaction between the heptad repeat regions HR-1 and -2 in the post-fusion conformation (Kilby et al., 1998). Peptides mimicking similar domains of other viral fusion proteins have also been characterized, including against the class I fusion proteins of IAV HA (Autoimmune Technologies, 2015; Badani et al., 2014), RSV F (Gaillard et al., 2017), SARS-CoV spike (Bosch et al., 2004; Sainz et al., 2006), the class II fusion proteins of Dengue and West Nile virus E (Hrobowski et al., 2005), and the class III fusion proteins of HSV-1 (Akkarawongsa et al., 2009). Small molecules that inhibit this transition against RSV (Razinkov et al., 2001) and Dengue virus (Leal et al., 2017) have been identified.

The humanized monoclonal antibodies palivizumab (Synagis, approved in 1998) and RSV-IGIV (immune globulin intravenous, Respigam, approved in 1996, discontinued), neutralize the antigenic site of the RSV attachment and fusion protein F (The IMpact-RSV Study Group, 1998). The mechanism of action of palivizumab is not well understood. It does not inhibit viral attachment or interactions with cellular membranes, and it remains unclear whether it inhibits fusion directly (Huang et al., 2010).

Maraviroc (Selzentry, approved in 2007) is an antagonist of the cellular co-receptor CCR5, which is used by a subset HIV strains (Dorr et al., 2005). Mariviroc binds to, and changes the conformation of, CCR5, a G-protein coupled receptor, in a manner such that the HIV attachment

and fusion protein gp120/gp41 cannot bind to it. gp120/gp41 determines the tropism of HIV isolates, binding to either CCR5 on macrophages (R5 strains) or CXCR4 on T-cells (X4 strains) (Raymond et al., 2015). HIV isolates at early stages of infections are predominantly R5. As the infection progress, X4-types become dominant (Kuhmann and Hartley, 2008). Maraviroc is effective at targeting infections with the R5, but not X4, strain of HIV, and selection for pre-existing X4 strains is one of the mechanisms of resistance (Raymond et al., 2015).

Antivirals that target proteins depend on specific interactions with their target proteins. They therefore have a narrow spectrum of activity, often active against only one virus, or even the subset of one. Moreover, viral fusion proteins are encoded in viral genomes, which rapidly evolve under selective pressures, resulting in the prompt selection for resistance (Greenberg and Cammack, 2004). Antiviral targets that are not encoded by the viral genome, such as the lipid envelope, may pose a higher barrier to resistance.

1.6.2 Antiviral molecules acting on viral lipids

Several antiviral molecules that target the lipids in the viral envelopes have already been characterized (**Figure 1.7**), although only one clinically approved antiviral may target lipids (De Clercq and Li, 2016). Docosanol (Abreva) is approved for the treatment of HSV-1 and -2 infections, but its mechanism of action, or actual targets, are still unclear. Docosanol is saturated 22-carbon primary alcohol and was first reported to have antiviral activity against otherwise unrelated enveloped viruses, including HSV-1, -2, and RSV, but not the non-enveloped poliovirus, (Katz et al., 1991). Docosanol co-purifies with cellular membrane lipids (Pope et al., 1996), but is rapidly metabolized (Pope et al., 1996). It has been proposed to inhibit virus-to-cell fusion (Pope et al., 1996; Sacks et al., 2001), but this mechanism of action is still highly debated (Spruance, 2002).

Many other small molecules, peptides, and antibodies that target the lipid envelope of envelope viruses have been identified and tested as potential antivirals. Arbidol (Blaising et al., 2014) is approved as a prophylactic and treatment for IAV and influenza B virus in Russia and China. Arbidol is an indole-derivative that interacts with tryptophan residues found in membrane proximal regions of many viral fusion proteins. It also interacts with the membrane at the level of the polar head groups (Teissier et al., 2011). Arbidol is active against the entry of both envelope and non-envelope viruses (Brooks et al., 2012; Pécheur et al., 2016), although the exact antiviral mechanism remains unknown. It may increase the affinity of viral glycoproteins for membranes, obstructing the necessary protein rearrangements (Teissier et al., 2011). However, other mechanisms of action have also been suggested, including the inhibition of clatherin-dependent trafficking (Blaising et al., 2013).

PD 404,182 is a small molecule that disrupts the integrity of the lipid envelopes of HIV and HCV without overt toxicity to cells (Chamoun et al., 2012). Although its mechanism of action is unclear, it may act via similar mechanisms to the RAFIs. PD 404,182 does not appear to directly interact with lipid envelopes, however, as it does not associate with liposomes. In addition, PD 404,182 is inactive against Dengue virus, which is closely related to HCV, or Sindbis virus, which is closely related to HIV, suggesting it may act on proteins, rather than on lipids (Chamoun et al., 2012).

A antiviral peptide derived from NS5a, C5a, is active against HIV and HCV, without overt toxicity to cells (Cheng et al., 2008). The peptide is an amphipathic helix, and was suggested to intercalate in virion membranes to disrupt the integrity of virion envelopes (Badani et al., 2014). However, the mechanism of action remains highly elusive, as it was also proposed to have immunogenic properties (Lin et al., 2011).

1.6.3 Lipid peroxide generators

Lipid peroxidation introduces a peroxide group to the hydrophobic region of unsaturated lipids. As a result, membranes with peroxidized lipids are disrupted, resulting in their permealization or disintegration.

Photoactive lipid peroxidators (**Figure 1.8**) absorb light and reach their excited state. Excited lipid peroxidators then promote the generation of reactive oxygen species through two pathways. In the first (type I) an electron or hydrogen atom is transferred to a substrate whereas in the latter (type II) the energy of the excited state is transferred to an oxygen molecule, resulting in the generation of singlet oxygen ($^1O_2$) (Bacellar et al., 2014; Foote, 1968). Singlet oxygen is a reactive excited-state oxygen that has a short half-life and slow diffusion rate.

LJ001 is a lipophilic rhodamine (oxazreolidine-2,4-dithione) derivative that generates singlet oxygen in a white light-dependent manner (Vigant et al., 2013; Wolf et al., 2010). LJ001 is active against the infectivity of various unrelated enveloped viruses, including HSV-1, -2, HIV, IAV, semliki forest virus, and Ebola virus (EBOV) (EC_{50} ~20-300 nM), while having no effect on the infectivity of the non-enveloped AdV (Vigant et al., 2013). LJ001 decreased the fluidity of membranes in a light-dependent manner, whereas the insertion of LJ001 in membranes alone does not affect the fluidity of membranes.

JL103 is a LJ001 derivative that absorbs visible light more efficiently (Vigant et al., 2013). Compared to LJ001, JL103 has approximately 10-fold higher potency (EC_{50} 0.5-13 nM for HIV, IAV, cytomegalovirus (CMV), HSV, and rift valley fever virus (RVFV); and 185 nM EBOV) (Vigant et al., 2013). LJ001 was postulated to reduce fluidity of membranes, rendering them unable to fuse (Hollmann et al., 2014). Peroxidation, by other agents, however, increases membrane fluidity which in turn renders the membranes unable to fuse (Huarte et al., 2016).

Quinone derivatives, such as the natural compounds hypocrellin A and B or hypericin found in St. Johns Wort, are active against envelope viruses, including HSV-1 (Hudson et al., 1997), IAV, VSV, and Sendai virus (Lenard et al., 1993) at nanomolar concentrations. They peroxidize lipids in a light-dependent manner (Jendželovská et al., 2016; Lenard et al., 1993), an effect which contributes to their antiviral activity (Hudson et al., 1997). Without light (λ 470-590 nm), the potency of hypocrellin A and B is reduced by 20-50 fold (Hudson et al., 1997). Hypericin and hypocrellin A and B have no overt cytotoxicity at effective concentrations, at least without light (Hudson et al., 1997).

Hypericin has two absorption peaks at λ 550 and 600 nm, with broad and weak absorptions at λ below 550 nm (Krishnamoorthy et al., 2005). Hypocrellin also has two peaks in the visible spectrum at λ 540 and 570 nm, as well as a broad peak at 470 nm (Krishnamoorthy et al., 2005). Synthetic quinone derivatives that absorb light in the UV rather than the visible spectrum have lower potencies than hypericin and hypocrellin A, indicating that absorption in the visible spectrum could be important for antiviral activity (Krishnamoorthy et al., 2005).

The mechanism of these quinone derivatives appear to be similar to that of certain tetrapyroles such as porphyrin and chlorophyllide, which also have light-dependent activity against envelope viruses, including HBV, HCV, Dengue virus, Marburg virus (Guo et al., 2011).

It is not known whether lipid peroxidation by these compounds has antiviral effects. Such studies are currently underway in our lab. Peroxyl radical generators (**Figure 1.8**) such as 2,2'-azobis (2,4-dimethylvaleronitrile) (AMVN) and 2,2′-azobis (2-amidinopropane) (AAPH) are very commonly used to study lipid peroxidation (Hanlon and Seybert, 1997). The azo bond of AMVN and AAPH decomposes to form two radicals (R・), which then react with oxygen molecules to produce peroxyl radicals (RO_2・). The polar AAPH generates radicals in aqueous

environments, whereas the hydrophobic AMVN generates them inside the membranes. Radicals produced by AAPH are scavenged by polar antioxidants such as ascorbic acid, whereas those produced by AMVN are scavenged by lipopohilic antioxidants such as α-tocopherol.

1.6.4 Modulators of fluidity

Modulators of membrane fluidity can also inhibit fusion between enveloped viruses and cells. Curcumin is a non-steroidal diarylheptanoid found in turmeric that has broad spectrum activity against otherwise unrelated enveloped viruses (Chen et al., 2013). Curcumin intercalates in the virion envelopes to decrease their fluidity, resulting in virions deficient in binding and fusion to cells (EC_{50} in micromolar range, no overt toxicity) (Anggakusuma et al., 2013). Curcumin inhibited both receptor binding and fusion directly (Anggakusuma et al., 2013).

Glycyrrhizin is another natural compound, found in licorice root, that decreases the fluidity of lipid bilayers (Harada, 2005). Glycyrrhizin is active against several unrelated enveloped viruses, including HIV, IAV, VSV (Harada, 2005), and severe acute respiratory syndrome corona virus (SARS-CoV) (Cinatl et al., 2003) . Curcumin and glycyrrhizine have no overt toxicity. However, their therapeutic indexes are narrow (> 2.94 and approximately 50, for curcumin and glycyrrhizine, respectively) (Anggakusuma et al., 2013; Harada, 2005).

Whereas the RAFIs also intercalate in virion envelopes to inhibit virus-to-cell fusion, they do not affect membrane fluidity (Colpitts et al., 2013), indicating the RAFIs act by a different mechanism of action than curcumin or glycyrrhizin.

1.6.5 Lipid-acting antiviral mechanisms in innate viral immunity

Cells may have evolved innate viral immunity mechanisms that modulate membrane properties to inhibit viral infection. HC25 (25-hydroxycholesterol) is a cholesterol-derivative, the synthesis

of which is induced by interferon during viral infection. It has broad-spectrum antiviral activity against a broad range of viruses, including IAV, HCV, and HSV (Blanc et al., 2013; Chen et al., 2014). HC25 downregulates cellular cholesterol levels, the principal regulator of cellular membrane fluidity (Blanc et al., 2013). HC25 has no direct effect on virions, but instead acts on the cells, being active when cells are treated prior or after infection (Anggakusuma et al., 2013). HC25 thus appears to act on cellular targets to decrease membrane fluidity.

Interferon induced transmembrane proteins (IFITM) restrict the infection of some unrelated enveloped viruses, including IAV and RSV, flaviviruses (west Nile virus and Dengue virus), VSV (Sun et al., 2005), and HIV (albeit to lesser extent than IAV) but not of some other enveloped viruses such as arenaviruses or a retrovirus (MLV). The mechanisms by which IFITMs restrict infection are not yet fully understood and probably diverse. One IFITM, IFITM3 is a transmembrane protein that localizes to endosomes. It restricts entry of IAV by modulating the properties of endosomal membrane, inhibiting pore formation after hemifusion has occurred (Desai et al., 2014). IFITM3 has also been proposed to inhibit virion-to-cell fusion by inhibiting the formation of negative curvatures for hemifusion (Li et al., 2013a).

1.6.6 Limitations of current antivirals

Most approved antivirals act directly on specific viral proteins. Development of drugs targeting specific enzymes or receptors requires specific knowledge of the target proteins, information which is not readily available for emerging pathogens. Antivirals that target steps conserved across multiple viral families have the potential to be useful against only partially characterized emerging pathogens.

1.7 Objectives and hypothesis

The research described in this thesis aims to examine the mechanism of action of the RAFIs. Two models were proposed. In one the RAFIs inhibit the fusion of enveloped viruses by increasing the energy required for the formation of the hemifusion stalk based on their physical properties, such as shape, rigidity and amphipathicity, rather than on chemical properties, such as reactive functional groups. In the other, the perylene moiety and absorption of visible light are required for activity. My hypothesis is that the RAFIs inhibit virus-to-cell fusion by biophysical mechanisms. If the hypothesis is correct, then chemically distinct molecules that have shape, rigidity, and amphipathicity similar to these of the RAFIs should also inhibit enveloped virus infectivity with similar efficacy. My first objective was to test chemically distinct molecules for their effects on the infectivity of enveloped viruses. If the RAFIs specifically target virus-to-cell fusions over cellular fusions, moreover, then their antiviral activities should be independent of their effects on cellular viability. Therefore, my second objective was to test the effect of chemically distinct RAFIs on cellular viability.

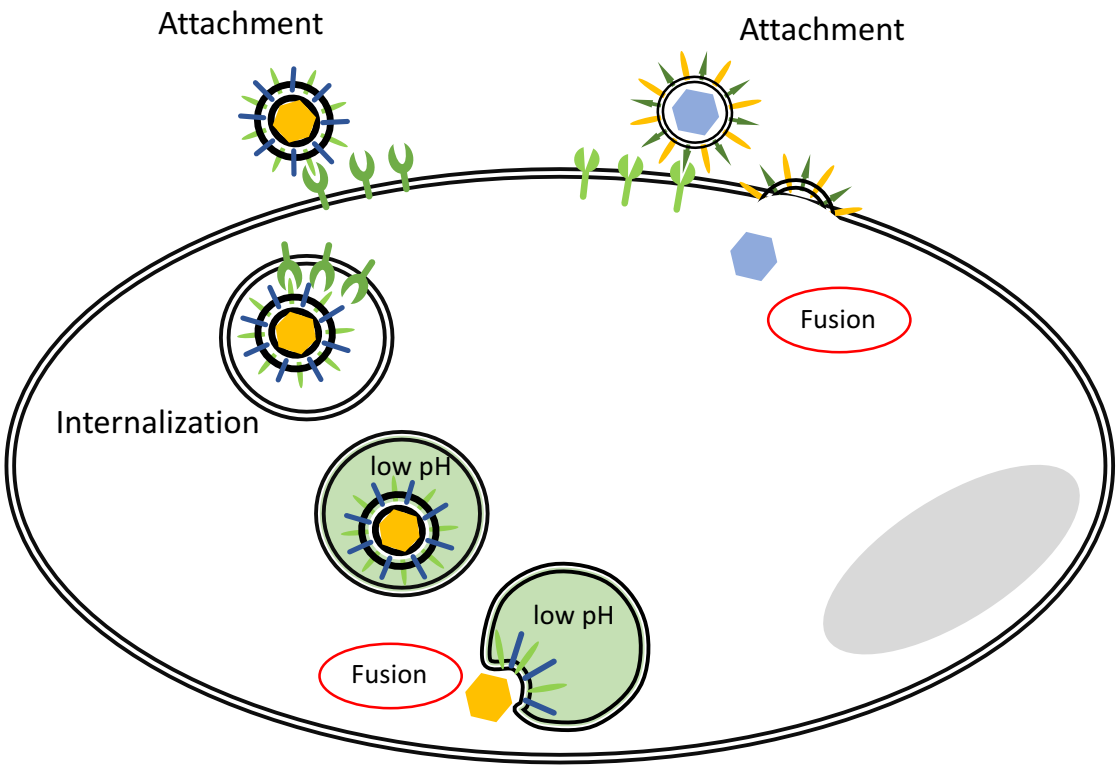

Figure 1.1 The lipid bilayers of envelope viruses must fuse with cellular membranes to infect cells

Viral entry begins with virion attachment to receptors or ligands on the cell surface. Most viruses are then internalized (**left**), to fuse with vesicle membranes. Viral fusion protein rearrangements are triggered by low pH or receptor binding. Some viruses fuse directly with the plasma membrane (**right**) upon receptor binding. Regardless of the entry pathway, however, all envelope viruses must fuse their envelopes with cellular membranes.

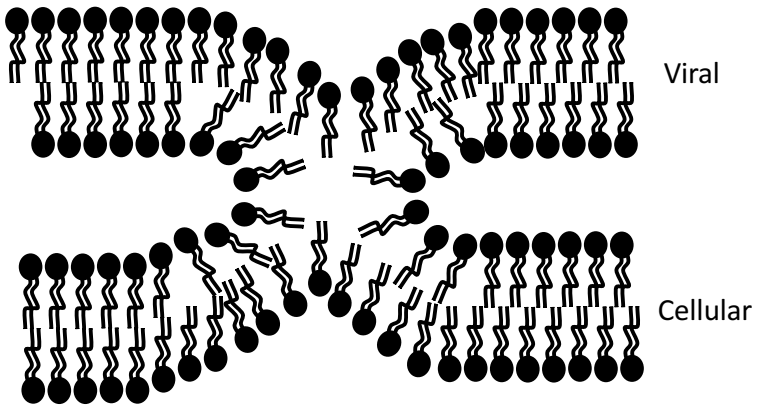

Figure 1.2 Membrane fusion proceeds through a hemifusion intermediate

In this structure, the outer leaflets have already fused whereas the inner leaflets have not. The outer leaflets must thus bend into a negative curvatures, which poses one of the energy barriers to fusion.

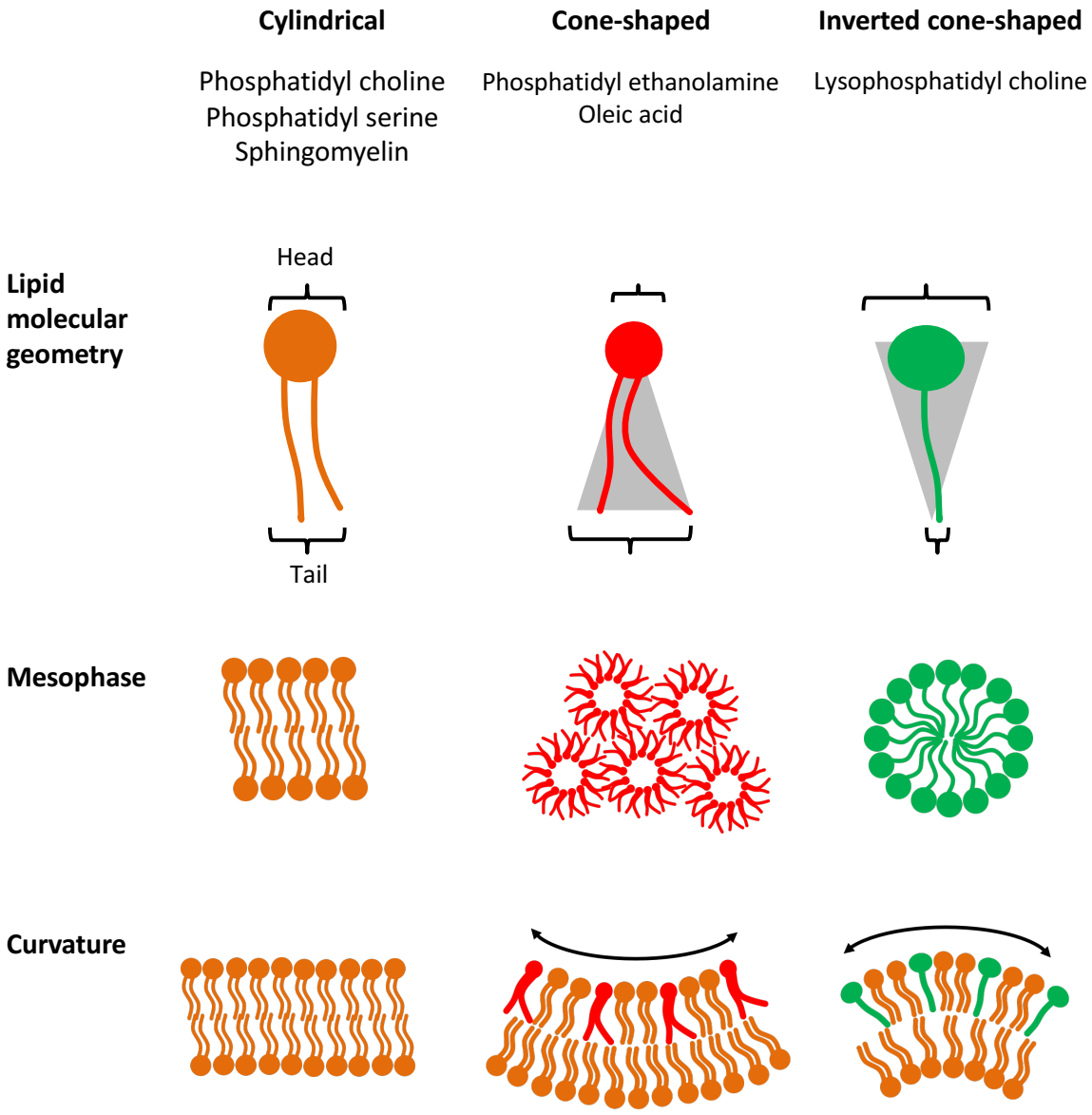

Figure 1.3 Lipid molecular geometries, mesophase structures, and their effects on membrane curvature

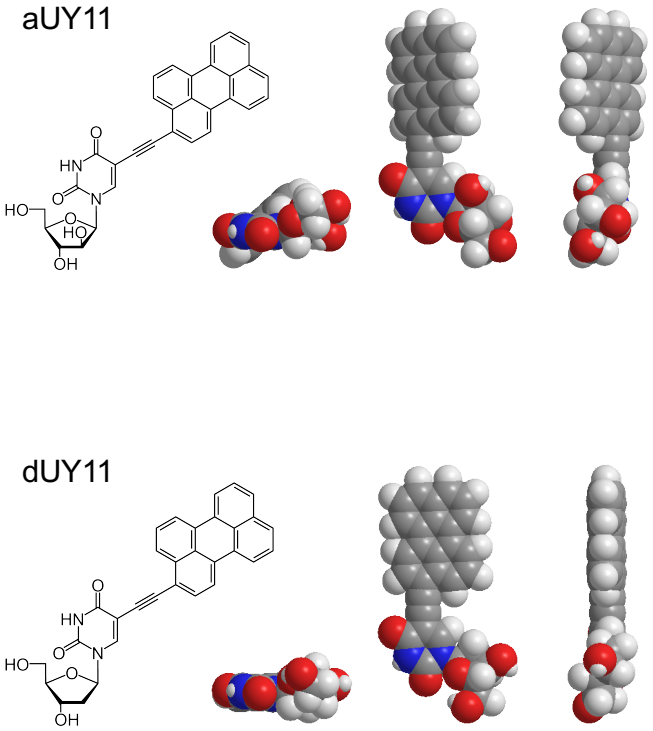

Figure 1.4 The RAFIs aUY11 and dUY11 have inverted cone shaped molecular geometries

Chemical and space filling structures orthogonal representations. aUY11 and dUY11 have rigid ethynylperylene hydrophobic moieties, and arabino-uracil or deoxyribose-uracil polar moieties, respectively. The cross sections of the polar moieties are larger than those of the hydrophobic moieties, giving them inverted cone molecular geometries. Grey, carbon; red, oxygen; blue, nitrogen; white, hydrogen.

Compounds with shorter hydrophobic moieties

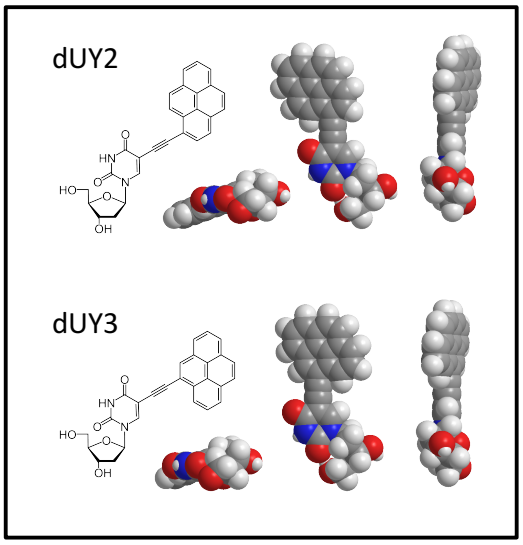

Compounds with non-planar or flexible hydrophobic moieties

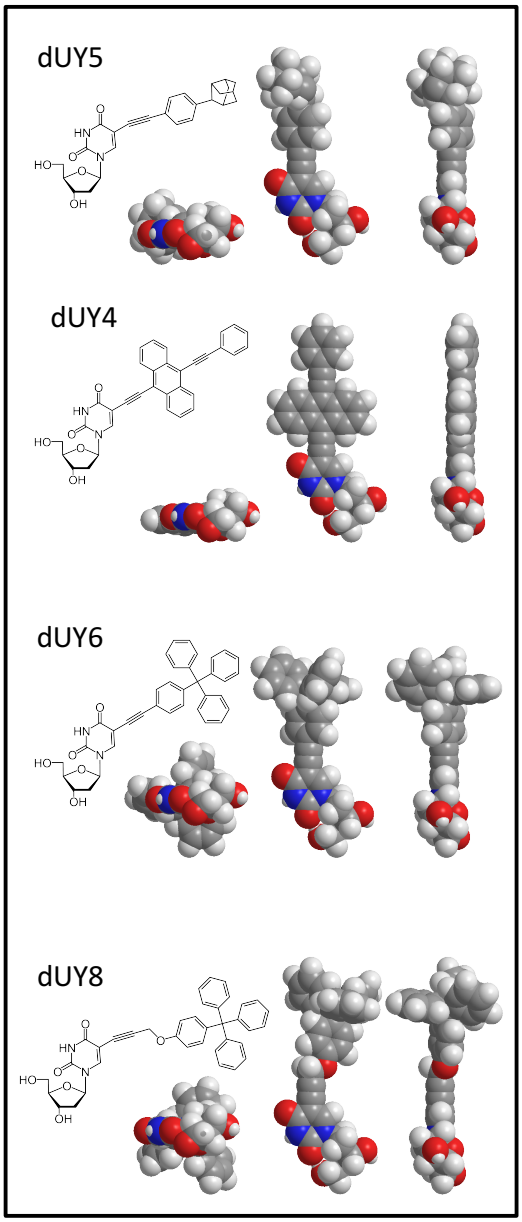

Compounds with non-planar and non-aromatic hydrophobic moieties

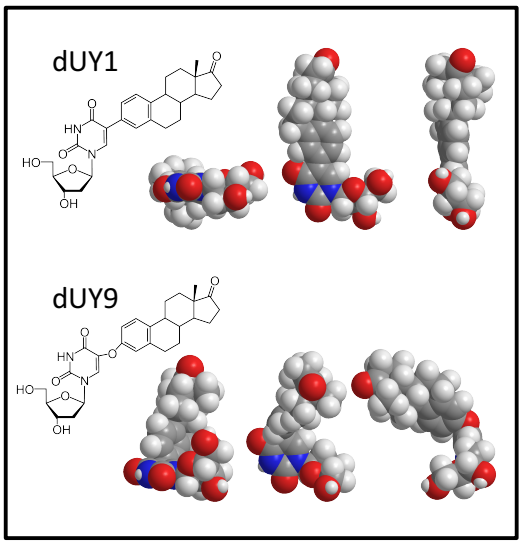

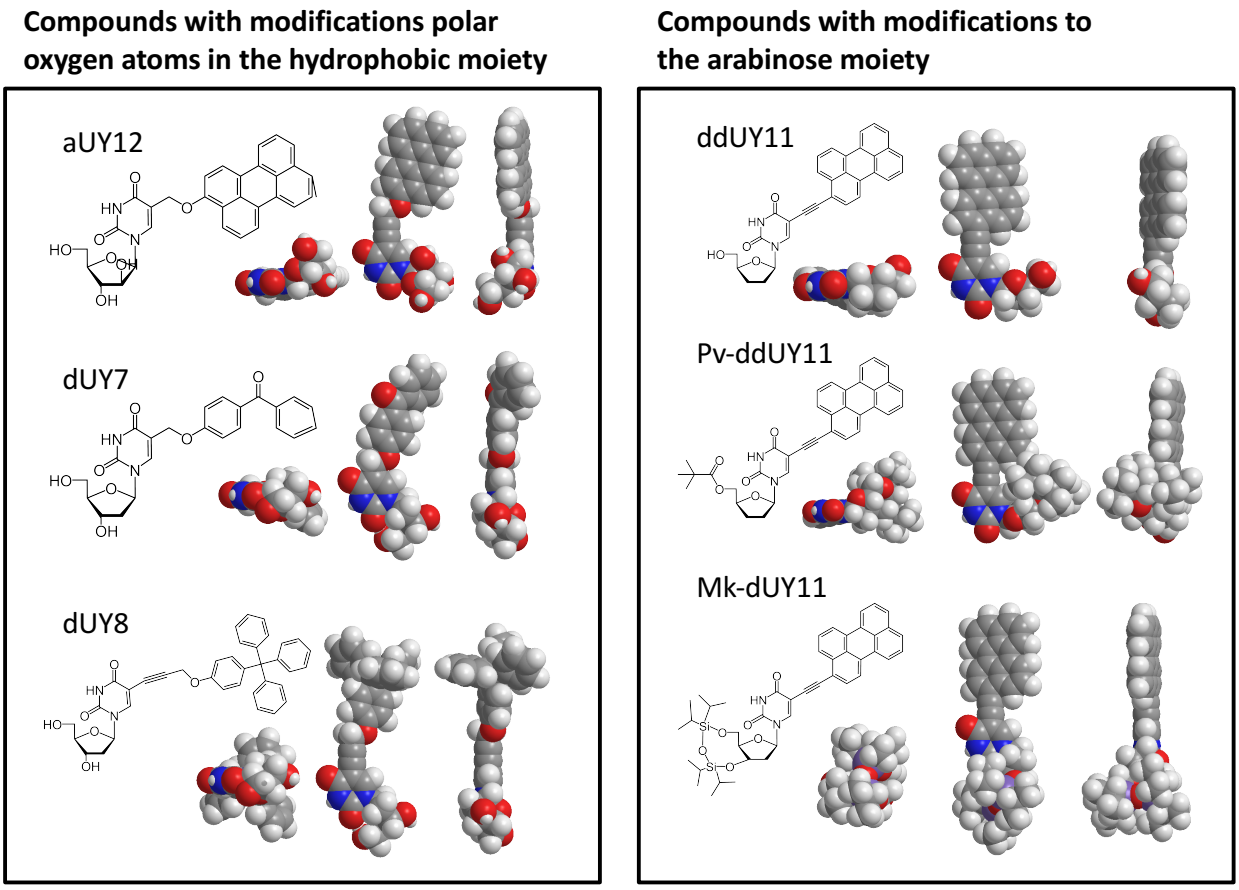

Figure 1.5 Previous structure activity relationship studies

Chemical and space filling structures orthogonal representations. Grey, carbon; red, oxygen; blue, nitrogen; purple, silicon; white, hydrogen. The activities of these compounds are published in (St. Vincent, *et al*., 2013).

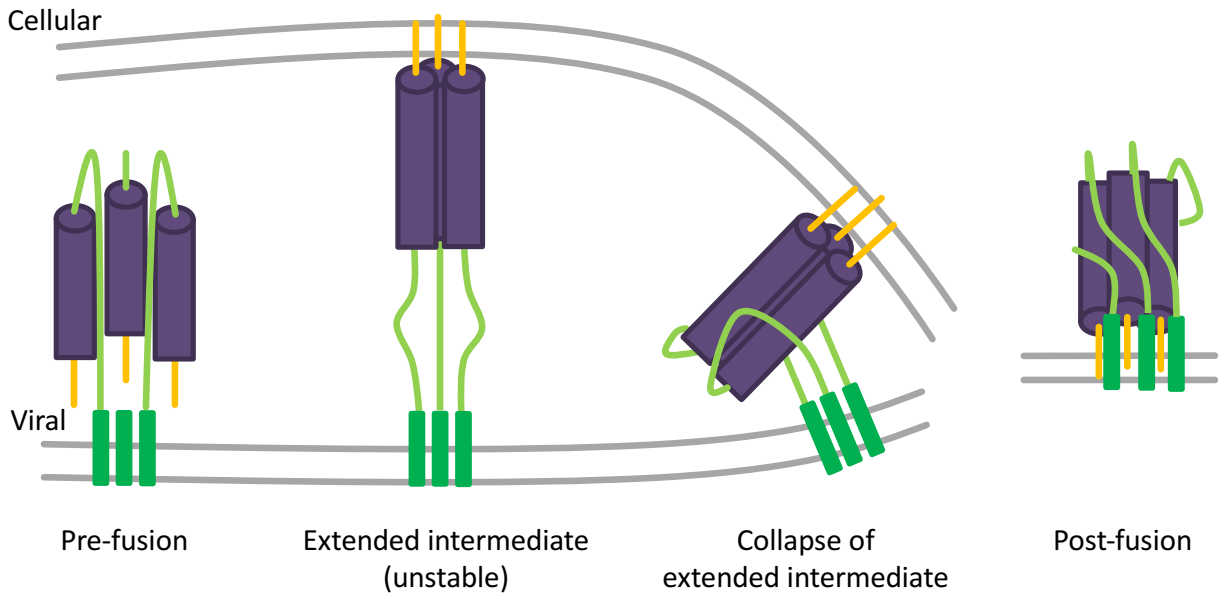

Figure 1.6 Viral fusion protein rearrangements

Despite structural differences, viral fusion protein rearrangements occur through similar mechanisms. In the pre-fusion conformation the TMD (dark green) is anchored in the viral membrane only. During fusion, the protein extends and a hydrophobic fusion peptide (orange) inserts in the cellular membrane. The collapse of this unstable intermediate results in the post-fusion conformation, in which the fusion peptide and the TMD are in the same membrane. Adapted from Harrison, 2008.

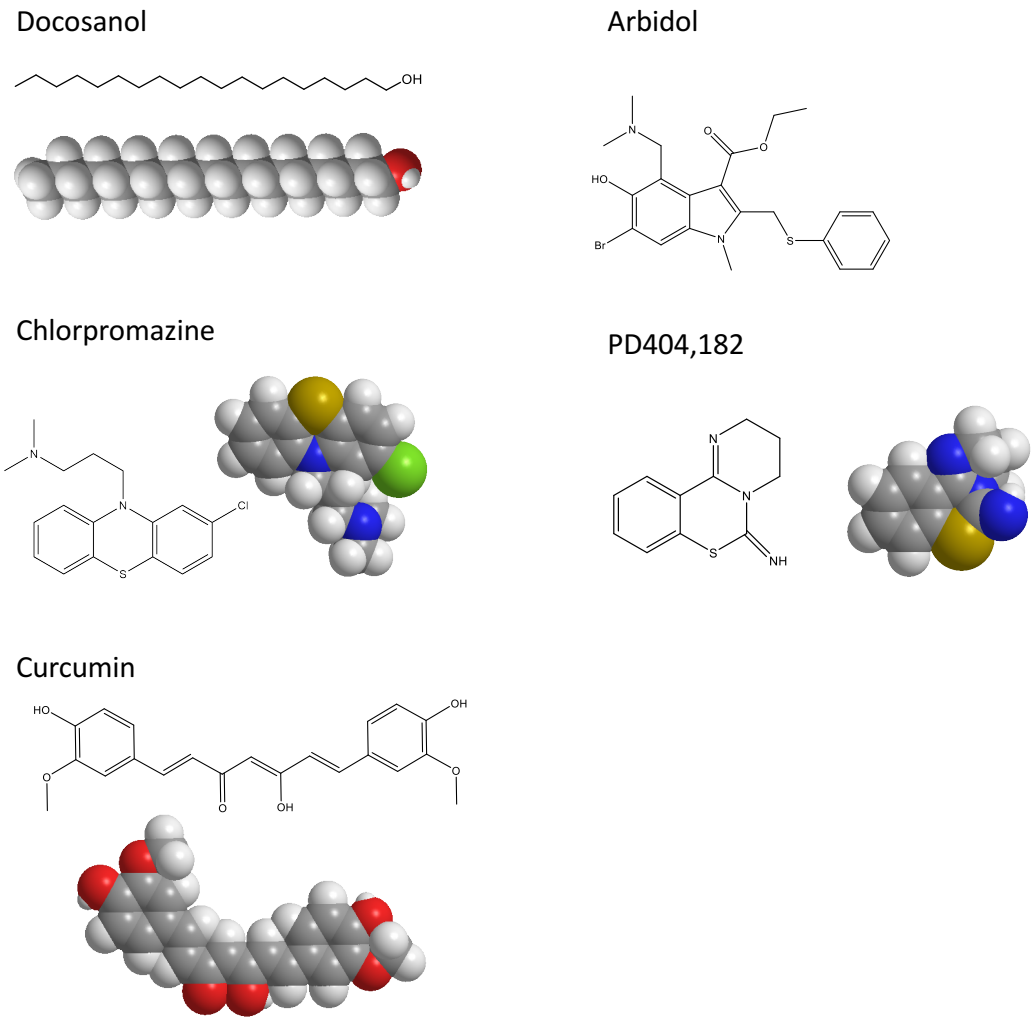

Figure 1.7 Compounds that act on viral lipids

Chemical and space filling structures. Grey, carbon; red, oxygen; blue, nitrogen; purple, silicon; yellow , sulfur; green, chloride; white, hydrogen..

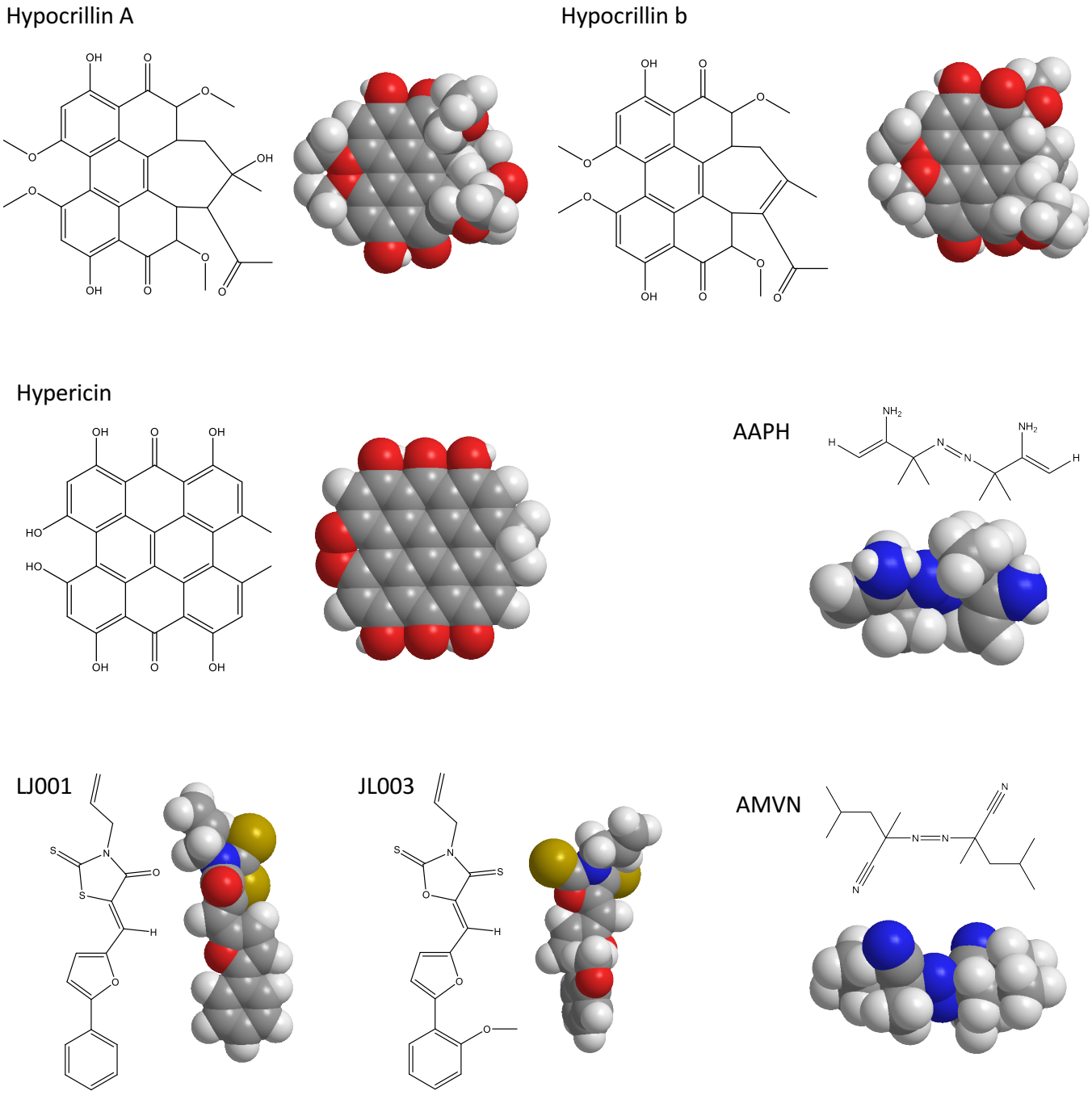

Figure 1.8 Lipid peroxidators

Chemical and space filling structures. Grey, carbon; red, oxygen; blue, nitrogen; purple, silicon; yellow , sulfur; white, hydrogen..

CHAPTER 2: MATERIALS AND METHODS

2.1 Antiviral compounds

Test compounds were synthesized by Alexey A. Chistov, Gleb V. Proskurin, Andrey V. Aralov, Egor A. Ulashchik, Philipp P. Streshnev, and Vadim V. Shmanai led by Vlademir Korshun (Shemyakin-Ovchinnikov Institute of Bioorganic Chemistry, Moscow, Russia). Compounds aUY11 (St Vincent et al., 2010; Chistov et al., accepted), dUY11 (Andronova et al., 2003), **3b** (Chistov et al., 2016), and **5a**,**b**–**7a**,**b** (Aralov et al., 2017) were prepared as described previously. The synthesis of **1a**,**b** and **8a**,**b**–**1a**,**b** will be reported elsewhere. The procedures for **2a**,**b**, **3a**, **4a**,**b**, **12a**,**b**, and **13** are described in (Speerstra et al., manuscript in preparation).

Compounds were dissolved in DMSO at 10 mM, aliquotted and stored at -20 °C. Compounds were dissolved in 37 °C DMEM just prior to use such that DMSO concentrations never exceeded 0.2%. Equivalent DMSO concentrations were used as vehicle control. All antiviral compounds are found in **Table 3.1-3**.

2.2 Chemicals and reagents

All RAFIs were dissolved in dimethylsulphoxide (DMSO ≥ 99.9%, Sigma-Aldrich, Oakville, ON, Canada). 3-(4,5-dimethylthiazol-2-yl)-2,5-diphenyltetrazolium (MTT, Sigma-Aldrich) dissolved at 5 mg/mL in warmed PBS (phosphate buffered saline, prepared as 1 mM KH_2PO_4, 150 mM NaCl, 3 mM Na_2HPO_4, adjusted to pH 7.4). MTT stock solutions were stored at 4 °C for up to 5 days. Isopropanol and DMSO (99.5%), purchased from Fisher (Ottawa, ON, Canada) and Sigma-Aldrich respectively, were used to solubilize formazan crystals in the MTT assay. RAFIs

were dissolved in 1-octanol (Sigma-Aldrich) to obtain their spectra in hydrophobic environments.

1,2-Dioleoyl-*sn*-glycero-3-phosphocholine (DOPC; Sigma-Aldrich) dissolved in chloroform (Fisher) was used for the preparation of liposomes. Catalog numbers for all chemicals are found in **Table 2.2**.

2.3 Cell culture reagents

Cells were cultured in Dulbecco's modified Eagle medium (DMEM, Invitrogen Life Technologies Inc., Burlington, ON, Canada), supplemented with 5% fetal bovine serum where indicated (PAA Laboratories, now GE Healthcare, Westborough, MA, USA). Phenol red free DMEM (Invitrogen) was used for MTT assays. Infected cells were overlayed with semisolid DMEM containing 2% methylcellulose and 5% FBS (Sigma-Aldrich) and were fixed and stained with crystal violet (1% [w/v] crystal violet, 17% [v/v] methanol in H_2O). PBS was prepared as 1 mM KH_2PO_4, 150 mM NaCl, 3 mM Na_2HPO_4, adjusted to pH 7.4. Catalog numbers for all main chemicals are described in **Table 2.3**.

2.4 Cells and viruses

African green monkey Vero fibroblasts (Vero; catalog number CCL-81, American Type Culture Collection, Manasses, VA, USA) were cultured in DMEM containing 5% FBS at 37 °C, 5% CO2. To passage cells, monolayers were washed once with 37 °C PBS and detached with trypsin-ethylenediaminetetraacetic acid (EDTA) (0.05%; Invitrogen) for approximately 5 minutes at 37 °C. Cells were then resuspended in 37 °C Dulbecco's modified Eagle's medium (DMEM), 5% fetal bovine serum (FBS).

HSV-1 (KOS) was obtained from the late Dr. Priscilla Schaffer (Harvard Medical School, Boston, MA). To propagate viral stocks, Vero cell monolayers at 70% confluency were inoculated with HSV-1 at a multiplicity of infection (MOI) 0.05 pfu/cell for 1 hour at 37 °C in 5% CO2, rocking and rotating the flask every 10 minutes. The inoculum was removed and cell monolayers were then washed twice with cold DMEM and overlayed with fresh DMEM. Infected cells were incubated in DMEM, 5% FBS for 48 hours at 33 °C until full cytopathic effect (CPE) was observed.

Infected cells were harvested with sterile disposable scrapers. Cells and supernatant were separated by centrifugation at 3,200 × g for 30 minutes in a swinging bucket rotor A-4-62 in Eppendorf 5810R centrifuge at 4 °C (Eppendorf Canada, Mississauga, ON, Canada). The supernatant was collected and cell-free virions were pelleted by centrifugation at 10,000 × g for 2 hours in a JA-14 rotor in a Beckman Coulter J-series centrifuge at 4°C (Beckman Coulter Inc., Mississauga, ON,Canada). Cell-associated virions were released by three freeze-thaw cycles in dry ice-ethanol and 37 °C water bath and three sonication cycles using an Ultrasonic Processor XL 2020 (Mandel Scientific Company, Guelph, ON, Canada) at a power setting of 3 and at 30 second intervals. Cellular debris was pelleted by centrifugation at 3,200 × g for 30 minutes in a swinging bucket rotor A-4-62 in an Eppendorf 5810R centrifuge at 4 °C. The resulting supernatant was used to resuspended cell-free virions. Viral stocks were aliquoted and stored at -80 °C.

2.5 Viral titrations

HSV-1 stocks were 10-fold serially diluted in DMEM on ice. Vero cell monolayers seeded on 6-well plates at 90% confluency were inoculated with 200 µL diluted virions for 1 hour at 37 °C.

Cells were then washed twice with 1 mL 4 °C serum-free DMEM. Infected cells were then overlayed with DMEM containing 5% FBS and 2% methyl cellulose (Sigma-Aldrich). Cells were incubated for approximately 48 hours or until plaques appeared. Cells were then fixed and stained with crystal violet (Sigma-Aldrich) and methanol (1% [w/v] crystal violet, 17% [v/v] methanol in H_2O).

2.6 Infectivity assay

Approximately 200 HSV-1 virions were exposed to test compound or DMSO vehicle for 10 minutes at 37 °C. Following treatment, confluent Vero cell monolayers were washed twice with serum-free Dulbecco's modified Eagle's minimal medium (DMEM) and then inoculated with the pre-treated virions in 5% CO_2 for 1 hour at 37 °C. Cells were then washed twice with 4°C DMEM to remove unbound virions, overlaid with semi-solid medium containing 5% FBS and 2% methyl cellulose, and incubated in 5% CO_2 at 37 °C until plaques became visible (approximately 48 hours). Viable cells were fixed and stained with crystal violet. Plaque numbers were normalized against the number of plaques produced by virions exposed to DMSO vehicle.

2.7 Cellular viability assay

Subconfluent Vero cell monolayers were incubated in medium containing test compound or DMSO vehicle for 24, 48, or 72 hours at 37 °C and 5% CO_2. Half of the medium was replaced every 24 hours with fresh drug-containing medium. Cell numbers and viability were assessed by the 3-(4,5-dimethylthiazol-2-yl)-2,5-diphenyltetrazolium (MTT) reduction assay, which evaluates mitochondrial activity, a correlate of cell number and viability (Berridge et al., 1996).

Following exposure to test compounds, cell monolayers were washed twice with 37°C DMEM. MTT dissolved in 37°C DMEM was then added to the cells and incubated in 5% CO_2 for 3 hours at 37 °C to allow for MTT reduction to formazan. MTT was removed and formazan crystals were solubilized in 1:1 DMSO:isopropanol. Formazan absorbance was read at 570 nm with background at 650 nm. As blank, MTT and test compound at the experimental concentrations, determined by spectrophotometry, were added together to untreated cells. Any effect of test compounds on MTT reduction was calculated as a percentage of DMSO ($I = [MTT_{DMSO} - MTT_{compound}] / MTT_{DMSO}$). Relative cell numbers were calculated as ($MTT_{t(x)} + MTT_{t(x)} * I$) / $MTT_{t(0)}$.

Cell numbers were expressed relative to t_0. Doubling times were calculated using GraphPad Prism, with the non-linear regression exponential growth fitting ($Y= Y_0^{k \cdot x}$, where Y_0 is relative cell number at time = 0 [normalized to 1], k is the growth constant in reciprocal hours, and x is time in hours). The doubling time $x_{doubling}$ is the time at which the relative cell number is two-fold Y_0, or $x_{doubling} = ln(2)/k$. Half cytostatic concentrations (CC_{50}) are the concentration at which the cell doubling times increase by two-fold.

2.8 Liposome preparation

β-oleoyl-γ-palmitoyl-L-α-phosphatidylcholine (POPC) was dissolved in chloroform in glass tubes and the chloroform evaporated overnight. POPC bilayers were hydrated in fusion buffer (180 mM Na_2HPO_4, 100 mM citric acid; pH 7.4) by vortexing. Large multi-lamellar liposomes were prepared using an Avanti liposome mini-extruder (Avanti Polar Lipids Inc., Alabaster, AL, USA). Hydrated POPC bilayers were loaded in an air-tight glass syringe and extruded through a

polycarbonate 200 nm filter to a syringe on the other side of the mini-extruder. Liposomes were passed through the filter ten times.

2.9 Absorbance and emission spectra

Test compounds were diluted to 10 μM in 1-octanol in10 mm polymethacrylate cuvettes (Sigma-Aldrich). Absorbance spectra were collected using a 10 mm polymethacrylate cuvette blanked with 1-octanol (BioDrop-DUO UV/Vis spectrometer, Montrèal Biotech Inc, Canada).

For emission spectra, test compounds were mixed to a concentration of 10 μM with 1-octanol, warm fusion buffer, or warm fusion buffer containing liposomes (2 nM DOPC). Emission spectra were collected using a QuantaMaster 40 scanning spectrofluorometer equipped with a 75-W Xenon lamp. RAFIs were excited at the first absorbance peak of the polyaromatic rings. Exicitation and emission wavelengths are found in **Table 2.4**. Background emission of the respective solvents was subtracted and spectra were internally normalized to the highest peak where possible (**5a** and **5b** produced no obvious peaks under certain conditions).

Table 2.1 Chemicals and reagents

Chemical name	Supplier	Catalog number
1-Octanol	Sigma-Aldrich (Oakville, ON, Canada)	111-87-5
Chloroform	Fisher (Ottawa, ON, Canada)	C-298-4
Methanol	Fisher	67-56-1
Citric acid monohydrate	Sigma-Aldrich	C1909
DMSO, 99.5%	Sigma-Aldrich	D1435
DMSO, ≥99.9%	Sigma-Aldrich	D8418
DOPC	Sigma-Aldrich	L1381
Isopropanol	Fisher	67-63-0
Methyl cellulose	Sigma-Aldrich	M0387
Thiazolyl Blue Tetrazolium Bromide	Sigma-Aldrich	M2128

Table 2.2 List of cell culture reagents

Chemical name	Supplier	Catalog number
Crystal Violet	Sigma-Aldrich	C3886
DMEM	Invitrogen (Life Technologies Inc., Burlington, ON, Canada)	11885
DMEM Phenol red free	Invitrogen	11054-001
FBS	PAA Laboratories (GE Healthcare, Westborough, MA, USA)	A15-70
Methyl Cellulose	Sigma-Aldrich	M0387
Trypsin-EDTA	Invitrogen	15400-054

Table 2.3 Excitation wavelengths RAFI spectra

RAFI	$\lambda_{excitation}$, nm
aUY11	440
dUY11	440
1a	382
1b	382
2a	440
2b	415
3a	440
3b	440
4a	440
4b	440
5a	440
5b	440
6a	425
6b	425
7a	415
7b	415
8a	440
8b	440
9a	440
9b	440
10a	440
10b	440
11a	440
11b	440
12a	440
12b	415
13	415

CHAPTER 3: RESULTS

My hypothesis is that the RAFIs inhibit virus-to-cell fusion based on their physical properties, such as shape, amphipathicity, and inverted cone shape. If this hypothesis is correct, then the RAFIs would act independently of their chemical groups. To test the hypothesis, I collaborated with chemists under the lead of Dr. Vladimir Korshun, who synthesized twenty-five chemical variations to aUY11 and dUY11 (**Figure 3.1**). These RAFIs are all amphipathic, although to varying extends, have rigid base-hydrophobic moiety interfaces, and inverted cone shapes.

If the mechanism of action of the RAFIs depend on their chemical groups, then the potencies of the RAFIs with chemical replacements of the sugar, base, linker, or perylene moieties would be expected to be lower than the potency of aUY11. Conversely, if the mechanism of action depends on the physical properties of the RAFIs, such as amphipathicity, rigidity, or inverted cone shape, then chemical distinct RAFIs with similar physical properties to aUY11 would also be expected to have similar potencies to aUY11.

To test the potencies of the RAFIs, HSV-1 virions were exposed to each of the RAFIs for 10 minutes prior to infection. Cell monolayers were then infected with treated virions for 1 hour. Any un-infectious virions were then washed away, and cell monolayers were overlayed with fresh semi-solid medium. After 48 hours, plaques developed, which were visualized by staining cells with crystal violet.

3.1 Perylene is not required for antiviral activity

Previous SAR studies had shown that a smaller 4-ring pyrene moiety preplacing the 5-ring perylene resulted in 1,000-fold reduction in antiviral activity (St Vincent et al., 2010), indicating

that either five aromatic rings as a chemical group or a hydrophobic moiety of sufficient length are required for activity. We tested these possibilities.

A compound with a smaller 4-ring pyrene together with a longer butadiynyl linker, giving the hydrophobic moiety a total length similar to that of aUY11, had antiviral activity similar to that of aUY11 (EC_{50}, 16 nM [aUY11]; 73 nM [**1a**]; **Figures 3.1, 3.2**; **Table 3.4**). The antiviral activity of compounds with smaller pyrene is thus recovered when the length of the hydrophobic moiety is maintained by increasing the length of the linker. The five-ring perylene moiety is not essential.

3.2 The minimal length of the hydrophobic moiety is 10.3 Å

RAFIs with hydrophobic moieties of different lengths tested the minimal required length for the hydrophobic moiety. The length of the hydrophobic moiety of aUY11, measured from the top of the perylene moiety to the bottom of the ethynyl linker, is 10.3 Å (*dimension b*; **Figures 3.1**, **3.2**, **3.3; Table 3.4**). Compounds with triazole moieties replacing the ethynyl linker, decreasing the length of the hydrophobic moiety to merely the length of the perylene moiety (8.3 Å), had 50 to 800-fold decreased antiviral activities (9.2 Å: EC_{50}, 2.3 μM [**6a**]; 0.89 μM [**6b**]; or 7.3 Å: EC_{50}, 12.4 μM [**7a**]; 4.38μM [**7b**]). Even shorter hydrophobic moieties (5.3 Å) resulted in > 1,000-fold decreased activity (EC_{50}, > 20 μM [**5a** and **5b**]). Hydrophobic moieties longer than that of aUY11 did not increase antiviral activities (12.3 Å: EC_{50}, 49 nM [**3a**]; 42 nM [**3b**]). The length of the hydrophobic moiety was inversely correlated with the antiviral activity (excluding compounds with 3-ethynylperylene, Pearson r -0.65, p 0.016; **Figure 3.4A**). Nonetheless, RAFIs with ethynylperylene hydrophobic moieties had EC_{50} ranging from 30 nM to > 20 μM, showing that the hydrophobic moiety is not the only factor determining potency.

RAFIs with hydrophobic moieties of varying widths tested whether activity depends on the width of the hydrophobic moiety. The width of the hydrophobic moiety of aUY11, measured from side to side of the perylene moiety, is 7.3 Å (**Table 3.4**). Wider hydrophobic moieties (up to 9.5 Å) did not affect antiviral activity (EC_{50}, 31 nM [**2a**] – 9.5 Å, 73 nM [**1a**] – 8.3 Å, **Table 3.4**, **Figure 3.4B**), whereas the two compounds with hydrophobic moieties narrower than 7.3 Å were > 1,000-fold less active (EC_{50}, > 20 μM [**5a** and **5b**]).

3.3 RAFIs with chemically distinct polar moieties had similar antiviral activities

Previous SAR studies showed that the hydroxyl groups in the arabino moiety had a modest 2-fold effect on antiviral activity, indicating the hydroxyl groups are not critical (St Vincent et al., 2010). We further tested the 2'-hydroxyl and other functional groups at this position. Elimination of the 2'-hydroxyl group did not affect the antiviral activity more than three-fold (EC_{50}, 31 nM [**2a**] or 0.608 μM [**2b**]; 49 nM [**3a**] or 32 nM [**3b**]; 2.3 μM [**6a**] or 0.89 μM [**6b**]; 12.4 μM; [**7a**] or 4.38 μM [**7b**]; for the respective compounds with or without the 2' hydroxyl group, respectively; **Table 3.4**, **Figure 3.5A**). Substitutions of the hydroxyl groups for small, less polar methyl ether groups did not affect antiviral activity either (EC_{50}, 52 nM [**4a**]; 46 nM [**4b**]; **Table 3.4**), supporting the conclusion that the hydroxyl-groups are not critical. The arabino moiety needs not be flexible either. A compound with an conformationally restrained arabino moiety had activity similar to that of aUY11 (EC_{50}, 46 nM [**4b**]; **Figure 3.2**, **Table 3.4**).

The arabino moiety is also replaceable by non-cyclic butylamide derivatives without affecting activity to a significant extent (EC_{50}, 29 nM [**9a**, 4-oxybutylamide]; 20 nM [**9b**, 4-oxybutylamide]; 60 nM [**10a**, 3,3-dimethyl-2,4-dioxybutylamide]; 50 nM [**10b**, 3,3-dimethyl-

2,4-dioxybutylamide]; 75 nM [**11a**, butylamide]) (**Figure 3.2**, **Table 3.4**). A smaller and negatively charged acetyl group substitution replacing the arabino sugar decreased activity by 20- to 120-fold (EC_{50} 1.90 μM [**8a**]; 350 nM [**8b**]).

The arabino sugar moiety is thus not required and can be substituted by polar (**9a**, **9b**, **10a**, and **10b**) or even relatively non-polar (**11a** and **11b**) groups (**Figure 3.2**, **Table 3.4**). However, small and charged substitutions for the arabino sugar decreased activity (**8a** and **8b**; **Figure 3.2**, **Table 3.4**).

Pivaloyloxymethyl (Pom) additions to N3 position had variable effects. Pom additions to compounds containing a 4-hydroxybutylamide group or a 3,3-dimethyl-2,4-dioxybutylamide had no major effect (EC_{50} 50 nM [**10b**] or 60 nM [**10a**]; 20 nM [**9b**] or 29 nM [**9a**], for compounds with or without POM, respectively **Figure 3.5B**). Pom additions increased the activity of the compound containing a small negatively charged acetic acid at position 1 by 5-fold (EC_{50} 350 nM [**8b**] or 1.89 μM [**8a**]), but decreased the activity of the compound containing a non-polar butylamide group by 125-fold (EC_{50} 9.38 μM [**11b**] or 75 nM [**11a**]; **Figure 3.5B**).

One compound tested the requirement of the carbonyl group (∂^-, hydrogen bond acceptor) at position 3 in the uracil moiety. Its replacement with a amine group (∂^+, hydrogen bond donor), converting it to cytidine, resulted in 465-fold decrease in antiviral activity (EC_{50}, 1.26 μM [**12a**]). The carbonyl group in the pyrimidine moiety can therefore not be replaced by an amine group (**Figure 3.2**, **Table 3.4**).

3.4 Cross sections of the polar moiety did not affect the antiviral activity

Although all dimensions of the flexible arabino moiety vary, the polar moiety of aUY11 in one conformation is 6.9 Å long (dimension *e*), 9.2 Å wide (dimension *f*), and 4.6 Å deep (dimension

g; **Figure 3.2**, **Table 3.4**). The cross section of its polar moiety (dimensions *f* and *g)* are thus larger than the cross section of its hydrophobic moiety (dimensions *c* and *d),* giving the inverted cone shape. None of the tested compounds were cone shaped (*i.e.* dimensions *f* and *g* smaller than *c* and *d*; **Figure 3.2**, **Table 3.4)**.

As the arabino moiety is replaceable by a variety of other polar moieties, we tested the effects of the size of the polar moiety on antiviral activity. There was no correlation between polar moiety length, width, or depth and the antiviral activity (**Figure 3.9**).

3.5 RAFIs with various hydrophobic moieties are not overtly cytotoxic

Half cytostatic values were not reached for the vast majority of the compounds at 20 μM, although most compounds with modifications to the hydrophobic moiety reduced cell doubling rates to some extent (**Table 3.4**, **Appendix 2**). Therefore, RAFIs with a variety of different hydrophobic moieties, including longer and wider than those of aUY11, have no major effects on cell viability (**Figure 3.4C**, **D**).

3.6 RAFIs with charged or non-polar moieties were cytostatic or cytotoxic

A compound with a cytidine moiety replacing the uridine moiety was cytostatic (CC_{50} < 0.6 μM, **12a**), but addition of an oxygen between the linker and the perylene moiety overcame cytotoxicity (CC_{50} > 20 μM; **12b**; **Table 3.4**), although it also disrupted antiviral activity. A compound with hydroxylated and methylated butylamide moieties replacing the arabino moiety and also a Pom group did not reach CC_{50} at 20 μM (**10b**), indicating that RAFIs without arabino moieties can also be tolerated. Nonetheless, most substitutions replacing the arabino moiety were either cytostatic or cytotoxic, including non-polar chains (CC_{50}, 1.7 μM – cytostatic, or 6 < CC_{50}

< 20 μM –cytotoxic; **11a**; CC_{50} < 0.6 μM – cytostatic, **11b**) or small charged groups (CC_{50} 7.5 μM –cytostatic, **8a**; **Table 3.4**). A compound with hydroxylated and methylated butylamide moieties replacing the arabino moiety and no Pom was also cytostatic (CC_{50} 9.6 μM, **10b**; **Table 3.4**).

3.7 Light absorption in the visible spectrum is not required

Most RAFIs absorb light at 440 and 474 nm (peak absorbance ratios approximately 1:1.2). The absorbance spectra for **2b**, **6a**, **6b**, **12b**, and **13** were blue-shifted, with absorption peaks at 415 and 440 nm (**Figure 3.6**). The two compounds with pyrene moieties replacing the perylene moieties had absorption peaks at 382 and 405 nm and absorbed little light at wavelengths > 425 nm (**1a** and **1b**; **Figure 3.6**), as would be expected from these hydrophobic moieties (**Figure 3.6**). One of them nonetheless retained good antiviral activity (**1a**, EC_{50} 0.073 μM), indicating that at least absorption in the visible spectrum is not required for activity.

3.8 Active RAFIs intercalate into lipid bilayers

To test the effects of the different substitutions on the ability of the test compounds to intercalate between the lipids of lipid bilayers, the fluorescence spectra were analyzed in aqueous or hydrophobic environments, or in aqueous environments containing liposomes.

Fluorescence emission spectra were determined at excitation wavelengths at the first absorbance peak. Like aUY11 and dUY11, most RAFIs had similar fluorescence spectra in hydrophobic environments or in polar environments containing liposomes, whereas the fluorescence intensity in aqueous environments was much weaker and characteristically distinct (**Figure 3.6**). The hydrophobic moieties of these compounds thus intercalate between the

hydrophobic acyl chains of the liposome bilayers. In contrast to most other compounds, **2b**, **12a** **12b**, and **13** were fluorescent in aqueous environments (**Figure 3.6**). Nonetheless, their fluorescence spectra in aqueous environments containing liposomes were more similar to those in hydrophobic than to those in aqueous environments, indicating that these compounds also intercalate between the hydrophobic acyl chains of the liposome bilayers (**Figure 3.6**).

Compounds **5a** and **5b** are only weakly fluorescent (**Figure 3.6**). However, their fluorescence spectra are still somewhat more similar when in aqueous environments containing liposomes or not, and most different in hydrophobic environments. These compounds are thus most unlikely to intercalate between the hydrophobic acyl chains of the liposome bilayers. With the exception of these two compounds, which had no activity (EC_{50} > 20 μM), all tested RAFIs intercalated in lipid bilayers. Intercalation is therefore required but not sufficient for antiviral activity.

Table 3.1 RAFIs based on uracil scaffold

The RAFIs were synthesized by Vlademir Korshun, Shemyakin-Ovchinnikov Institute of Bioorganic Chemistry, Moscow, Russia.

	Compound	R1	R2	X
aUY11	5-(perylen-3-ylethynyl)-arabino-uridine	arabinose	H	perylen-3-ylethynyl
dUY11	5-(perylen-3-ylethynyl)-2′-deoxyuridine	deoxyribose	H	perylen-3-ylethynyl
1a	5-(pyren-1-ylbutadiynyl)-2′-deoxyuridine	deoxyribose	H	pyren-1-ylbutadiynyl
1b	5-(pyren-4-ylbutadiynyl)-2′-deoxyuridine	deoxyribose	H	pyren-4-ylbutadiynyl
2a	5-(perylen-2-ylethynyl)-arabino-uridine	arabinose	H	perylen-2-ylethynyl
2b	5-(perylen-2-ylethynyl)-2′-deoxyuridine	deoxyribose	H	perylen-2-ylethynyl
3a	5-(perylen-3-ylbutadiynyl)-arabino-uridine	arabinose	H	perylen-3-ylbutadiynyl
3b	5-(perylen-3-ylbutadiynyl)-2′-deoxyuridine	deoxyribose	H	perylen-3-ylbutadiynyl
4a	5-(perylen-3-ylethynyl)-2′-O-methyl-uridine	2′-O-methyl-ribose	H	perylen-3-ylethynyl
4b	5-(perylen-3-ylethynyl)-LNA-uridine	2′-O-4′C-methylene-ribose	H	perylen-3-ylethynyl
5a	5-(4-phenyl-1,2,3-triazol-1-yl)uridine	ribose	H	4-phenyl-1,2,3-triazol-1-yl
5b	5-(4-phenyl-1,2,3-triazol-1-yl)-2′-deoxyuridine	deoxyribose	H	4-phenyl-1,2,3-triazol-1-yl
6a	5-[4-(perylen-3-yl)-1,2,3-triazol-1-yl]uridine	ribose	H	4-(perylen-3-yl)-1,2,3-triazol-1-yl
6b	5-[4-(perylen-3-yl)-1,2,3-triazol-1-yl]-2′-deoxy-uridine	deoxyribose	H	4-(perylen-3-yl)-1,2,3-triazol-1-yl
7a	5-[4-(perylen-2-yl)-1,2,3-triazol-1-yl]uridine	ribose	H	4-(perylen-2-yl)-1,2,3-triazol-1-yl
7b	5-[4-(perylen-2-yl)-1,2,3-triazol-1-yl]-2′-deoxy-uridine	deoxyribose	H	4-(perylen-2-yl)-1,2,3-triazol-1-yl
8a	5-(perylen-3-ylethynyl)-uracil-1-acetic acid	acetic acid	H	perylen-3-ylethynyl
8b	3-pivaloyloxymethyl-5-(perylen-3-ylethynyl)-uracil-1-acetic acid	acetic acid	Pom	perylen-3-ylethynyl

9a	5-(perylen-3-ylethynyl)-uracil-1-acetic acid, 4-oxybutylamide	N-(4-oxybutyl)acetamide	H	perylen-3-ylethynyl
9b	3-pivaloyloxymethyl-5-(perylen-3-ylethynyl)-uracil-1-acetic acid, 4-oxybutylamide	N-(4-oxybutyl)acetamide	Pom	perylen-3-ylethynyl
10a	5-(perylen-3-ylethynyl)-uracil-1-acetic acid, 3,3-dimethyl-2,4-dioxybutylamide	N-(3,3-dimethyl-2,4-dioxybutyl)acetamide	H	perylen-3-ylethynyl
10b	3-pyvaloyloxymethyl-5-(perylen-3-ylethynyl)-uracil-1-acetic acid, 3,3-dimethyl-2,4-dioxybutylamide	N-(3,3-dimethyl-2,4-dioxybutyl)acetamide	Pom	perylen-3-ylethynyl
11a	5-(perylen-3-ylethynyl)-uracil-1-acetic acid, butylamide	N-butylacetamide	H	perylen-3-ylethynyl
11b	3-pyvaloyloxymethyl-5-(perylen-3-ylethynyl)-uracil-1-acetic acid, butylamide	N-butylacetamide	Pom	perylen-3-ylethynyl

Table 3.2 RAFIs based on cytidine scaffold

	Compound	R1	X
12a	5-(perylen-3-ylethynyl)-2′-deoxycytidine	deoxyribose	perylen-3-ylethynyl
12b	5-(perylen-3-ylmethyloxymethylethynyl)-2′-deoxycytidine	deoxyribose	perylen-3-ylmethyloxymethyl

Table 3.3 RAFIs based on furanosyl scaffold

	Compound	R1	X
13	3-(2-deoxy-β-*D*-ribofuranosyl)-6-(perylen-2-yl)furo[2,3-*d*]-pyrimidin-2(3H)-one.	deoxyribose	perylene-2-yl

	Dimensions							Activities			
		Hydrophobic moiety			Polar moiety			EC_{50}, µM	CC_{50}, µM		TI
	a	*b*	*c*	*d*	*e*	*f*	*g*		cytostatic	cytotoxic	
aUY11	17.2	10.3	7.3	2.6	6.9	9.2	4.6	0.016	> 20	> 20	> 1,250
9b	18.9	10.3	7.3	2.6	8.6	9.2	7.6	0.02	0.82	$2<CC_{50}<6$	41
9a	18.9	10.3	7.3	2.6	8.6	7.3	7.6	0.029	0.82	$2<CC_{50}<6$	39
2a	17.8	10.3	9.5	2.6	6.9	9.2	4.6	0.031	> 20	> 20	> 645
3b	19.3	12.3	7.3	2.6	6.9	8.9	4.6	0.032	> 20	> 20	> 625
dUY11	17.2	10.3	7.3	2.6	6.9	8.9	4.6	0.043	> 20	> 20	> 465
4b	16.2	10.3	7.3	2.6	6.9	10.2	5.9	0.046	> 20	> 20	> 435
3a	19.2	12.3	7.3	2.6	6.9	9.2	4.6	0.049	> 20	> 20	> 408
10b	18.6	10.3	7.3	2.6	8.3	9.2	6.3	0.05	> 20	> 20	> 400
4a	16.2	10.3	7.3	2.6	6.9	8.6	5.6	0.052	> 20	> 20	> 385
10a	18.6	10.3	7.3	2.6	8.3	8.3	7.4	0.06	9.6	> 20	> 160
1a	17.2	10.3	8.3	2.6	6.9	8.9	4.6	0.073	> 20	> 20	> 274
11a	18.6	10.3	7.3	2.6	8.3	8.3	6.8	0.075	1.7	$6<CC_{50}<20$	22.7
8b	17.7	10.3	7.3	2.6	7.4	13	6.3	0.35	> 20	> 20	> 57.1
2b	17.8	10.3	9.5	2.6	6.9	8.9	4.6	0.608	> 20	> 20	> 32.9
6b	17.2	9.2	8.9	2.6	9.9	9.2	4.6	0.89	> 20	> 20	> 22
13	15.5	8.6	8.6	2.6	6.9	8.9	4.6	1.06	> 20	> 20	> 12.6
12a	17.2	10.3	7.3	2.6	6.9	8.9	4.6	1.26	< 0.6	> 20	< 0.48
8a	15.3	10.3	7.3	2.6	5.3	6.9	4.9	1.9	7.5	> 20	4
6a	17.2	9.2	8.9	2.6	9.9	8.9	4.6	2.3	> 20	> 20	> 8.7
7b	14.5	7.3	7.3	2.6	9.9	9.2	4.6	4.38	> 20	> 20	> 4.6
1b	17.2	10.3	8.3	2.6	6.9	8.9	4.6	5.95	> 20	> 20	> 3.4
11b	18.6	10.3	7.3	2.6	8.3	8.9	6.8	9.38	< 0.6	> 20	< 0.06
7a	14.5	7.3	7.3	2.6	9.9	8.9	4.6	12.4	> 20	> 20	> 1.6
12b	17.8	7.9	7.3	2.6	8.6	8.9	4.6	> 20	> 20	> 20	≤ 1
5b	13.9	5.3	5.9	2.6	9.9	9.2	4.6	> 20	> 20	> 20	≤ 1
5a	13.9	5.3	5.9	2.6	9.9	8.9	4.6	> 20	> 20	> 20	≤ 1

Table 3.4 RAFIs ranked by antiviral activity

Yellow, equal to the dimension of aUY11 (*a,* 17.2 Å; *b,* 10.3 Å; c, 7.3 Å; *d*, 2.6 Å; *e*, 6.9 Å; *f*, 9.2 Å; or *g*, 4.6 Å); green, larger than the dimension of aUY11 (yellow green [*a*, 17.7-17.8 Å; *c*, 8.3 Å; or *d*, 8.3-8.6 Å]; light green [*a*, 18.6 Å; *c*, 8.3-8.6 Å; or *g,* 5.9-6.2 Å]; darkest green [*a*, >18.9 Å; *b*, >10.9 Å; *c*, >8.9 Å; *e,* >9.9 Å; or *g*, >6.8 Å]; red, smaller than the dimension of aUY11: light pink [*a*, 16.2 Å; *b*, 9.2 Å; or *f*, 8.3 Å]; dark pink [*a*, 15.3 Å; *b*, 8.6 Å; *f*, 8.6 Å; *e,* 9.9 Å; or *g*, 6.8 Å]; darkest red [*a*, <14.5 Å; *b*, <7.3 Å; *c*, <5.9 Å; *e,* <5.3 Å; or *g*, <7.3 Å]. EC_{50} < 100 nM (green), 100 nM < EC_{50} < 500 nM (yellow); 500 nM ≤ EC_{50} < 1 μM (light pink); 500 nM ≤ EC_{50} < 1.5 μM (dark pink); or ≤ 1.5 μM (red); CC_{50} > 20 μM (green), 20 < CC_{50} < 6 μM (yellow), 6 < CC_{50} < 2 μM (light pink), 2 < CC_{50} < 0.6 μM (dark pink), or < 0.6 μM (red); selective indexes (SI) > 600 (green), 200 ≤ SI < 600 (light green), 100 ≤ SI < 200 (yellow green); 30 ≤ SI < 100 (yellow); 10 ≤ SI < 30 (light pink); 4 ≤ SI < 10 (dark pink); or SI ≤ 4 (red).

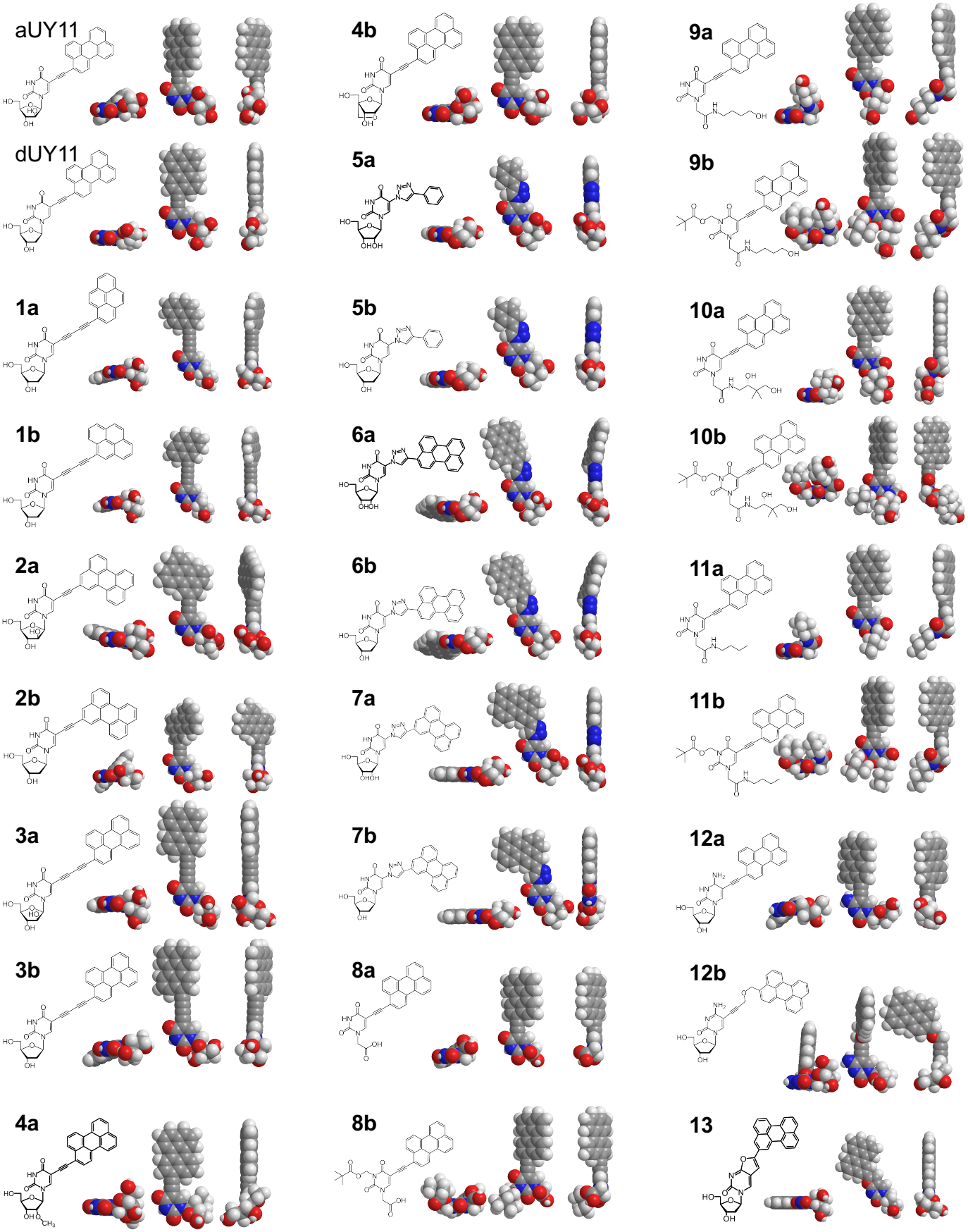
aUY11
dUY11
1a
1b
2a
2b
3a
3b
4a
4b
5a
5b
6a
6b
7a
7b
8a
8b
9a
9b
10a
10b
11a
11b
12a
12b
13

Figure 3.1 Chemical and space filling structures

Chemical and space filling structures of aUY11, dUY11 and twenty-five new RAFIs in three orthogonal orientations. Gray, carbon; red, oxygen; blue, nitrogen; white, hydrogen.

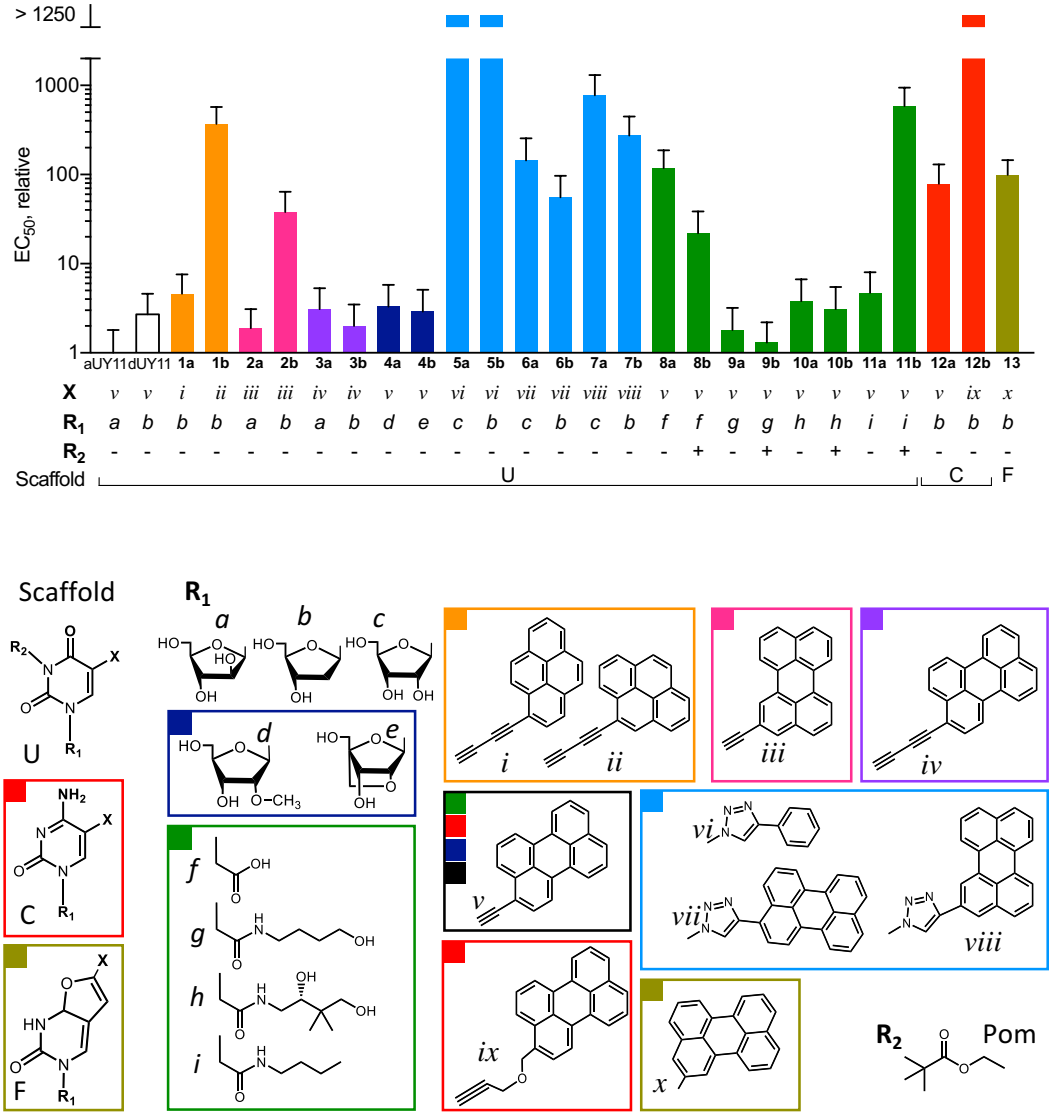

Figure 3.2 Most of the RAFI moieties can be replaced with chemically distinct ones

Bar graphs presenting EC_{50} of test compound relative to that of aUY11. Average ± 95% confidence interval (n = 3). Colors of the bars correspond the colors of the modifications shown below.

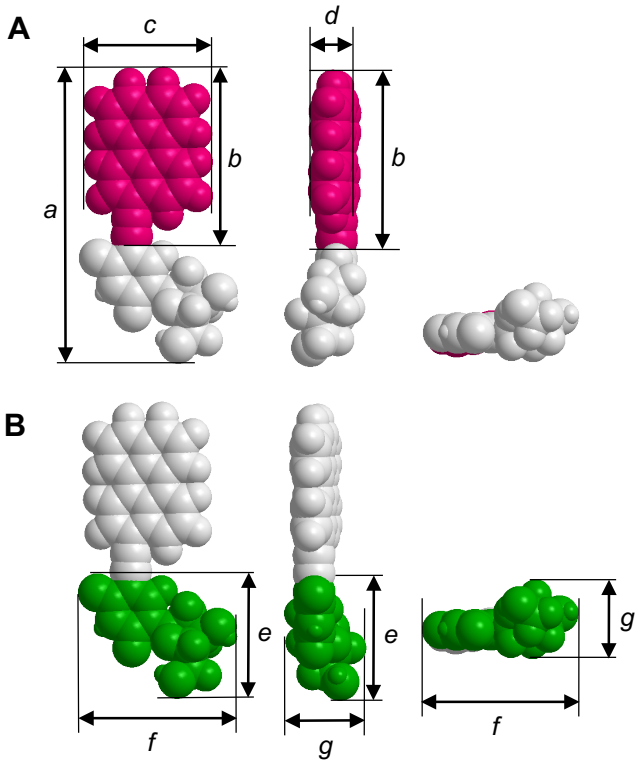

Figure 3.3 Dimensions of the hydrophobic and polar moieties

Space filling structure of the RAFI aUY11 in three orthogonal perspectives, indicating dimensions of the hydrophobic (**A**, pink) or polar (**B**, green) moiety. The cross sections of the polar moiety (dimensions *f* and *g*) are larger than those of the hydrophobic moieties (dimensions *c* and *d*), giving the inverted cone shape.

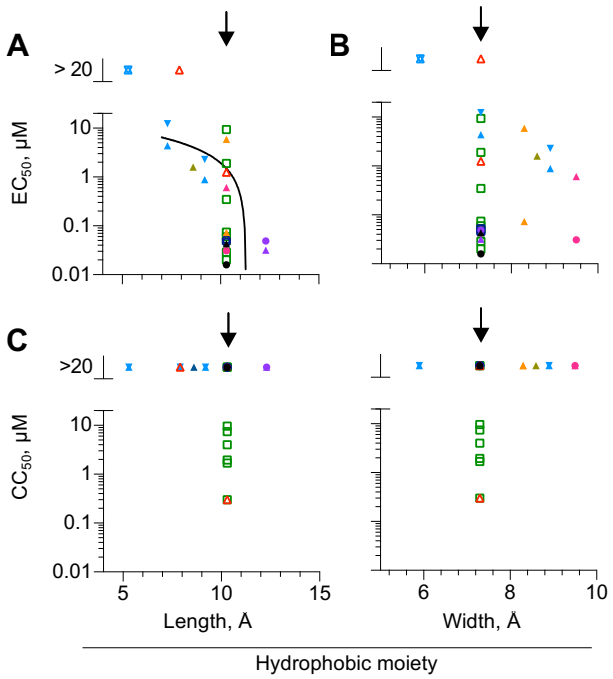

Figure 3.4 Antiviral activities depend on the length of the hydrophobic moiety

The antiviral (**A**, **B**) and cytostatic (**C**, **D**) activities of the RAFIs with modifications in the hydrophobic (filled) and polar (open) moieties plotted against the length (**A** and **C**) or width (**B** and **D**) of the hydrophobic moiety. Colors moieties as in **Figure 2**; circles, arabino; triangles, deoxyribose; squares, other. Arrow, RAFIs with the same hydrophobic moiety as that of aUY11. The antiviral activities of the 10 active compounds with distinct hydrophobic moieties correlate to the length of the hydrophobic moiety (Pearson r -0.678, p 0.011).

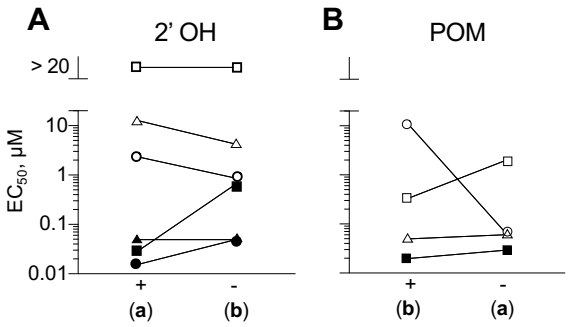

Figure 3.5 Antiviral activities were independent of two functional groups

A. Antiviral activities of RAFIs with **(a)** or without **(b)** 2' hydroxyl group for compounds with hydrophobic moieties *i* (aUY11 and dUY11, open circles), *iii* (**2**, open triangles), *vi* (**5**, open squares), *vii* (**6**, closed circles), or *viii* (**7**, closed squares). 2' hydroxyl did not affect antiviral activity (paired t-test p 0.98).

B. Antiviral activities of RAFIs with (**a**) or without (**b**) the pivaloyloxymethyl group for compounds with polar moieties *f* (**8**, open squares), *g* (**9**, open triangles), *h* (**10**, closed squares), or *h* (**11**, open circles). The pivaloyloxymethyl did not affect antiviral activity (paired t-test p 0.68).

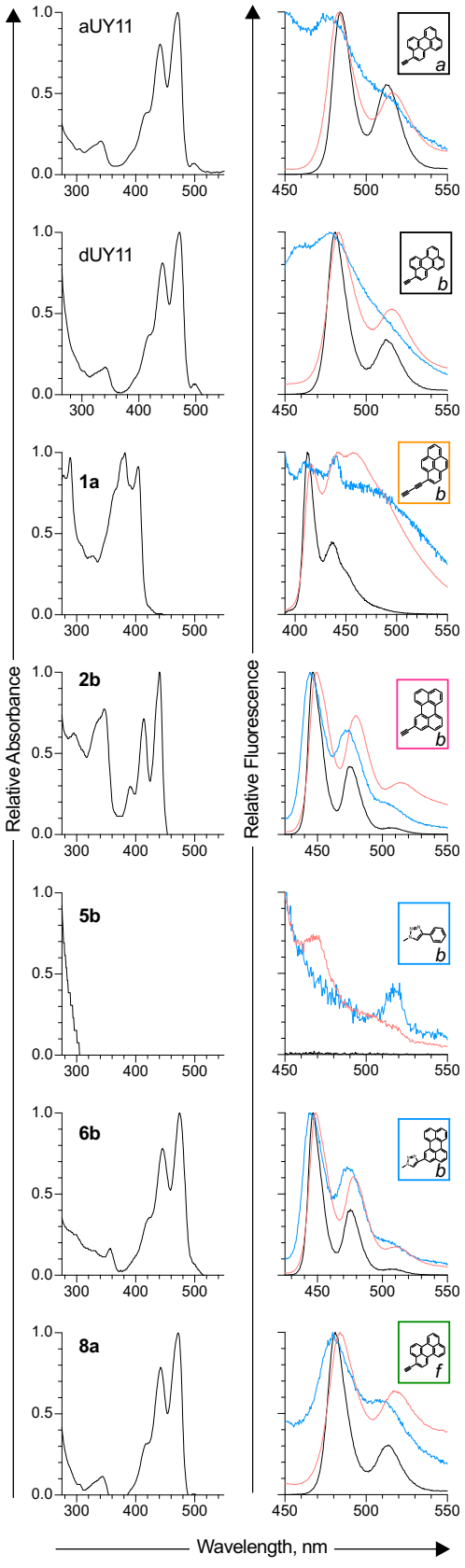
aUY11
dUY11
1a
2b
5b
6b
8a
a
b
b
b
b
b
f
Relative Absorbance
Relative Fluorescence
Wavelength, nm
1.0
0.5
0.0
300
400
500
450
500
550

Figure 3.6 RAFIs with distinct hydrophobic and polar moieties intercalate into lipid bilayers

Left: Absorbance spectra of aUY11, or representative RAFIs with pyrenebutadiynyl (**1a**), polar linker (**6b**), or small polar (**8a**) or hydrophobic (**5b**) moieties. Insets: structure of the hydrophobic moieties: arabinose (*a*), deoxyribose (*b*), or acetyl (*f*) polar moieties.

Right: Emission spectra of aUY11, or representative RAFIs in aqueous (blue) or non-polar environments (octanol, black), or in aqueous environments containing liposomes (orange). The spectra of dUY11, **6b**, and **8a** is similar in aqueous environments containing liposomes or in hydrophobic environments, indicating that they intercalate into the hydrophobic environment of the lipid bilayers. The spectrum of **5b** is more similar in liposomes or aqueous buffer than in hydrophobic environments (black on the x-axis), indicating that it does not intercalate into lipid bilayers.

Absorbance and emission spectra of all compounds are shown in **Appendix 3**.

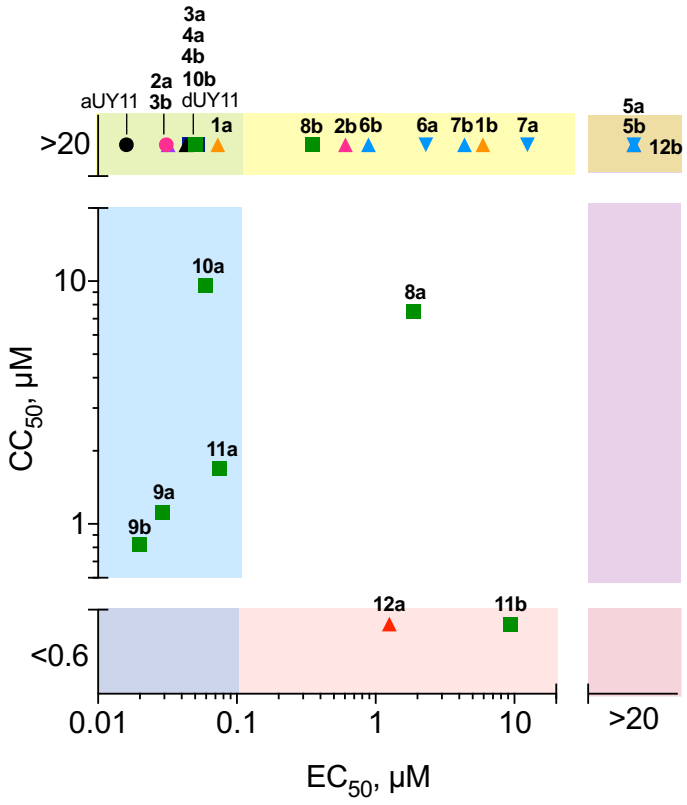

Figure 3.7 Antiviral and cytostatic activities are independent

CC_{50} plotted against EC_{50} on logarithmic scale. There is no correlation between the antiviral and cellular activities of the five compounds with $EC_{50} < 20\ \mu M$ and $0.6\ \mu M < CC_{50} < 20\ \mu M$ (Spearman coefficient, 0.54; p 0.30). Colors moieties as in **Figure 3.2**; circles, arabino; triangles, deoxyribose; squares, other.

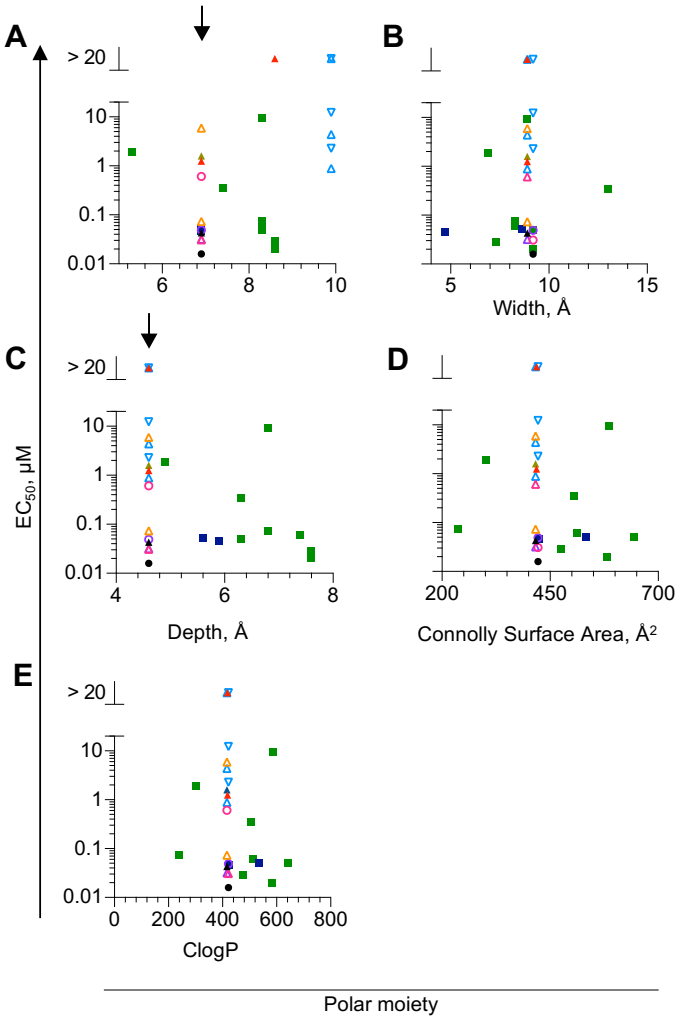

Figure 3.8 Dimensions of the polar moiety did not correlate with activity

The activities of RAFIs are plotted against the dimensions (A-C), surface area (D), or partition coefficient (ClogP; E) of the polar moiety. Antiviral activities do not correlate with the dimensions or polarity of the polar moiety (Pearson's r 0.54, length [dimension *e*]; 0.18, width [dimension *f*]; 0.07, depth [dimension *g*]; 0.24, Connolly surface area; or 0.59, ClogP).

CHAPTER 4: DISCUSSION

Antivirals that act on lipids to target viral fusion have the potential to have broad-spectrum antiviral activities with a high barrier to selection for resistance. However, only one clinical antiviral may target viral lipids, docosanol. Several approaches to target viral lipids have already been proposed. Antiviral compounds that appear to induce peroxidative damage to viral phospholipids such as LJ001 and hypericin have broad spectrum activity against otherwise unrelated envelope viruses (Prince et al., 2000; Wolf et al., 2010). Modulators of membrane fluidity also have broad spectrum antiviral activities. Curcumin, a non-steroidal diarylheptanoid found in turmeric, for example, intercalates in the lipid envelopes of HCV virions decreasing fluidity, and resulting in deficiency in binding and fusion (EC_{50} 8.46 μM) (Anggakusuma et al., 2013). Glycyrrhizin, a compound from licorice root, which also decreases the fluidity of lipid bilayers (Harada, 2005), is active at high micromolar concentrations against several unrelated enveloped viruses, including HIV, IAV, VSV (Harada, 2005), and SARS (Cinatl et al., 2003). The mechanism of action of the possibly lipid-targeting docosanol (Abreva), a 22-C saturated alcohol approved for the treatment of HSV-1 infections (Sacks et al., 2001), remains unclear (Spruance, 2002).

The RAFIs inhibit the infectivity of otherwise unrelated envelope viruses. They increase the energy required for membranes to adopt negative curvatures and directly inhibit virion-to-cell-fusion (Colpitts et al., 2013; St Vincent et al., 2010). Whereas cells also depend on fusions through the hemifusion stalk, the RAFIs are not overtly cytotoxic and have no apparent effects on intracellular fusions or mitosis (Colpitts et al., 2013; St Vincent et al., 2010).

We propose that the RAFIs act by a mechanism that depends on their inverted cone physical molecular shape. If this model is correct, then the activity would not depend on the presence of specific chemical groups. In an alternative model, the perylene moiety of the RAFIs may induce lipid peroxidation upon excitation by visible light, thus decreasing the fluidity of viral envelopes, in turn resulting in impaired fusion (Vigant et al., 2014).

In this thesis, I describe the evaluation of twenty-five chemically distinct compounds with overall similar shapes and physical characteristics to the lead RAFIs aUY11 and dUY11. While this SAR study identified the critical requirements for activity and cytotoxicity, it also indirectly tested the hypothesis that the RAFIs increase the activation energy by biophysical, rather than by biochemical, mechanisms. The activity of the RAFI was found to be independent of most chemical moieties, the perylene moiety in particular, but to correlate with the biophysical characteristics in the moieties. In contrast, cytotoxicity was found to be determined by the chemical groups in the polar moiety. Activity and cytotoxicity were thus found to be independent of each other.

My hypothesis was that the RAFIs increase the activation energy required for fusion by mechanisms depending on their inverted cone physical molecular shape, rigidity and amphipathicity. If the mechanism of the RAFIs depends on these physical characteristics, then other, chemically distinct compounds with similar biophysical characteristics would be expected to have similar activities as aUY11 or dUY11.

Consistently with the inverted cone shape model, I found that the RAFIs act independently of most chemical moieties, including the perylene, ethynyl, and arabinose moieties. Nonetheless, the carbonyl group on the 3-position of the uracil base could not be replaced by an amine. Carbonyl groups have δ^- polarity and accepts two hydrogen bonds, whereas amine groups have δ^-

polarity and donate two hydrogen bonds. Negative polarity or the ability to accept hydrogen bonds may thus be requirements for the mechanism of action of the RAFIs. Activity was found to depend on the length of the hydrophobic moiety. It was already known that RAFIs with a smaller ethynyl pyrene moiety (6.1 Å long) had lower potency than aUY11 (EC_{50}, 51 μM [dUY2]; 40 μM [dUY3] (Orlov et al., 2016; St Vincent et al., 2010). I now show that activity was recovered by extension of the linker, increasing the total length of the hydrophobic moiety to 10.3 Å (EC_{50} 73 nM, **1a**). Intercalation of the hydrophobic moiety of the RAFIs to a depth of ~10 Å may thus be required for their mechanism of action. Ten Angstroms would position the rigid poly aryl group approximately two thirds into the hydrophobic core of the bilayer leaflet.

Inverted cone shape phospholipids with longer hydrophobic acyl chains inhibit virus-to-cell fusion with lower potencies than those with shorter chains (Chernomordik et al., 1995b, 1997; Szule et al., 2002). For example, palmitoyl LPC (16:0), the acyl chains of which extend to approximately 20 Å into the lipid bilayer (Binder and Gawrisch, 2001), is more active than stearoyl LPC (18:0), which reaches deeper in the bilayer (22 Å) (Binder and Gawrisch, 2001). Shorter hydrophobic moieties give such phospholipids a more pronounced inverted cone shape (Chernomordik et al., 1995b, 1997; Szule et al., 2002). The RAFIs described here have even shorter hydrophobic moieties. The optimal length of their hydrophobic moieties is at least 10.3 Å, and activity does not decrease much with hydrophobic moieties of up to 12.3 Å long, still much shorter than that of palmytoyl LPC. It would be interesting to test in the future longer hydrophobic moieties, such as compounds with ethynylpentacene (13.1 Å, **Figure 4.2**) hydrophobic moieties.

The dimensions of the polar moieties of the compounds described in this study are within the range of the dimensions of the polar head groups and backbones of common phospho- or sphingolipids (**Table 4.1**, **Figure 4.1**).

Lipid bilayers adopt spontaneous curvatures according to the relative geometries of the polar head groups and hydrophobic acyl chains. Any bending away from this spontaneous curvature could result in disruption of the polar-hydrophobic interface, which is opposed by the hydrophobic effect (Helfrich, 1973). When lipid leaflets deviate from the spontaneous curvature, the radius of the acyl chains changes. To accommodate these differences in acyl chain radius, lipid acyl chains splay (the two acyl chains of one lipid move away or towards each other) or tilt (acyl chains bent away from the plane of the lipid leaflet) (Chernomordik and Kozlov, 2003; Cohen and Melikyan, 2004). The requirement for rigid hydrophobic moieties of 10 Å long (and 7.3 Å wide) of the RAFIs may suggest an additional role to the inverted cone shape requirement, in which the RAFIs act by posing a physical barrier to the acyl chain splay or tilt needed in the negative curvatures.

Although compounds with hydrophobic moieties shorter than 10.3 Å have decreased potency, they still intercalate in lipid bilayers, (9.2 Å, EC_{50} 2.3 μM [**6a**], 0.89 μM [**6b**]; 7.3 Å: 12.4 μM [**7a**], 4.38 μM [**7b**]; 8.6 Å: 1.06 μM [**13**]). These compounds may partition in lipid bilayers less than compounds with longer hydrophobic moiety, resulting in lower membrane concentrations. Alternatively, length of the hydrophobic moiety could be required for the mechanism of action, as would be expected under the inverted cone shape model.

4.1.1 Requirement of rigidity and conjugation

The activity of the RAFIs depends on the rigidity of their hydrophobic moieties, as shown in previous SAR studies (St Vincent et al., 2010) (**Figure 1.3**). Rigidity in the arabinose moiety did

not increase activity, but it remains unclear if rigidity of the aromatic base is required for activity. To test any requirement for rigidity in the base, RAFIs with flexible polar scaffolds would be evaluated, such as cyclic diazine, or pyrroles, or non-cyclic amide moieties could be synthesized and tested (**Figure 4.2**).

The base scaffold, ethynyl linker, and perylene moiety are part of a conjugated system, which contributes to the rigidity of these moieties. Conjugation may thus also be required. Most compounds in this study, including those with triazole linkers (**5a**-**7b**), have hydrophobic moieties conjugated with the scaffold base. **12b**, which has an oxygen in the linker, breaking the conjugation, is not active, but neither does it intercalate into the lipid bilayers. Further SAR studies should thus test the relative contributions of rigidity and conjugation. For example, RAFIs with rigid, non-aromatic steroid scaffolds such as cholane replacing the ethynyl perylene hydrophobic moiety (**Figure 4.2**), would test the relative contributions of rigidity and conjugation. Similar RAFIs with cholesterol hydrophobic moieties have been tested (dUY1, dUY9, **Figure 1.3**) (St Vincent et al., 2010), but these compounds had polar carbonyl groups in the hydrophobic moiety, however, which not surprisingly, led to lower potency (EC_{50} 60 μM, aUY1; >200 μM, dUY1).

4.1.2 Bilayer intercalation

Intercalation in the lipid bilayer was required for activity. Compounds that did not intercalate in lipid bilayers, had no antiviral, cytostatic or cytotoxic activities (**5a**, **5b**, and **12b**). **12a** intercalates in lipid bilayers and is cytostatic but only weakly antiviral, indicating that bilayer intercalation not sufficient. Polar additions to the hydrophobic moiety of **12a**, resulting in decreased amphipathicity and lower affinity with lipid bilayers, decreased cytostatic and

disrupted antiviral activities (**12b**, **Figure 3.1**). Lipid bilayer intercalation is thus also required for cytotoxicity.

Bilayer intercalation was not sufficient for activity, however. **1b**, **2b**, **8b**, **11b** and **13** intercalated in bilayers, but had >100-fold lower potency compared to aUY11. The pyrene-containing compounds **1a** and **1b** are very similar in structure and dimensions (**Figure 3.1**, **Table 3.4**), although their emission spectra differ. **1b** has two distinct emission peaks in hydrophobic environments, characteristic of pyrene moieties, which were not observed for **1a**. Similarly, **2b** (deoxyribose; EC_{50} 0.608 μM) has lower potency compared to its counterpart **2a** (arabinose; EC_{50} 0.031 μM). Whereas these compounds are highly similar in structure and dimensions, their absorbance spectra differ. **2b** is blue-shifted compared to **2a** and does not absorb light at wavelengths > 450 nm, whereas **2a** does. This spectral shift was not observed for other deoxyribose/arabinose counterparts **3a**/**3b**, or for deoxyribose/ribose counterparts **6a**/**6b** or **7a**/**7b**. The peaks observed in the spectrum of **2b** are instead more similar to those of **12b** and **13**, both of which have polar oxygen atoms in the linker region.

4.1.3 Specificity for virus-to-cell fusion

Whereas viral and cellular fusions proceed through similar lipid rearrangements, the favorable therapeutic indexes of the RAFIs indicate that viral fusion can be targeted in a manner that is specific for virus-to-cell fusion. Cells tolerate RAFIs with different hydrophobic moieties, including 2-ethynylperylene, 3-butadiynylperylene, butadynylpyrene and triazole perylene moieties. In contrast, chemical modifications to the polar moiety were less well tolerated. For example, RAFIs that had butylamide groups replacing the arabino moiety all reached $CC_{50} < 20$ μM. A compound with a cytidine replacing the uracil moiety was also cytostatic (**Table 3.4, Appendix 2**).

If the RAFIs inhibited virus-to-cell and cellular fusions by the same mechanism, then the antiviral and cytostatic activities would be correlated. However, there was no correlation between antiviral and cytostatic activities between the six compounds with EC_{50} < 20 μM and 0.6 < CC_{50} < 20 μM (Spearman coefficient, 0.54; p 0.30, **Figure 3.7**). Compounds with EC_{50} from 30 nM to > 20 μM are equally non-cytostatic, whereas cytostatic compounds have EC_{50} > 1 μM.

The mechanisms for specificity for virus-to-cell fusion but not for cellular fusions is not yet fully understood, but two models have been proposed. In one, specificity is determined by the differences in energy availability, vesicle diameter, or lipid composition between viruses and cells, as described in **section 1.4.7** (Colpitts and Schang, 2014; St Vincent et al., 2010). In the other, it is determined by the capacity of cells to repair damaged membranes, another energy-consuming process that extracellular virions cannot perform (Vigant et al., 2013).

Viral and cellular fusions differ in various ways. The energy for cellular fusion comes from metabolism. SNAREs store energy from ATP to bring the fusing membranes in close proximity and to destabilize them (Bombardier and Munson, 2015; McMahon et al., 2010). Cells also have the ability to actively regulate and remodel membrane curvatures (Salzer et al., 2017). The composition of the outer and inner leaflets of cellular membranes are tightly regulated by ATP-driven lipases and flippases (Montigny et al., 2016). The prevalence of non-cylindrical, curvature altering lipids are typically low in membranes, but is upregulated upon lipase stimulation (Ivanova et al., 2001). Lysolipids have been found to be upregulated in cells with significant exocytotic fusion events (Blaschko et al., 1967). SNAREs may actively recruit fusogenic lipids to the fusion sites (Fratti et al., 2004; Wickner et al., 2017). Cells also use proteins to actively modulate membrane curvatures. Some proteins stabilize curved membrane structures by the

insertion of amphipathic domains in one leaflet of the bilayer (*e.g.* COPII), or by interacting with membrane with curved protein surfaces (*e.g.* BAR-domains). Clathrin cages modulate the curvature of cellular membranes by binding to membrane lipids (Zimmerberg and Kozlov, 2006). In contrast, viruses are metabolically inert. The energy available for viral fusion is released solely by attachment, binding and rearrangement of their glycoproteins (Chernomordik et al., 1998; Epand, 2003; Harrison, 2008; Mittal et al., 2003; White and Whittaker, 2016; Zaitseva et al., 2005), and they cannot actively remodel membrane curvatures.

The lipid rearrangements during viral and cellular fusions are similar and both are inhibited by inverted cone shape lipids. While the fusion proteins are different, as described above and in **section 1.4.1,** they have functional and structural similarities. Like class I viral fusion proteins, SNAREs bring membranes in close contact through the formation of coiled coils (Wesolowski and Paumet, 2010). The SNARE TMDs also contribute to membrane destabilization, similarly to the TMDs and fusion peptides of viral fusion peptides. Class II viral fusion proteins are structural and functional homologs to the *C. elegans* fusion protein EEF-1, which is involved in embryonic development (Pérez-Vargas et al., 2014). It is therefore surprising to find a small molecule that inhibits virus-to-cell fusion with such discrimination against cellular fusions. The RAFIs could be used as small molecule probes to study the critical difference between virion-to-cell and cellular fusion, and in the process finding the mechanisms for the unexpected specificity.

4.1.4 Lipid peroxidation model

An alternative model for the mechanism of action of the RAFIs has also been proposed, in which the RAFIs insert in the viral envelopes where they produce light-induced peroxidative damage, resulting in virions that cannot fuse with cellular membranes (Vigant et al., 2014). In this model absorption of visible light and the perylene moiety are required (Orlov et al., 2016; Vigant et al.,

2013, 2014). The RAFIs would then damage lipids upon excitation by visible light, decreasing the fluidity of viral envelopes, thus resulting in impaired fusion (Vigant et al., 2013, 2014). The RAFIs do not overtly decrease membrane fluidity, however (Colpitts et al., 2013), and typically neither do phospholipids (Jurkiewicz et al., 2012; Megli et al., 2009; Van der Paal et al., 2016).

Other antiviral compounds that damage virion envelopes upon exposure to light have been identified. For example, LJ001, a rhodamine derivative, inserts in lipid bilayers where it produces singlet oxygen species that peroxidize unsaturated fatty acid chains in the envelope when exposed to light (Vigant et al., 2013; Wolf et al., 2010). Hypericin also produces singlet oxygen (type II) and superoxide anion (type I) when exposed to light and has light-dependent broad-spectrum activity against fusion of VSV, IAV, HIV, and Sendai virus, among others (Lenard et al., 1993). Other such molecules are the porphyrins, which disrupt virion structure through the generation of singlet oxygen (Guo et al., 2011). Porphoryns were are active against HBV, HCV, and HIV, among others (Guo et al., 2011).

The activity of antiviral molecules proposed to act by peroxidative mechanisms increases when their absorption shifts into the visible light (Vigant et al., 2015). Previous analysis of the absorption spectra of four RAFIs led to the conclusion that absorption at visible spectra was required for antiviral activity (Orlov et al., 2016). In that study, a RAFI with an ethynylpyrene moiety which absorbed mostly in the UV spectrum and little at wavelengths > 400 nm, had reduced activity (EC_{50}, 980 nM [dUY2] (Orlov et al., 2016)). I now reach the conclusion that neither light absorption at visible spectra nor the perylene moiety are required. **1a**, which lacks the perylene moiety and absorbs little light at > 425 nm, retains good potency (EC_{50}, 73 nM [**1a**], **Figure 3.6**).

4.2 Future directions

4.2.1 Explore the requirement for inverted cone shape

The current study evaluates the antiviral activities of chemically distinct compounds but with overall similar physical features (i.e. inverted-cone shape, rigidity and amphipathicity) as aUY11 or dUY11. Consequently, all RAFIs in this study are inverted-cone shaped. To test the requirement for inverted cone shapes, future SAR studies may include compounds that have either cylindrical or conical shapes. Under my hypothesis, such RAFIs would not be expected to have antiviral activity. For example, compounds without arabinose moieties, have cylindrical geometries. If the inverted cone molecular geometry is required for antiviral activity, cylindrical compounds would not be expected to be active. Alternatively, if cylindrical compounds are found to be active, then the intercalation of a rigid, planar hydrophobic moiety may be required, either to generate lipid peroxidation (as proposed by Vigant, *et al.,* 2013), or to restrict acyl chain rearrangements (as discussed in **section 4.1.2**)

Under the inverted cone shape model, RAFIs that have more pronounced inverted cone shapes than that of aUY11, such as compounds with hydrophobic moieties of smaller cross sections than that of perylene would be expected to have higher potencies than aUY11. For example, anthracenes (length hydrophobic moiety, 11.1 Å), tetracenes (12.1 Å), or pentacenes (13.1 Å) instead of perylene could be synthesized and tested (**Figure 4.2**). While SAR studies of RAFIs with these moieties can help determine the physical and chemical requirements of the RAFIs, these moieties are not suitable in antivirals, as these moieties are carcinogenic.

Inhibition of fusion by inverted cone shaped lipids is reversed by the addition of cone shaped lipids (Chernomordik et al., 1995b; Pécheur, 2007). If the inverted cone shape of the

RAFIs is required for activity, then co-treatment of the RAFIs with amphipathic molecules of cone shaped molecular geometries would be expected to reverse inhibition. To test this model, cone shaped lipids such as oleic acid at concentrations below toxic concentrations could be mixed with RAFI treatments in lipid mixing fusion assays, as described previously (Colpitts et al., 2013).

4.2.2 Further SAR studies to test the base scaffold

The SAR studies described in this thesis indicate that most of the chemical moieties of the RAFIs are not essential. The nucleobase scaffold could not be replaced, however. Various factors may contribute to the requirement of this moiety, such as the chemical composition, polarity, or geometry. Further SAR studies are required to evaluate each of these properties.

One compound with a cytosine moiety replacing the uracil moiety had lower potency than aUY11. Cytosine differs from uracil in that it has an amine group instead of the carbonyl uracil group, which alters the polarity from ∂^- to ∂^+. Future directions may include testing whether the carbonyl group on the 3-position of the uracil moiety is required or whether it can be replaced by other groups with similar polarity, such as alcohols or fluoride atoms (**Figure 4.2**). Other chemical modifications could include small non-polar additions (*e.g.* methyl groups, **Figure 4.2**), which were tolerated in the arabino moiety.

4.2.3 Explore the lipid peroxidation model

If the RAFIs acted by a photochemically activated mechanism, then they would not be active when not exposed to light. Infectivity assays without any light exposure during or after RAFI treatment are currently underway in our lab. Moreover, under the photochemical activation model, lipid peroxidation would depend on the presence of unsaturated lipids. The RAFIs would

thus not inhibit fusion between liposomes composed of exclusively saturated lipids. This model can be tested in *in vitro* lipid mixing assays between liposomes composed of saturated lipids, such as dipalmitoylphosphatidylcholine (DPPC). A similar assay, using unsaturated DOPC liposomes fusing to each other, has already been established in our lab (Colpitts et al., 2013).

The mechanism of specificity of lipid peroxidants for viruses over cells is not known, or even whether viruses are more sensitive to such antivirals than cells. Experiments that test the relative sensitivities of viruses and cells to lipid peroxidation by radical peroxyl generators AMVN and AAPH inactivates virions are currently underway in our lab.

4.3 Conclusion

Although lipid bilayer fusion is required for entry of all enveloped viruses, it is also required for various cellular processes. It is generally accepted that virus-to-cell fusion and cellular lipid bilayer fusion proceed through the same hemifusion state by the same core biophysical principles.

Using a structure-activity relationship approach, I show in this thesis that chemically distinct compounds that are amphipathic, rigid, and have inverted cone-shapes have similar potencies against the infectivity of one enveloped virus, HSV-1. The mechanism of action of the RAFIs is therefore more consistent with biophysical rather than biochemical properties determining their antiviral activities.

I identified the properties of the RAFIs required for antiviral activity and cytotoxicity, including amphipathicity, chemical groups and sizes of the hydrophobic and polar moieties. The perylene group or absorbance in the visible spectra are not required or sufficient. The favorable

therapeutic indexes of these compounds indicate that lipid bilayer fusions can be targeted in a manner that is specific for virus-to-cell fusions. The distinction between antiviral and cytostatic activities of the RAFIs opens the possibility to the rational design of therapeutics that specifically inhibit virus-to-cell fusions.

	Length, Å	Width, Å	Depth, Å	Connolly accessible surface area, Å^2
Arabinose-uracil	6.9	9.2	4.6	421
Sphingomyelin	9.2	8.6	4.8	552
Phosphatidic serine	7.2	10.7	2.6	513
Phosphatidic choline	6.6	9.8	4.8	453
Phosphatidic ethanolamine	7.4	10.1	5.5	416

Table 4.1 Dimensions and Connolly surface area of arabinose-uracil or the polar portions (head groups and backbones) of common membrane lipids

Colors dimensions; same as in **Table 3.4**.

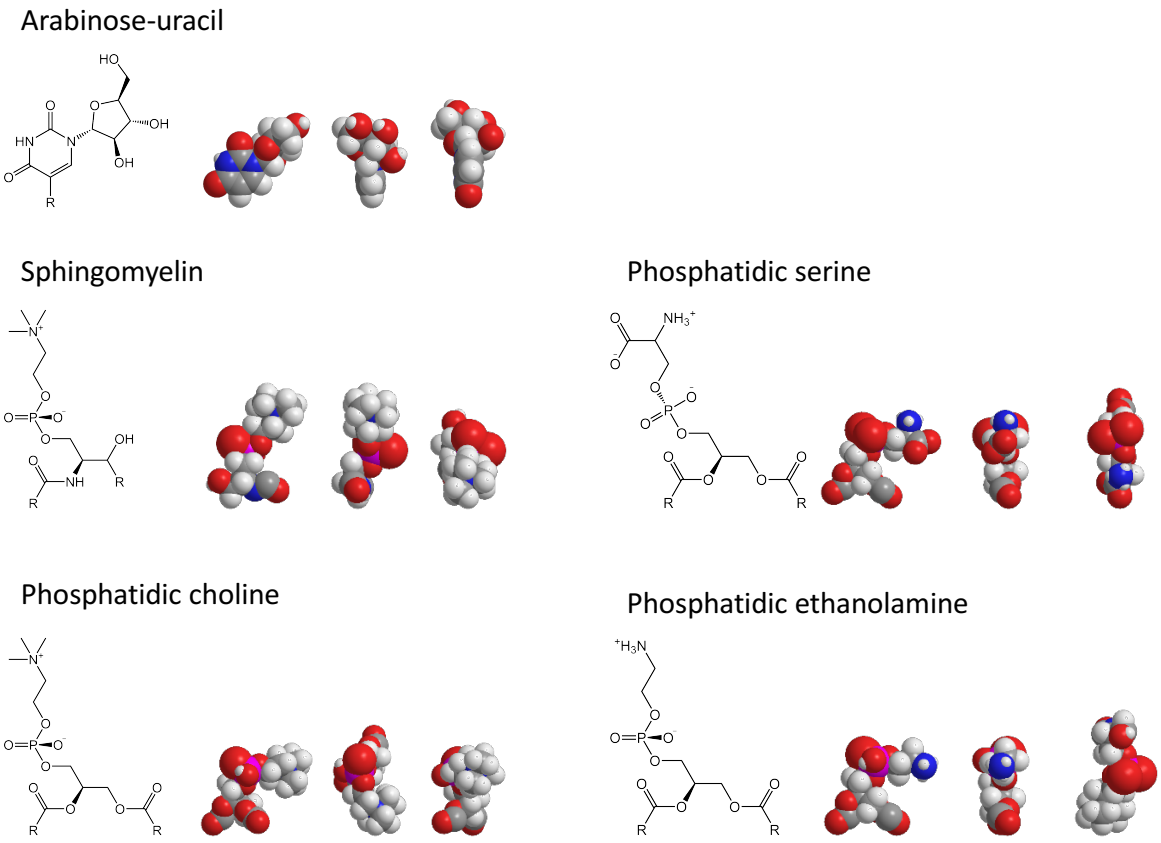

Figure 4.1 Polar moieties of common membrane lipids and aUY11

Chemical and space filling structures of the aUY11 polar moieties arabinose-uracil or the polar lipid head group and backbone in three orthogonal orientations. Gray, carbon; red, oxygen; blue, nitrogen; pink, phosphorus; white, hydrogen.

Compounds with modifications to the base scaffold

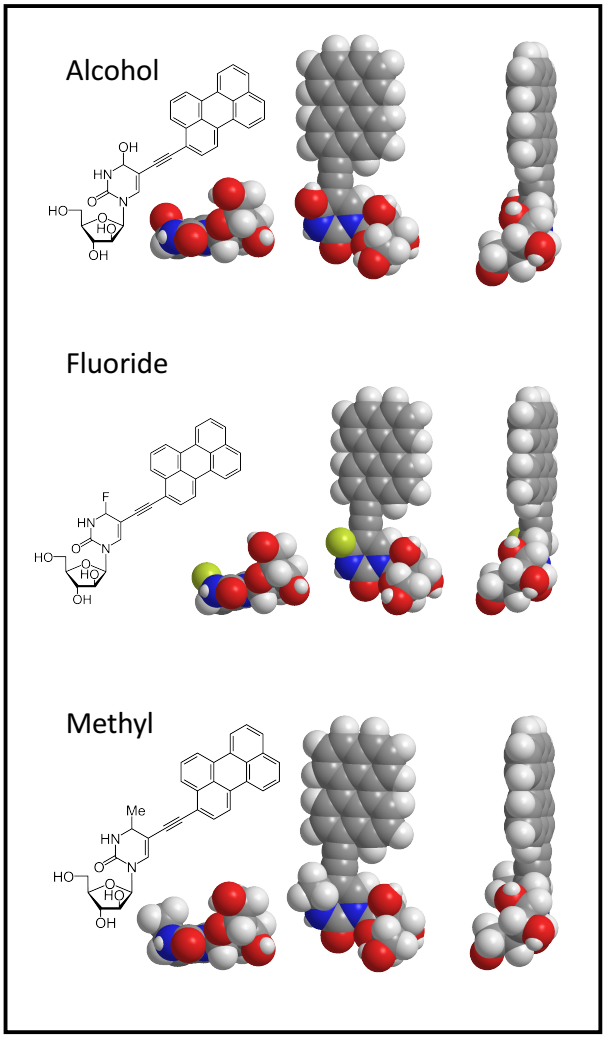

Compounds with modifications to the base scaffold

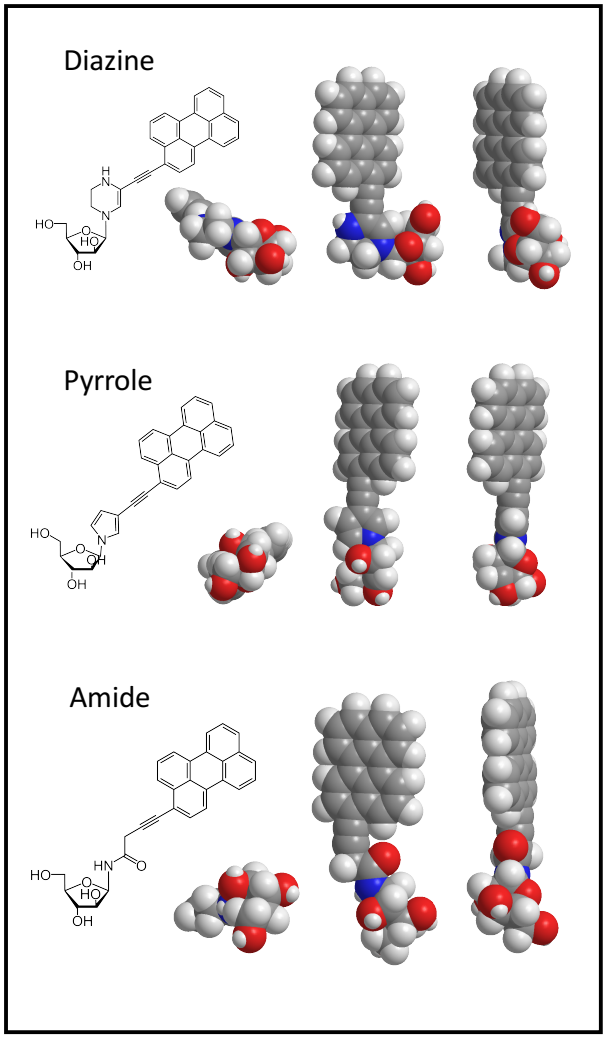

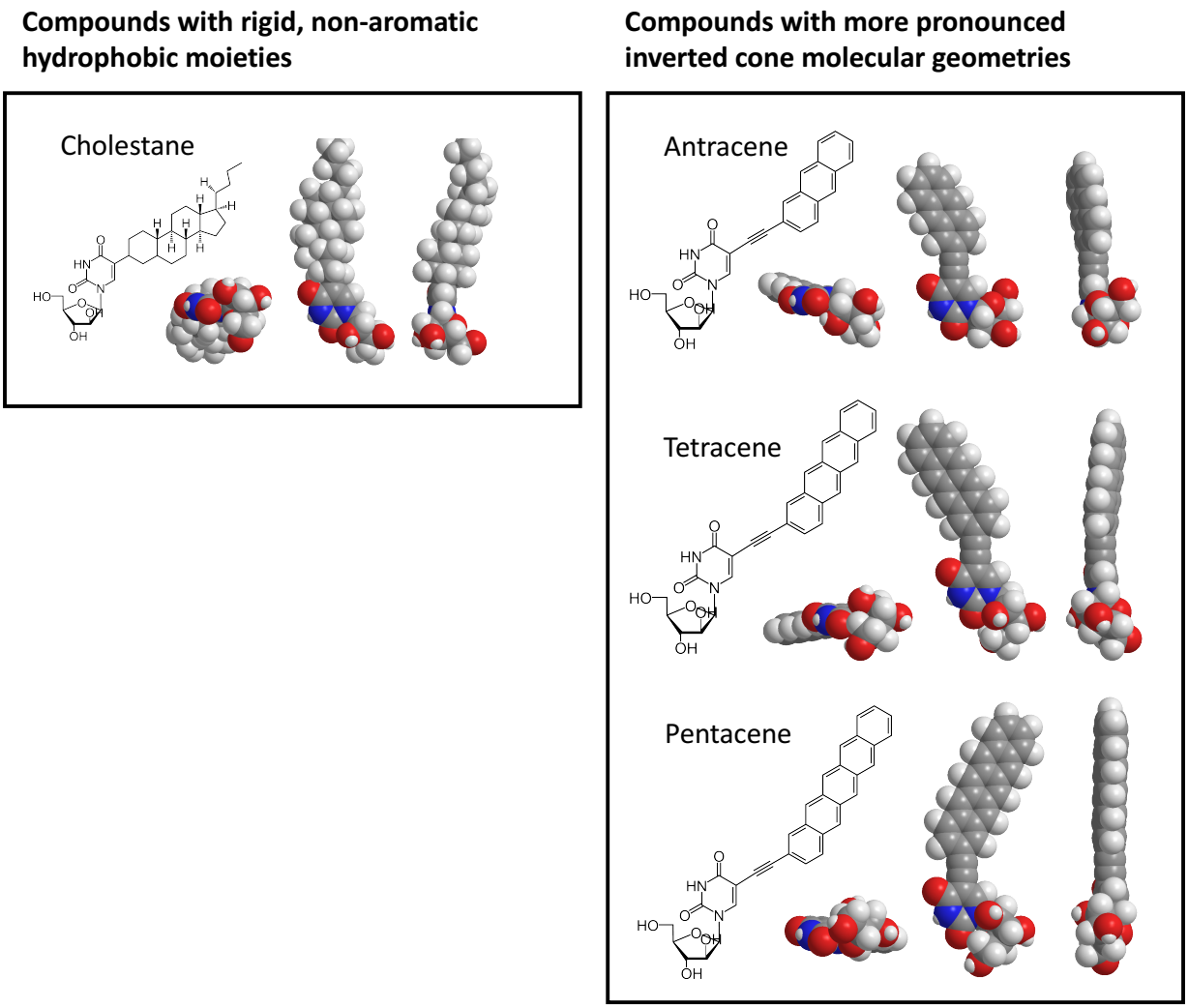

Figure 4.2 Future SAR studies

Chemical and space filling structures in three orthogonal orientations. Gray, carbon; red, oxygen; blue, nitrogen; yellow; fluoride; white, hydrogen.

REFERENCES

Adams, O., Bonzel, L., Kovacevic, A., Mayatepek, E., Hoehn, T., and Vogel, M. (2010). Palivizumab-Resistant Human Respiratory Syncytial Virus Infection in Infancy. Clin. Infect. Dis. *51*, 185–188.

Adu-Gyamfi, E., Kim, L.S., Jardetzky, T.S., and Lamb, A. (2016). Flexibility of the Head-Stalk Linker Domain of Paramyxovirus HN Glycoprotein Is Essential for Triggering Virus Fusion. *90*, 9172–9181.

Aeffner, S., Reusch, T., Weinhausen, B., and Salditt, T. (2012). Energetics of stalk intermediates in membrane fusion are controlled by lipid composition. Proc. Natl. Acad. Sci. *109*, E1609–E1618.

Akhtar, J., and Shukla, D. (2009). Viral entry mechanisms: cellular and viral mediators of herpes simplex virus entry. FEBS J. *276*, 7228–7236.

Akkarawongsa, R., Pocaro, N.E., Case, G., Kolb, A.W., and Brandt, C.R. (2009). Multiple peptides homologous to herpes simplex virus type 1 glycoprotein B inhibit viral infection. Antimicrob. Agents Chemother. *53*, 987–996.

Aloia, R.C., Tian, H., and Jensen, F.C. (1993). Lipid composition and fluidity of the human immunodeficiency virus envelope and host cell plasma membranes. Proc. Natl. Acad. Sci. U. S. A. *90*, 5181–5185.

Andronova, V.L., Skorobogatyi, M.V., Manasova, E.V., Berlin, Y.A., Korshun, V.A., and Galegov, G.A. (2003). Antiviral activity of some 5-arylethynyl 2'-deoxyuridine derivatives. Russ. J. Bioorg. Chem. *29*, 262–266.

Anggakusuma, Colpitts, C.C., Schang, L.M., Rachmawati, H., Frentzen, A., Pfaender, S., Behrendt, P., Brown, R.J.P., Bankwitz, D., Steinmann, J., et al. (2013). Turmeric curcumin inhibits entry of all hepatitis C virus genotypes into human liver cells. Gut 1137–1149.

Apellániz, B., Ivankin, A., Nir, S., Gidalevitz, D., and Nieva, J.L. (2011). Membrane-proximal external HIV-1 gp41 motif adapted for destabilizing the highly rigid viral envelope. Biophys. J. *101*, 2426–2435.

Aralov, A. V, Proskurin, G. V, Orlov, A.A., Kozlovskaya, L.I., Chistov, A., Kutyakov, S. V, Karganova, G.G., Palyulin, V.A., Dmitry, I., and Korshun, V.A. (2017). Perylenyltriazoles inhibit reproduction of enveloped viruses. Eur. J. Med. Chem. *in press*.

Asokan, A., Hamra, J.B., Govindasamy, L., Agbandje-McKenna, M., and Samulski, R.J. (2006). Adeno-Associated Virus Type 2 Contains an Integrin 5 1 Binding Domain Essential for Viral Cell Entry. J. Virol. *80*, 8961–8969.

Autoimmune Technologies, L. (2015). A Phase 1, Randomized, Double-blind, Placebo-controlled Assessment of the Safety, Tolerability and Pharmacokinetics of Escalating Single and Repeat Doses of Flufirvitide-3 Dry Powder for Inhalation in Healthy Subjects.

Bacellar, I.O.L., Pavani, C., Sales, E.M., Itri, R., Wainwright, M., and Baptista, M.S. (2014). Membrane damage efficiency of phenothiazinium photosensitizers. Photochem. Photobiol. *90*, 801–813.

Badani, H., Garry, R.F., and Wimley, W.C. (2014). Peptide entry inhibitors of enveloped viruses: The importance of interfacial hydrophobicity. Biochim. Biophys. Acta

- Biomembr. *1838*, 2180–2197.

Berridge, M., Tan, A., McCoy, K., and Wang, R. (1996). The biochemical and cellular basis of cell proliferation assays that use tetrazolium salts. Biochemica 4–9.

Bhattacharyya, S., War, K.L., Ruthel, G., Bavari, S., Aman, M.J., and Hope, T.J. (2010). Ebola virus uses clathrin-mediated endocytosis as an entry pathway. *401*, 18–28.

Binder, H., and Gawrisch, K. (2001). Effect of unsaturated lipid chains on dimensions, molecular order and hydration of membranes. J. Phys. Chem. B *105*, 12378–12390.

Blaising, J., Lévy, P.L., Polyak, S.J., Stanifer, M., Boulant, S., and Pécheur, E.I. (2013). Arbidol inhibits viral entry by interfering with clathrin-dependent trafficking. Antiviral Res. *100*, 215–219.

Blaising, J., Polyak, S.J., and Pécheur, E.I. (2014). Arbidol as a broad-spectrum antiviral: An update. Antiviral Res. *107*, 84–94.

Blanc, M., Hsieh, W.Y., Robertson, K.A., Kropp, K.A., Forster, T., Shui, G., Lacaze, P., Watterson, S., Griffiths, S.J., Spann, N.J., et al. (2013). The Transcription Factor STAT-1 Couples Macrophage Synthesis of 25-Hydroxycholesterol to the Interferon Antiviral Response. Immunity *38*, 106–118.

Blanchard, E., Belouzard, S., Goueslain, L., Wakita, T., Dubuisson, J., Wychowski, C., and Rouille, Y. (2006). Hepatitis C Virus Entry Depends on Clathrin-Mediated Endocytosis. *80*, 6964–6972.

Blaschko, H., Firemark, H., Smith, A.D., and Winkler, A.H. (1967). Lipids of the Adrenal Medulla LYSOLECITHIN, A CHARACTERISTIC CONSTITUENT OF CHROMAFFIN GRANULES. Biochem. J *104*, 545–549.

Bobardt, M.D., Cheng, G., de Witte, L., Selvarajah, S., Chatterji, U., Sanders-Beer, B.E., Geijtenbeek, T.B., Chisari, F. V, and Gallay, P.A. (2008). Hepatitis C virus NS5A anchor peptide disrupts human immunodeficiency virus. Proc Natl Acad Sci U S A *105*, 5525–5530.

Bombardier, J.P., and Munson, M. (2015). Three steps forward, two steps back: Mechanistic insights into the assembly and disassembly of the SNARE complex. Curr. Opin. Chem. Biol. *29*, 66–71.

Bosch, B.J., Martina, B.E., Van Der Zee, R., Lepault, J., Haijema, B.J., Versluis, C., Heck, A.J., De Groot, R., Osterhaus, A.D., and Rottier, P.J. (2004). Severe acute respiratory syndrome coronavirus (SARS-CoV) infection inhibition using spike protein heptad repeat-derived peptides. Proc Natl Acad Sci U S A *101*, 8455–8460.

Brooks, M.J., Burtseva, E.I., Ellery, P.J., Marsh, G.A., Lew, A.M., Slepushkin, A.N., Crowe, S.M., and Tannock, G.A. (2012). Antiviral Activity of Arbidol, a Broad-Spectrum Drug for Use Against Respiratory Viruses, Varies According to Test Conditions. J. Med. Virol. *84*, 170–181.

Bruce, E.A., Digard, P., and Stuart, A.D. (2010). The Rab11 Pathway Is Required for Influenza A Virus Budding and Filament Formation. J. Virol. *84*, 5848–5859.

Brügger, B., Glass, B., Haberkant, P., Leibrecht, I., Wieland, F.T., and Kräusslich, H.-G.G. (2006). The {HIV} lipidome: a raft with an unusual composition. Proc. Natl. Acad. Sci. {U.S.A.} *103*, 2641–2646.

Bullough, P.A., Hughson, F.M., Skehel, J.J., and Wiley, D.C. (1994). Structure of influenza haemagglutinin at the pH of membrane fusion. Nature *371*, 37–43.

Byrnes, a P., and Griffin, D.E. (1998). Binding of Sindbis virus to cell surface heparan sulfate. J. Virol. *72*, 7349–7356.

Campelo, F., McMahon, H.T., and Kozlov, M.M. (2008). The Hydrophobic Insertion Mechanism of Membrane Curvature Generation by Proteins. Biophys. J. *95*, 2325–2339.

Carr, C.M., and Kim, P.S. (1993). A spring-loaded mechanism for the conformational change of influenza hemagglutinin. Cell *73*, 823–832.

Chamoun, A.M., Chockalingam, K., Bobardt, M., Simeon, R., Chang, J., Gallay, P., and Chen, Z. (2012). PD 404,182 is a virocidal small molecule that disrupts hepatitis C virus and human immunodeficiency virus. Antimicrob. Agents Chemother. *56*, 672–681.

Chan, D.C., Fass, D., Berger, J.M., and Kim, P.S. (1997). Core structure of gp41 from the HIV envelope glycoprotein. Cell *89*, 263–273.

Chang, C.-W., and Jackson, M.B. (2015). Synaptobrevin Transmembrane Domain Influences Exocytosis by Perturbing Vesicle Membrane Curvature. Biophys. J. *109*, 76–84.

Chanturiya, A., Chernomordik, L. V, and Zimmerberg, J. (1997). Flickering fusion pores comparable with initial exocytotic pores occur in protein-free phospholipid bilayers. Proc. Natl. Acad. Sci. U. S. A. *94*, 14423–14428.

Chen, C., and Zhuang, X. (2008). Epsin 1 is a cargo-specific adaptor for the clathrin-mediated endocytosis of the influenza virus. *2008*.

Chen, Y.A., and Scheller, R.H. (2001). SNARE-mediated membrane fusion. Nat. Rev. Mol. Cell Biol. *2*, 98–106.

Chen, J., Lee, K.H., Steinhauer, D.A., Stevens, D.J., Skehel, J.J., and Wiley, D.C. (1998). Structure of the hemagglutinin precursor cleavage site, a determinant of influenza pathogenicity and the origin of the labile conformation. Cell *95*, 409–417.

Chen, T., Chen, D., Wen, H., Ou, J., Chiou, S., Chen, J., Wong, M., and Hsu, W. (2013). Inhibition of Enveloped Viruses Infectivity by Curcumin. *8*, 1–11.

Chen, Y., Götte, M., Liu, J., and Park, P.W. (2008). Microbial subversion of heparan sulfate proteoglycans. Mol. Cells *26*, 415–426.

Chen, Y., Wang, S., Yi, Z., Tian, H., Aliyari, R., Li, Y., Chen, G., Liu, P., Zhong, J., Chen, X., et al. (2014). Interferon-Inducible Cholesterol-25-Hydroxylase Inhibits Hepatitis C Virus Replication via Distinct Mechanisms. Sci. Rep. *4*, 7242.

Cheng, G., Montero, A., Gastaminza, P., Whitten-Bauer, C., Wieland, S.F., Isogawa, M., Fredericksen, B., Selvarajah, S., Gallay, P.A., Ghadiri, M.R., et al. (2008). A Virocidal Amphipathic α-Helical Peptide That Inhibits Hepatitis C Virus Infection in vitro. Proc. Natl. Acad. Sci. U. S. A. *105*, 3088–3093.

Chernomordik, L. V., and Kozlov, M.M. (2005). Membrane hemifusion: Crossing a chasm in two leaps. Cell *123*, 375–382.

Chernomordik, L. V, and Kozlov, M.M. (2003). Protein-lipid interplay in fusion and fission of biological membranes. Annu. Rev. Biochem. *72*, 175–207.

Chernomordik, L. V, and Kozlov, M.M. (2008). Mechanics of membrane fusion. Nat. Struct. Mol. Biol. *15*, 675–683.

Chernomordik, L., Kozlov, M., and Zimmerberg, J. (1995a). Lipids in biological membrane fusion. J. Membr. Biol. *14*, 1–14.

Chernomordik, L., Leikina, E., Cho, M.S., and Zimmerberg, J. (1995b). Control of baculovirus gp64-induced syncytium formation by membrane lipid composition. J Virol

69, 3049–3058.

Chernomordik, L., Chanturiya, a, Green, J., and Zimmerberg, J. (1995c). The hemifusion intermediate and its conversion to complete fusion: regulation by membrane composition. Biophys. J. *69*, 922–929.

Chernomordik, L. V, Vogel, S.S., Sokoloff, A., Onaran, H.O., Leikina, E.A., and Zimmerberg, J. (1993). Lysolipids Reversibly Inhibit Ca-2+-Dependent, Gtp-Dependent and Ph-Dependent Fusion of Biological-Membranes. Febs Lett. *318*, 71–76.

Chernomordik, L. V., Kozlov, M.M., Melikyan, G.B., Abidor, I.G., Markin, V.S., and Chizmadzhev, Y.A. (1985). The shape of lipid molecules and monolayer membrane fusion. BBA - Biomembr. *812*, 643–655.

Chernomordik, L. V., Frolov, V.A., Leikina, E., Bronk, P., and Zimmerberg, J. (1998). The pathway of membrane fusion catalyzed by influenza hemagglutinin: Restriction of lipids, hemifusion, and lipidic fusion pore formation. J. Cell Biol. *140*, 1369–1382.

Chernomordik, L. V., Zimmerberg, J., and Kozlov, M.M. (2006). Membranes of the world unite! J. Cell Biol. *175*, 201–207.

Chernomordik, L.V., Leikina, E., Frolov, V., Bronk, P., and Zimmerberg, J. (1997). An early stage of membrane fusion mediated by the low pH conformation of influenza haemagglutinin depends upon membrane lipids. J.Cell.Biol *136*, 81–93.

Chistov, A.A., Kutyakov, S. V., Ustinov, A. V., Aparin, I.O., Glybin, A. V., Mikhura, I. V., and Korshun, V.A. (2016). 2-Ethynylperylene and improved synthesis of 3-ethynylperylene. Tetrahedron Lett. *57*, 1003–1005.

Chistov, A.A., Kutyakov, S.V., Guz, A.V., Mikhura, I.V., Ustinov, A.V., and Korshun, V.A. (2017). Improved large-scale synthesis of 5-(perylen-3-ylethynyl)-arabino-uridine (aUY11), the broad-spectrum antiviral. Org. Prep. Proc. Int. *49*, accepted.

Chlanda, P., Mekhedov, E., Waters, H., Schwartz, C.L., Fischer, E.R., Ryham, R.J., Cohen, F.S., Blank, P.S., and Zimmerberg, J. (2016). The hemifusion structure induced by influenza virus haemagglutinin is determined by physical properties of the target membranes. Nat. Microbiol. 16050.

Chowdary, T.K., Cairns, T.M., Atanasiu, D., Cohen, G.H., Eisenberg, R.J., and Heldwein, E.E. (2010). Crystal structure of the conserved herpesvirus fusion regulator complex gH-gL. Nat. Struct. Mol. Biol. *17*, 882–888.

Cinatl, J., Morgenstern, B., Bauer, G., Chandra, P., Rabenau, H., and Doerr, H.W. (2003). Glycyrrhizin, an active component of liquorice roots, and replication of SARS-associated coronavirus. Lancet *361*, 2045–2046.

Clarke, R.W. (2016). Forces and Structures of the Herpes Simplex Virus (HSV) Entry Mechanism. ACS Infect. Dis. *1*, 403–415.

De Clercq, E., and Li, G. (2016). Approved Antiviral Drugs over the Past 50 Years. Clin. Microbiol. Rev. *29*, 695–747.

Cohen, F.S., and Melikyan, G.B. (2004). The energetics of membrane fusion from binding, through hemifusion, pore formation, and pore enlargement. J. Membr. Biol. *199*, 1–14.

Colpitts, C.C., and Baumert, T.F. (2016). Hepatitis C virus cell entry: a target for novel antiviral strategies to address limitations of direct acting antivirals. Hepatol. Int. *10*, 741–748.

Colpitts, C.C., and Schang, L.M. (2014). A small molecule inhibits virion attachment to heparan sulfate- or sialic Acid-containing glycans. J. Virol. *88*, 7806–7817.

Colpitts, C.C., Ustinov, A. V, Epand, R.F., Epand, R.M., Korshun, V. a, and Schang, L.M. (2013). 5-(Perylen-3-yl)ethynyl-arabino-uridine (aUY11), an arabino-based rigid amphipathic fusion inhibitor, targets virion envelope lipids to inhibit fusion of influenza virus, hepatitis C virus, and other enveloped viruses. J. Virol. *87*, 3640–3654.

Cooper, R.S., and Heldwein, E.E. (2015). Herpesvirus gB: A finely tuned fusion machine. Viruses *7*, 6552–6569.

Cross, K.J., Wharton, S.A., Skehel, J.J., Wiley, D.C., and Steinhauer, D.A. (2001). Studies on influenza haemagglutinin fusion peptide mutants generated by reverse genetics. EMBO J. *20*, 4432–4442.

Crublet, E., Andrieu, J.P., Vivès, R.R., and Lortat-Jacob, H. (2008). The HIV-1 envelope glycoprotein gp120 features four heparan sulfate binding domains, including the co-receptor binding site. J. Biol. Chem. *283*, 15193–15200.

Desai, T.M., Marin, M., Chin, C.R., Savidis, G., Brass, A.L., and Melikyan, G.B. (2014). IFITM3 Restricts Influenza A Virus Entry by Blocking the Formation of Fusion Pores following Virus-Endosome Hemifusion. PLoS Pathog. *10*.

Dessau, M., and Modis, Y. (2013). Crystal structure of glycoprotein C from Rift Valley fever virus. Proc Natl Acad Sci U S A *110*, 1696–1701.

Diizgiineg, N., Straubinger, R.M., Baldwin, P.A., and Friend, D.S. (1985). Proton-Induced Fusion of Oleic Acid-Phosphatidylethanolamine Liposomes +. 3091–3098.

Dorr, P., Westby, M., Dobbs, S., Griffin, P., Irvine, B., Macartney, M., Mori, J., Rickett, G., Smith-Burchnell, C., Napier, C., et al. (2005). Maraviroc (UK-427,857), a Potent, Orally Bioavailable, and Selective Small-Molecule Inhibitor of Chemokine Receptor CCR5 with Broad-Spectrum Anti-Human Immunodeficiency Virus Type 1 Activity. Nature *49*, 4721–4732.

Edinger, T.O., Pohl, M.O., and Stertz, S. (2014). Entry of influenza A virus: host factors and antiviral targets. J. Gen. Virol. *95*, 263–277.

Efrat, A., Chernomordik, L. V, and Kozlov, M.M. (2007). Point-like protrusion as a prestalk intermediate in membrane fusion pathway. Biophys. J. *92*, L61–L63.

Eisenberg, R.J., Atanasiu, D., Cairns, T.M., Gallagher, J.R., Krummenacher, C., and Cohen, G.H. (2012). Herpes virus fusion and entry: A story with many characters. Viruses *4*, 800–832.

Engel, S., Heger, T., Mancini, R., Herzog, F., Hayer, A., and Helenius, A. (2011). Role of Endosomes in Simian Virus 40 Entry and Infection. *85*, 4198–4211.

Epand, R.M. (2003). Fusion peptides and the mechanism of viral fusion. Biochim. Biophys. Acta - Biomembr. *1614*, 116–121.

Fang, J., and Iwasa, K.H. (2007). Effects of Chlorpromazine and Trinitrophenol on the Membrane Motor of Outer Hair Cells. Biophys. J. *93*, 1809–1817.

Fätkenheuer, G., Pozniak, A.L., Johnson, M. a, Plettenberg, A., Staszewski, S., Hoepelman, A.I.M., Saag, M.S., Goebel, F.D., Rockstroh, J.K., Dezube, B.J., et al. (2005). Efficacy of short-term monotherapy with maraviroc, a new CCR5 antagonist, in patients infected with HIV-1. Nat. Med. *11*, 1170–1172.

Floyd, D.L., Ragains, J.R., Skehel, J.J., Harrison, S.C., and Oijen, A.M. Van (2008). Single-particle kinetics of influenza virus membrane fusion.

Foote, C.S. (1968). Mechanisms of Photosensitized Oxidation. Science (80-.). *162*, 963–970.

Fratti, R.A., Jun, Y., Merz, A.J., Margolis, N., Wickner, W., and Wickner, B. (2004). Interdependent assembly of specific regulatory lipids and membrane fusion proteins into the vertex ring domain of docked vacuoles. J. Cell Biol. *167*, 1087–1098.

Fuller, N., and Rand, R.P. (2001). The influence of lysolipids on the spontaneous curvature and bending elasticity of phospholipid membranes. Biophys. J. *81*, 243–254.

Gaillard, V., Galloux, M., Garcin, D., Eléouët, J.-F., Goffic, R. Le, Larcher, T., Rameix-Welti, M.-A., Boukadiri, A., Héritier, J., Segura, J.-M., et al. (2017). A Short Double-Stapled Peptide Inhibits Respiratory Syncytial Virus Entry and Spreading. Antimicrob. Agents Chemother. *61*, 1–19.

Gaudin, Y. (2000a). Rabies virus-induced membrane fusion pathway. J. Cell Biol. *150*, 601–611.

Gaudin, Y. (2000b). Reversibility in fusion protein conformational changes. The intriguing case of rhabdovirus-induced membrane fusion. Subcell. Biochem. *34*, 379–408.

van Genderen, I.L., Brandimarti, R., Torrisi, M.R., Campadelli, G., and van Meer, G. (1994). The phospholipid composition of extracellular herpes simplex virions differs from that of host cell nuclei. Virology *200*, 831–836.

Gerl, M.J., Sampaio, J.L., Urban, S., Kalvodova, L., Verbavatz, J., Binnington, B., Lindemann, D., Lingwood, C.A., Shevchenko, A., Schroeder, C., et al. (2012). Quantitative analysis of the lipidomes of the influenza virus envelope and MDCK cell apical membrane. *196*, 213–221.

Gianni, T., Piccoli, a, Bertucci, C., and Campadelli-Fiume, G. (2006). Heptad repeat 2 in herpes simplex virus 1 gH interacts with heptad repeat 1 and is critical for virus entry and fusion. J. Virol. *80*, 2216–2224.

Greenberg, M.L., and Cammack, N. (2004). Resistance to enfuvirtide, the first HIV fusion inhibitor. J. Antimicrob. Chemother. *54*, 333–340.

Grote, E., Baba, M., Ohsumi, Y., and Novick, P.J. (2000). Geranylgeranylated SNAREs are dominant inhibitors of membrane fusion. J. Cell Biol. *151*, 453–465.

Gunther Ausborn, S., Preator, A., and Stegmann, T. (1995). Inhibition of membrane fusion by lysophosphatidylcholine. Biochemistry *270*, 29279–29285.

Guo, H., Pan, X., Mao, R., Zhang, X., Wang, L., Lu, X., Chang, J., Guo, J.T., Passic, S., Krebs, F.C., et al. (2011). Alkylated porphyrins have broad antiviral activity against hepadnaviruses, flaviviruses, filoviruses, and arenaviruses. Antimicrob. Agents Chemother. *55*, 478–486.

Han, X., Bushweller, J.H., Cafiso, D.S., and Tamm, L.K. (2001). Membrane structure and fusion-triggering conformational change of the fusion domain from influenza hemagglutinin. *8*, 715–720.

Hanlon, M.C., and Seybert, D.W. (1997). The pH dependence of lipid peroxidation using water-soluble azo initiators. Free Radic. Biol. Med. *23*, 712–719.

Harada, S. (2005). The broad anti-viral agent glycyrrhizin directly modulates the fluidity of plasma membrane and HIV-1 envelope. Biochem. J. *392*, 191–199.

Harrison, S.C. (2008). Viral membrane fusion. Nat. Struct. Mol. Biol. *15*, 690–698.

Heldwein, E.E., Lou, H., Bender, F.C., Cohen, G.H., Eisenberg, R.J., and Harrison, S.C. (2006). Crystal structure of glycoprotein B from herpes simplex virus 1. Science

(80-.). *313*, 217–220.

Helenius, A. (2013). Virus entry : What has pH got to do with it ? *15*, 2013.

Helfrich, W. (1973). Steric interactions of fluid membranes in multilayer systems. Z. Naturforsch.A *33*, 305–315.

Hollmann, A., Castanho, M. a R.B., Lee, B., and Santos, N.C. (2014). Singlet oxygen effects on lipid membranes: implications for the mechanism of action of broad-spectrum viral fusion inhibitors. Biochem. J. *459*, 161–170.

Hrobowski, Y.M., Garry, R.F., and Michael, S.F. (2005). Peptide inhibitors of dengue virus and West Nile virus infectivity. Virol. J. *2*, 49.

Huang, K., Incognito, L., Cheng, X., Ulbrandt, N.D., and Wu, H. (2010). Respiratory Syncytial Virus-Neutralizing Monoclonal Antibodies Motavizumab and Palivizumab Inhibit Fusion. J. Virol. *84*, 8132–8140.

Huarte, N., Carravilla, P., Cruz, A., Lorizate, M., Nieto-garai, J.A., Kräusslich, H., Pérez-gil, J., Requejo-isidro, J., and Nieva, J.L. (2016). Functional organization of the HIV lipid envelope. Nat. Publ. Gr. 1–14.

Hudson, J.B., Imperial, V., Haugland, R.P., and Diwu, Z. (1997). Antiviral activities of photoactive perylenequinones. Photochem. Photobiol. *65*, 352–354.

Ivanova, P.T., Cerda, B.A., Horn, D.M., Cohen, J.S., McLafferty, F.W., and Brown, H.A. (2001). Electrospray ionization mass spectrometry analysis of changes in phospholipids in RBL-2H3 mastocytoma cells during degranulation. Proc Natl Acad Sci U S A *98*, 7152–7157.

Jackson, M.B., and Chapman, E.R. (2008). The fusion pores of Ca2+ -triggered exocytosis. Nat. Struct. Mol. Biol. *15*, 684–689.

Jendželovská, Z., Jendželovský, R., Kuchárová, B., and Fedoročko, P. (2016). Hypericin in the Light and in the Dark: Two Sides of the Same Coin. Front. Plant Sci. *7*, 560.

Jun, Y., and Wickner, W. (2007). Assays of vacuole fusion resolve the stages of docking , lipid mixing , and content mixing. *104*, 13010–13015.

Jurkiewicz, P., Olzyńska, A., Cwiklik, L., Conte, E., Jungwirth, P., Megli, F.M., and Hof, M. (2012). Biophysics of lipid bilayers containing oxidatively modified phospholipids: Insights from fluorescence and EPR experiments and from MD simulations. Biochim. Biophys. Acta - Biomembr. *1818*, 2388–2402.

Karunakaran, S., and Fratti, R.A. (2013). The Lipid Composition and Physical Properties of the Yeast Vacuole Affect the Hemifusion-Fusion Transition. Traffic *14*, 650–662.

Katsov, K., Müller, M., and Schick, M. (2006). Field Theoretic Study of Bilayer Membrane Fusion : II . Mechanism of a Stalk-Hole Complex. *90*, 915–926.

Katz, D.H., Marcellettit, J.F., Khalilt, M.H., Popet, L.E., and Katzt, L.E.E.R. (1991). Antiviral activity of 1-docosanol , an inhibitor of lipid-enveloped viruses including herpes simplex. *88*, 10825–10829.

Kemble, G.W., Danieli, T., and White, J.M. (1994). Lipid-anchored influenza hemagglutinin promotes hemifusion, not complete fusion. Cell *76*, 383–391.

Khan, A.G., Whidby, J., Miller, M.T., Scarborough, H., Zatorski, A. V, Cygan, A., Price, A. a, Yost, S. a, Bohannon, C.D., Jacob, J., et al. (2014). Structure of the core ectodomain of the hepatitis C virus envelope glycoprotein 2. Nature *509*, 381–384.

Kielian, M.C., and Helenius, A. (1984). Role of cholesterol in fusion of Semliki

Forest virus with membranes. J. Virol. *52*, 281–283.

Kielian, M., Chanel-Vos, C., and Liao, M. (2010). Alphavirus entry and membrane fusion. Viruses *2*, 796–825.

Kilby, J.M., Hopkins, S., Venetta, T.M., DiMassimo, B., Cloud, G.A., Lee, J.Y., Alldredge, L., Hunter, E., Lambert, D., Bolognesi, D., et al. (1998). Potent suppression of HIV-1 replication in humans by T-20, a peptide inhibitor of gp41-mediated virus entry. Nat. Med. *4*, 1302–1307.

Kong, L., Giang, E., Nieusma, T., Kadam, R.U., Cogburn, K.E., Hua, Y., Dai, X., Stanfield, R.L., Burton, D.R., Ward, A.B., et al. (2013). Hepatitis C virus E2 envelope glycoprotein core structure. Science *342*, 1090–1094.

Kozlov, M.M., and Chernomordik, L. V (2015). Membrane tension and membrane fusion. Curr. Opin. Struct. Biol. *33*, 61–67.

Kozlovsky, Y., and Kozlov, M.M. (2002). Stalk Model of Membrane Fusion: Solution of Energy Crisis. Biophys. J. *82*, 882–895.

Kozlovsky, Y., Chernomordik, L. V, and Kozlov, M.M. (2002). Lipid intermediates in membrane fusion: formation, structure, and decay of hemifusion diaphragm. Biophys. J. *83*, 2634–2651.

Kozlovsky, Y., Efrat, A., Siegel, D.P., and Kozlov, M.M. (2004). Stalk phase formation: effects of dehydration and saddle splay modulus. Biophys. J. *87*, 2508–2521.

Krey, T., D'Alayer, J., Kikuti, C.M., Saulnier, A., Damier-Piolle, L., Petitpas, I., Johansson, D.X., Tawar, R.G., Baron, B., Robert, B., et al. (2010). The disulfide bonds in glycoprotein E2 of hepatitis C virus reveal the tertiary organization of the molecule. PLoS Pathog. *6*.

Krishnamoorthy, G., Webb, S.P., Nguyen, T., Chowdhury, P.K., Halder, M., Wills, N.J., Carpenter, S., Kraus, G. a, Gordon, M.S., and Petrich, J.W. (2005). Synthesis of hydroxy and methoxy perylene quinones, their spectroscopic and computational characterization, and their antiviral activity. Photochem. Photobiol. *81*, 924–933.

Kuhmann, S.E., and Hartley, O. (2008). Targeting chemokine receptors in HIV: a status report. Annu. Rev. Pharmacol. Toxicol. *48*, 425–461.

Kuzmin, P.I., Zimmerberg, J., Chizmadzhev, Y.A., and Cohen, F.S. (2001). A quantitative model for membrane fusion based on low-energy intermediates. *98*, 7235–7240.

Kweon, D.-H., Kong, B., and Shin, Y.-K. (2017). Hemifusion in Synaptic Vesicle Cycle. Front. Mol. Neurosci. *10*, 65.

Lai, A.L., and Freed, J.H. (2015). The Interaction between Influenza HA Fusion Peptide and Transmembrane Domain Affects Membrane Structure. Biophys. J. *109*, 2523–2536.

Lamb, R.A., and Jardetzky, T.S. (2007). Structural basis of viral invasion: lessons from paramyxovirus F. Curr. Opin. Struct. Biol. *17*, 427–436.

Leal, E.S., Aucar, M.G., Gebhard, L.G., Iglesias, N.G., Pascual, M.J., Casal, J.J., Gamarnik, A. V, Cavasotto, C.N., and Bollini, M. (2017). Discovery of novel Dengue virus entry inhibitors via a structure-based approach. Bioorg. Med. Chem. Lett. *In press*.

Lee, J., and Lentz, B.R. (1997). Evolution of lipidic structures during model membrane fusion and the relation of this process to cell membrane fusion. Biochemistry *36*, 6251–6259.

Lee, M., Yang, J., Jo, E., Lee, J.-Y., Kim, H.-Y., Bartenschlager, R., Shin, E.-C., Bae,

Y.-S., and Windisch, M.P. (2017). A Novel Inhibitor IDPP Interferes with Entry and Egress of HCV by Targeting Glycoprotein E1 in a Genotype-Specific Manner. Sci. Rep. *7*, 44676.

Lenard, J., Rabson, A., and Vanderoef, R. (1993). Photodynamic inactivation of infectivity of human immunodeficiency virus and other enveloped viruses using hypericin and rose bengal: inhibition of fusion and syncytia formation. Proc. Natl. Acad. Sci. U. S. A. *90*, 158–162.

Lentz, B.R. (2006). Seeing is believing: The stalk intermediate. Biophys. J. *91*, 2747–2748.

Lentz, B.R., and Lee, J.K. (1999). Poly(ethylene glycol) (PEG)-mediated fusion between pure lipid bilayers: a mechanism in common with viral fusion and secretory vesicle release? Mol. Membr. Biol. *16*, 279–296.

Levine, S., Kaliaber-Franco, R., and Paradiso, P.R. (1987). Demonstration that glycoprotein G is the attachment protein of respiratory syncytial virus. J. Gen. Virol. *68*, 2521–2524.

Li, K., Markosyan, R.M., Zheng, Y.M., Golfetto, O., Bungart, B., Li, M., Ding, S., He, Y., Liang, C., Lee, J.C., et al. (2013a). IFITM Proteins Restrict Viral Membrane Hemifusion. PLoS Pathog. *9*.

Li, Y., Wang, J., Kanai, R., and Modis, Y. (2013b). Crystal structure of glycoprotein E2 from bovine viral diarrhea virus. Pnas *110*, 6805–6810.

Lin, H., Yang, Y., Yu, S., Hsiao, K., Liu, C., Sia, C., and Chow, Y. (2013). Caveolar Endocytosis Is Required for Human PSGL-1-Mediated. *87*, 9064–9076.

Lin, Q., Fang, D., Hou, X., Le, Y., Fang, J., Wen, F., Gong, W., Chen, K., Wang, J.M., and Su, S.B. (2011). HCV peptide (C5A), an amphipathic α-helical peptide of hepatitis virus C, is an activator of N-formyl peptide receptor in human phagocytes. J. Immunol. *186*, 2087–2094.

Lindau, M., and Almers, W. (1995). Structure and function of fusion pores in exocytosis and ectoplasmic membrane fusion. Curr. Opin. Cell Biol. *7*, 509–517.

Liu, Q., Zhou, Y., and Yang, Z. (2016). The cytokine storm of severe influenza and development of immunomodulatory therapy. Cell. Mol. Immunol. *13*, 3–10.

Liu, S.T.H., Sharon-Friling, R., Ivanova, P., Milne, S.B., Myers, D.S., Rabinowitz, J.D., Brown, H.A., and Shenk, T. (2011). Synaptic vesicle-like lipidome of human cytomegalovirus virions reveals a role for SNARE machinery in virion egress. Proc. Natl. Acad. Sci. U. S. A. *108*, 12869–12874.

Lommer, B., Runge, A., Drechsel, D., Ohya, T., and Miaczynska, M. (2009). Reconstitution of Rab- and SNARE-dependent membrane fusion by synthetic endosomes. *459*.

Lorieau, J.L., Louis, J.M., and Bax, A. (2010). The complete influenza hemagglutinin fusion domain adopts a tight helical hairpin arrangement at the lipid:water interface. Proc Natl Acad Sci U S A *107*, 11341–11346.

Lu, X., Zhang, F., Mcnew, J.A., and Shin, Y. (2005). Membrane Fusion Induced by Neuronal SNAREs Transits through Hemifusion. *280*, 30538–30541.

Macovei, A., Radulescu, C., Lazar, C., Petrescu, S., Durantel, D., Dwek, R.A., Zitzmann, N., Nichita, N.B., Lyon, D., and Est, I.F.R.L. (2010). Hepatitis B Virus Requires Intact Caveolin-1 Function for Productive Infection in HepaRG Cells □. *84*, 243–253.

Markosyan, R.M., Cohen, F.S., and Melikyan, G.B. (2000). The lipid-anchored ectodomain of influenza virus hemagglutinin (GPI-HA) is capable of inducing nonenlarging fusion pores. Mol. Biol. Cell *11*, 1143–1152.

Martens, S., and McMahon, H.T. (2008). Mechanisms of membrane fusion: disparate players and common principles. Nat. Rev. Mol. Cell Biol. *9*, 543–556.

Maurer, U.E., Zeev-Ben-Mordehai, T., Pandurangan, A.P., Cairns, T.M., Hannah, B.P., Whitbeck, J.C., Eisenberg, R.J., Cohen, G.H., Topf, M., Huiskonen, J.T., et al. (2013). The structure of herpesvirus fusion glycoprotein B-bilayer complex reveals the protein-membrane and lateral protein-protein interaction. Structure *21*, 1396–1405.

Mayer, A. (2002). Membrane Fusion in Eukaryotic Cells. Annu. Rev. Cell Dev. Biol. *18*, 289–314.

McMahon, H.T., and Gallop, J.L. (2005). Membrane curvature and mechanisms of dynamic cell membrane remodelling. Nature *438*, 590–596.

McMahon, H.T., Kozlov, M.M., and Martens, S. (2010). Membrane Curvature in Synaptic Vesicle Fusion and Beyond. Cell *140*, 601–605.

McNew, J.A. (2000). Close Is Not Enough: SNARE-dependent Membrane Fusion Requires an Active Mechanism that Transduces Force to Membrane Anchors. J. Cell Biol. *150*, 105–118.

Meers, P., Ali, S., Erukulla, R., and Janoff, A.S. (2000). Novel inner monolayer fusion assays reveal differential monolayer mixing associated with cation-dependent membrane fusion. Biochim. Biophys. Acta - Biomembr. *1467*, 227–243.

Megli, F.M., Russo, L., and Conte, E. (2009). Spin labeling EPR studies of the properties of oxidized phospholipid-containing lipid vesicles. Biochim. Biophys. Acta - Biomembr. *1788*, 371–379.

Melikyan, G.B., White, J.M., and Cohen, F.S. (1995). Gpi-Anchored Influenza Hemagglutinin Induces Hemifusion To Both Red-Blood-Cell and Planar Bilayer-Membranes. J. Cell Biol. *131*, 679–691.

Melikyan, G.B., Markosyan, R.M., Roth, M.G., and Cohen, F.S. (2000). A point mutation in the transmembrane domain of the hemagglutinin of influenza virus stabilizes a hemifusion intermediate that can transit to fusion. Mol. Biol. Cell *11*, 3765–3775.

Mercer, J., and Helenius, A. (2008). Vaccinia virus uses macropinocytosis and apoptotic mimicry to enter host cells. Science *320*, 531–535.

Mercer, J., and Helenius, A. (2012). Gulping rather than sipping: macropinocytosis as a way of virus entry. Curr. Opin. Microbiol. *15*, 490–499.

Miao, Z., Xie, Z., Miao, J., Ran, J., Feng, Y., and Xia, X. (2017). Regulated Entry of Hepatitis C Virus into Hepatocytes. *1*, 1–19.

Mitchell, C.A., Ramessar, K., and O'Keefe, B.R. (2017). Antiviral lectins: Selective inhibitors of viral entry. Antiviral Res. *142*, 37–54.

Mittal, A., Leikina, E., Chernomordik, L. V, and Bentz, J. (2003). Kinetically differentiating influenza hemagglutinin fusion and hemifusion machines. Biophys. J. *85*, 1713–1724.

Modis, Y., Ogata, S., Clements, D., and Harrison, S.C. (2004). Structure of the dengue virus envelope protein after membrane fusion. Nature *427*, 313–319.

Mohler, W. a, Shemer, G., del Campo, J.J., Valansi, C., Opoku-Serebuoh, E., Scranton, V., Assaf, N., White, J.G., and Podbilewicz, B. (2002). The type I membrane

protein EFF-1 is essential for developmental cell fusion. Dev. Cell *2*, 355–362.

Montigny, C., Lyons, J., Champeil, P., Nissen, P., and Lenoir, G. (2016). On the molecular mechanism of flippase- and scramblase-mediated phospholipid transport. Biochim. Biophys. Acta - Mol. Cell Biol. Lipids *1861*, 767–783.

Morikawa, K., Zhao, Z., Date, T., Miyamoto, M., Murayama, A., Akazawa, D., Tanabe, J., Sone, S., and Wakita, T. (2007). The Roles of CD81 and Glycosaminoglycans in the Adsorption and Uptake of Infectious HCV Particles. J. Med. Virol. *79*, 714–723.

Murray, D.H., Jahnel, M., Lauer, J., Avellaneda, M.J., Brouilly, N., Cezanne, A., Morales-Navarrete, H., Perini, E.D., Ferguson, C., Lupas, A.N., et al. (2016). An endosomal tether undergoes an entropic collapse to bring vesicles together. Nature *537*, 107–111.

Nemerow, G.R. (2000). Cell Receptors Involved in Adenovirus Entry. *274*, 1–4.

Nicola, A. V. (2016). Herpesvirus Entry into Host Cells Mediated by Endosomal Low pH. Traffic *17*, 965–975.

Nieva, J.L., Bron, R., Corver, J., and Wilschut, J. (1994). Membrane fusion of Semliki Forest virus requires sphingolipids in the target membrane. EMBO J. *13*, 2797–2804.

Oelkers, M., Witt, H., Halder, P., Jahn, R., and Janshoff, A. (2016). SNARE-mediated membrane fusion trajectories derived from force-clamp experiments. Proc. Natl. Acad. Sci. *113*, 13051–13056.

Orlov, A.A., Chistov, A.A., Kozlovskaya, L.I., Ustinov, A. V, Korshun, V.A., Karganova, G.G., and Osolodkin, D.I. (2016). Rigid amphipathic nucleosides suppress reproduction of the tick-borne encephalitis virus. Medchemcomm *7*, 495–499.

Van der Paal, J., Neyts, E.C., Verlackt, C.C.W., and Bogaerts, A. (2016). Effect of lipid peroxidation on membrane permeability of cancer and normal cells subjected to oxidative stress. Chem. Sci. *7*, 489–498.

Pannuzzo, M., De Jong, D.H., Raudino, A., and Marrink, S.J. (2014). Simulation of polyethylene glycol and calcium-mediated membrane fusion. J. Chem. Phys. *140*.

Park, H.E., Gruenke, J. a, and White, J.M. (2003). Leash in the groove mechanism of membrane fusion. Nat. Struct. Biol. *10*, 1048–1053.

Pécheur, É.T.E. (2007). Lipids as modulators of membrane fusion mediated by viral fusion proteins. 887–899.

Pécheur, E.-I., Borisevich, V., Halfmann, P., Morrey, J.D., Smee, D.F., Prichard, M., Mire, C.E., Kawaoka, Y., Geisbert, T.W., and Polyak, S.J. (2016). The Synthetic Antiviral Drug Arbidol Inhibits Globally Prevalent Pathogenic Viruses. J. Virol. *90*, JVI.02077-15.

Pelkmans, L., Pu, D., and Helenius, A. (2002). Local Actin Polymerization and Dynamin Recruitment in SV40-Induced Internalization of Caveolae. *296*, 535–540.

Pérez-Vargas, J., Krey, T., Valansi, C., Avinoam, O., Haouz, A., Jamin, M., Raveh-Barak, H., Podbilewicz, B., and Rey, F.A. (2014). Structural basis of eukaryotic cell-cell fusion. Cell *157*, 407–419.

Pietschmann, T. (2017). Clinically approved ion channel inhibitors close gates for hepatitis C virus –and open doors for drug repurposing in viral infectious diseases. J. Virol. *91*, JVI.01914-16.

Pope, L.E., Marcelletti, J.F., Katz, L.R., and Katz, D.H. (1996). Anti-herpes simplex virus activity of n-docosanol correlates with intracellular metabolic conversion of the

drug. J. Lipid Res. *37*, 2167–2178.

Prince, A.M., Pascual, D., Meruelo, D., Liebes, L., Mazur, Y., Dubovi, E., Mandel, M., and Lavie, G. (2000). Strategies for Evaluation of Enveloped Virus Inactivation in Red Cell Concentrates Using Hypericin. Photochem. Photobiol. *71*, 188–195.

Prinz, W.A., and Hinshaw, J.E. (2009). Membrane-bending proteins. Crit. Rev. Biochem. Mol. Biol. *44*, 278–291.

Qiao, H., Armstrong, R.T., Melikyan, G.B., Cohen, F.S., and White, J.M. (1999). A specific point mutant at position 1 of the influenza hemagglutinin fusion peptide displays a hemifusion phenotype. Mol Biol Cell *10*, 2759–2769.

Raff, A.B., Woodham, A.W., Raff, L.M., Skeate, J.G., Yan, L., Silva, M. Da, and Schelhaas, M. (2013). The Evolving Field of Human Papillomavirus Receptor Research : a Review of Binding and Entry. *87*, 6062–6072.

Raman, R., Sasisekharan, V., and Sasisekharan, R. (2005). Structural Insights into biological roles of protein-glycosaminoglycan interactions. Chem. Biol. *12*, 267–277.

Rand, R.P., and Parsegian, V.A. (1989). Hydration forces between phospholipid bilayers. BBA - Rev. Biomembr. *988*, 351–376.

Rand, R.P., Fuller, N.L., Gruner, S.M., and Parsegian, V.A. (1990). Membrane curvature, lipid segregation, and structural transitions for phospholipids under dual-solvent stress. Biochemistry *29*, 76–87.

Ratcliff, A.N., Shi, W., and Arts, E.J. (2013). HIV-1 resistance to maraviroc conferred by a CD4 binding site mutation in the envelope glycoprotein gp120. J. Virol. *87*, 923–934.

Rauma, T., Tuukkanen, J., Bergelson, J.M., Denning, G., and Hautala, T. (1999). Rab5 GTPase regulates adenovirus endocytosis. J Virol *73*, 9664–9668.

Raymond, S., Maillard, A., Amiel, C., Peytavin, G., Trabaud, M.A., Desbois, D., Bellecave, P., Delaugerre, C., Soulie, C., Marcelin, A.G., et al. (2015). Virological failure of patients on maraviroc-based antiretroviral therapy. J. Antimicrob. Chemother. *70*, 1858–1864.

Razinkov, V., Gazumyan, A., Nikitenko, A., Ellestad, G., and Krishnamurthy, G. (2001). RFI-641 inhibits entry of respiratory syncytial virus via interactions with fusion protein. Chem. Biol. *8*, 645–659.

Reiss, K., Stencel, J.E., Liu, Y., Blaum, B.S., Reiter, D.M., Feizi, T., Dermody, T.S., and Stehle, T. (2012). The GM2 Glycan Serves as a Functional Coreceptor for Serotype 1 Reovirus. *8*.

Rey, F.A. (2006). Molecular gymnastics at the herpesvirus surface. EMBO Rep. *7*, 1000–1005.

Risselada, H.J., Bubnis, G., and Grubmüller, H. (2014). Expansion of the fusion stalk and its implication for biological membrane fusion. Proc. Natl. Acad. Sci. U. S. A. *111*, 1–6.

Roche, S., Rey, F.A., and Bressanelli, S. (2007). Structure of the Prefusion Form of the Vesicular Stomatitis virus glycoprotein G. Science (80-.). *315*, 843–848.

Rossman, J.S., Leser, G.P., and Lamb, R.A. (2012). Filamentous influenza virus enters cells via macropinocytosis. J. Virol. *86*, 10950–10960.

Sacks, S.L., Thisted, R.A., Jones, T.M., Barbarash, R.A., Mikolich, D.J., Ruoff, G.E., Jorizzo, J.L., Gunnill, L.B., Katz, D.H., Khalil, M.H., et al. (2001). Clinical efficacy of topical docosanol 10% cream for herpes simplex labialis: A multicenter, randomized,

placebo-controlled trial. J. Am. Acad. Dermatol. *45*, 222–230.

Saeed, M.F., Kolokoltsov, A.A., Albrecht, T., and Davey, R.A. (2010). Cellular Entry of Ebola Virus Involves Uptake by a Macropinocytosis-Like Mechanism and Subsequent Trafficking through Early and Late Endosomes. *6*.

Sainz, B., Mossel, E.C., Gallaher, W.R., Wimley, W.C., Peters, C.J., Wilson, R.B., and Garry, R.F. (2006). Inhibition of severe acute respiratory syndrome-associated coronavirus (SARS-CoV) infectivity by peptides analogous to the viral spike protein. Virus Res. *120*, 146–155.

Salzer, U., Kostan, J., and Djinović-Carugo, K. (2017). Deciphering the BAR code of membrane modulators. Cell. Mol. Life Sci. *0*, 0.

Sauter, N.K., Hanson, H.J.E., Glick, G.D., Brown, J.H., Crowther, R.L., Park, S., Skehel, J.J., and Wiley, D.C. (1992). Binding of Influenza Virus Hemagglutinin to Analogs of Its Cell-Surface Receptor , Sialic Acid : Analysis by Proton Nuclear Magnetic Resonance Spectroscopy and. 9609–9621.

Scheiffele, P., Rietveld, A., Wilk, T., and Simons, K. (1999). Influenza Viruses Select Ordered Lipid Domains during Budding from the Plasma Membrane *. *274*, 2038–2044.

Schroth-Diez, B., Ludwig, K., Baljinnyam, B., Kozerski, C., Huang, Q., and Herrmann, A. (2000). The role of the transmembrane and of the intraviral domain of glycoproteins in membrane fusion of enveloped viruses. Biosci. Rep. *20*, 571–595.

Schulz, W.L., Haj, A.K., and Schiff, L.A. (2012). Reovirus uses multiple endocytic pathways for cell entry. J. Virol. *86*, 12665–12675.

Sieczkarski, S.B., and Whittaker, G.R. (2002). Influenza Virus Can Enter and Infect Cells in the Absence of Clathrin-Mediated Endocytosis Influenza Virus Can Enter and Infect Cells in the Absence of Clathrin-Mediated Endocytosis. J. Virol. *76*, 10455–10464.

Sieczkarski, S.B., Whittaker, G.R., and Sn, R. (2003). Differential Requirements of Rab5 and Rab7 for Endocytosis of Influenza and Other Enveloped Viruses. 333–343.

Skehel, J.J., and Wiley, D.C. (1998). Coiled coils in both intracellular vesicle and viral membrane fusion. Cell *95*, 871–874.

Skehel, J.J., and Wiley, D.C. (2000). Receptor Binding and Membrane Fusion in Virus Entry: The Influenza Hemagglutinin. Annu. Rev. Biochem. *69*, 531–569.

Söllner, T.H. (2003). Regulated exocytosis and SNARE function (Review). Mol. Membr. Biol. *20*, 209–220.

Spear, P.G. (2004). Herpes simplex virus: Receptors and ligands for cell entry. Cell. Microbiol. *6*, 401–410.

Speerstra, S., Chistov, A.A., Proskurin, G. V, Aralov, A., Ulashchik, E.A., Streshnev, P.P., Vadim V Shmanai, Korshun, V., and Luis, S. Antivirals Acting on Viral Envelopes via Biophysical Mechanisms of Action. Submitt. Publ. submitted for publication.

Spruance, S.L. (2002). N-docosanol (Abreva) for herpes labialis: Problems and questions. J. Am. Acad. Dermatol. *47*, 457–458.

Stachowiak, J.C., Brodsky, F.M., and Miller, E.A. (2013). A cost-benefit analysis of the physical mechanisms of membrane curvature. Nat. Cell Biol. *15*, 1019–1027.

Stampfer, S.D., Lou, H., Cohen, G.H., Eisenberg, R.J., and Heldwein, E.E. (2010). Structural basis of local, pH-dependent conformational changes in glycoprotein B from herpes simplex virus type 1. J. Virol. *84*, 12924–12933.

St Vincent, M.R., Colpitts, C.C., Ustinov, A. V, Muqadas, M., Joyce, M. a, Barsby, N.L., Epand, R.F., Epand, R.M., Khramyshev, S. a, Valueva, O. a, et al. (2010). Rigid amphipathic fusion inhibitors, small molecule antiviral compounds against enveloped viruses. Proc. Natl. Acad. Sci. U. S. A. *107*, 17339–17344.

Stencel-Baerenwald, J.E., Reiss, K., Reiter, D.M., Stehle, T., and Dermody, T.S. (2014). The sweet spot: defining virus–sialic acid interactions. Nat. Rev. Microbiol. *12*, 739–749.

Sun, X., Yau, V.K., Briggs, B.J., and Whittaker, G.R. (2005). Role of clathrin-mediated endocytosis during vesicular stomatitis virus entry into host cells. Virology *338*, 53–60.

Szule, J.A., Fuller, N.L., and Rand, R.P. (2002). The effects of acyl chain length and saturation of diacylglycerols and phosphatidylcholines on membrane monolayer curvature. Biophys. J. *83*, 977–984.

Tanford, C. (1978). The Hydrophobic Effect and the Organization of Living Matter. Science *200*, 1012–1018.

Teissier, E., Zandomeneghi, G., Loquet, A., Lavillette, D., Lavergne, J.P., Montserret, R., Cosset, F.L., Böckmann, A., Meier, B.H., Penin, F., et al. (2011). Mechanism of inhibition of enveloped virus membrane fusion by the antiviral drug arbidol. PLoS One *6*.

The IMpact-RSV Study Group (1998). Palivisumab, a humanized respiratory syncytial virus monoclonal antibody, reduces hospitalization from respiratory syncytial virus infection in high-risk infants. Pediatrics *102*, 531–537.

Tse, F.W., Iwata, A., and Almers, W. (1993). Membrane flux through the pore formed by a fusogenic viral envelope protein during cell fusion. J. Cell Biol. *121*, 543–552.

Turner, A., Bruun, B., Minson, T., and Browne, H. (1998). Glycoproteins gB, gD, and gHgL of herpes simplex virus type 1 are necessary and sufficient to mediate membrane fusion in a Cos cell transfection system. J. Virol. *72*, 873–875.

Vigant, F., Lee, J., Hollmann, A., Tanner, L.B., Akyol Ataman, Z., Yun, T., Shui, G., Aguilar, H.C., Zhang, D., Meriwether, D., et al. (2013). A mechanistic paradigm for broad-spectrum antivirals that target virus-cell fusion. PLoS Pathog. *9*, e1003297.

Vigant, F., Hollmann, A., Lee, J., Santos, N.C., Jung, M.E., and Lee, B. (2014). The rigid amphipathic fusion inhibitor dUY11 acts through photosensitization of viruses. J. Virol. *88*, 1849–1853.

Vigant, F., Santos, N.C., and Lee, B. (2015). Broad-spectrum antivirals against viral fusion. Nat. Rev. Microbiol. *13*, 426–437.

Vogel, S.S., Leikina, E.A., and Chernomordik, L. V. (1993). Lysophosphatidylcholine reversibly arrests exocytosis and viral fusion at a stage between triggering and membrane merger. J. Biol. Chem. *268*, 25764–25768.

de Vries, E., Tscherne, D.M., Wienholts, M.J., Cobos-Jiménez, V., Scholte, F., García-Sastre, A., Rottier, P.J.M., and de Haan, C.A.M. (2011). Dissection of the influenza a virus endocytic routes reveals macropinocytosis as an alternative entry pathway. PLoS Pathog. *7*.

Waters, L., Mandalia, S., Randell, P., Wildfire, A., Gazzard, B., and Moyle, G. (2008). The impact of HIV tropism on decreases in CD4 cell count, clinical progression, and subsequent response to a first antiretroviral therapy regimen. Clin. Infect. Dis. *46*,

1617–1623.

Weed, D.J., Pritchard, S.M., Gonzalez, F., Aguilar, H.C., and Nicola, A. V (2016). Mildly acidic pH triggers an irreversible conformational change in the fusion domain of herpes simplex virus 1 glycoprotein B and inactivation of viral entry. J. Virol. JVI.02123-16.

Weissenhorn, W., Carfí, A., Lee, K.-H., Skehel, J.J., and Wiley, D.C. (1998). Crystal Structure of the Ebola Virus Membrane Fusion Subunit, GP2, from the Envelope Glycoprotein Ectodomain. Mol. Cell *2*, 605–616.

Wesolowski, J., and Paumet, F. (2010). SNARE motif: A common motif used by pathogens to manipulate membrane fusion. Virulence *1*, 319–324.

White, J.M., and Whittaker, G.R. (2016). Fusion of Enveloped Viruses in Endosomes. Traffic *17*, 593–614.

Wickner, W., Rizo, J., and Kozminski, K.G. (2017). A cascade of multiple proteins and lipids catalyzes membrane fusion. *28*, 707–711.

Wiley, D.C., Wilson, I. a, and Skehel, J.J. (1981). Structural identification of the antibody-binding sites of Hong Kong influenza haemagglutinin and their involvement in antigenic variation. Nature *289*, 373–378.

Wilson, I. a, Skehel, J.J., and Wiley, D.C. (1981). Structure of the haemagglutinin membrane glycoprotein of influenza virus at 3 A resolution. Nature *289*, 366–373.

Winsor, J., Hackney, D.D., and Lee, T.H. (2017). The crossover conformational shift of the GTPase atlastin provides the energy driving ER fusion. J. Cell Biol. jcb.201609071.

Wisskirchen, K., Lucifora, J., Michler, T., and Protzer, U. (2014). New pharmacological strategies to fight enveloped viruses. Trends Pharmacol. Sci. *35*, 470–478.

Wittels, M., and Spear, P.G. (1991). Penetration of cells by herpes simplex virus does not require a low pH-dependent endocytic pathway. Virus Res. *18*, 271–290.

Wolf, M.C., Freiberg, A.N., Zhang, T., Akyol-Ataman, Z., Grock, A., Hong, P.W., Li, J., Watson, N.F., Fang, A.Q., Aguilar, H.C., et al. (2010). A broad-spectrum antiviral targeting entry of enveloped viruses. Proc. Natl. Acad. Sci. U. S. A. *107*, 3157–3162.

Wong, J.L., Koppel, D.E., Cowan, A.E., and Wessel, G.M. (2007). Short Article Membrane Hemifusion Is a Stable Intermediate of Exocytosis. 653–659.

Xiao, F., Fofana, I., Thumann, C., Mailly, L., Alles, R., Robinet, E., Meyer, N., Schaeffer, M., Habersetzer, F., Doffoël, M., et al. (2014). Synergy of entry inhibitors with direct-acting antivirals uncovers novel combinations for prevention and treatment of hepatitis C. Gut 1–12.

Xu, Y., Liu, Y., Lou, Z., Qin, L., Li, X., Bai, Z., Pang, H., Tien, P., Gao, G.F., and Rao, Z. (2004). Structural basis for coronavirus-mediated membrane fusion: Crystal structure of mouse hepatitis virus spike protein fusion core. J. Biol. Chem. *279*, 30514–30522.

Xu, Y., Zhang, F., Su, Z., McNew, J.A., and Shin, Y.-K. (2005). Hemifusion in SNARE-mediated membrane fusion. Nat. Struct. Mol. Biol. *12*, 417–422.

Yamauchi, Y., and Helenius, A. (2013). Virus entry at a glance. J. Cell Sci. *126*, 1289–1295.

Yang, L., and Huang, H.W. (2002). Observation of a membrane fusion intermediate structure. Science *297*, 1877–1879.

Yeagle, P.L., Smith, F.T., Young, J.E., and Flanagan, T.D. (1994). Inhibition of membrane fusion by lysophosphatidylcholine. Biochemistry *33*, 1820–1827.

Zaitseva, E., Mittal, A., Griffin, D.E., and Chernomordik, L. V. (2005). Class II fusion protein of alphaviruses drives membrane fusion through the pathway as class I proteins. J. Cell Biol. *169*, 167–177.

Zampighi, G.A., Zampighi, L.M., Fain, N., Lanzavecchia, S., Simon, S.A., and Wright, E.M. (2006). Conical Electron Tomography of a Chemical Synapse: Vesicles Docked to the Active Zone are Hemi-Fused. Biophys. J. *91*, 2910–2918.

Zeev-Ben-Mordehai, T., Vasishtan, D., Siebert, C.A., and Grünewald, K. (2014). The full-length cell-cell fusogen EFF-1 is monomeric and upright on the membrane. Nat. Commun. *5*, 3912.

Zhou, Q., Lai, Y., Bacaj, T., Zhao, M., Lyubimov, A.Y., Uervirojnangkoorn, M., Zeldin, O.B., Brewster, A.S., Sauter, N.K., Cohen, A.E., et al. (2015). Architecture of the synaptotagmin – SNARE machinery for neuronal exocytosis.

Zimmerberg, J., and Kozlov, M.M. (2006). How proteins produce cellular membrane curvature. Nat. Rev. Mol. Cell Biol. *7*, 9–19.

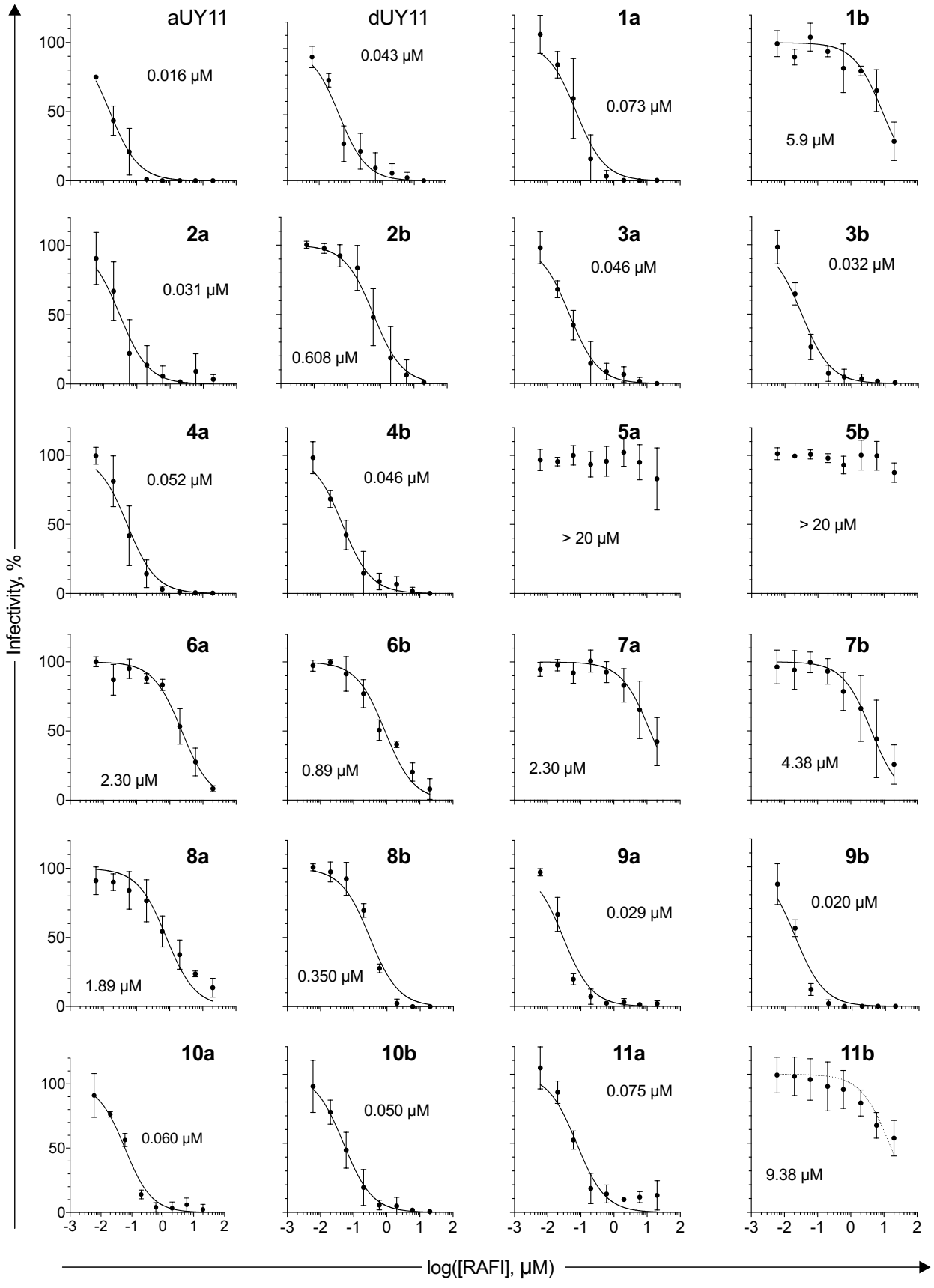
aUY11
0.016 μM
dUY11
0.043 μM
1a
0.073 μM
1b
5.9 μM
2a
0.031 μM
2b
0.608 μM
3a
0.046 μM
3b
0.032 μM
4a
0.052 μM
4b
0.046 μM
5a
> 20 μM
5b
> 20 μM
6a
2.30 μM
6b
0.89 μM
7a
2.30 μM
7b
4.38 μM
8a
1.89 μM
8b
0.350 μM
9a
0.029 μM
9b
0.020 μM
10a
0.060 μM
10b
0.050 μM
11a
0.075 μM
11b
9.38 μM
Infectivity, %
100
50
0
-3 -2 -1 0 1 2
log([RAFI], μM)

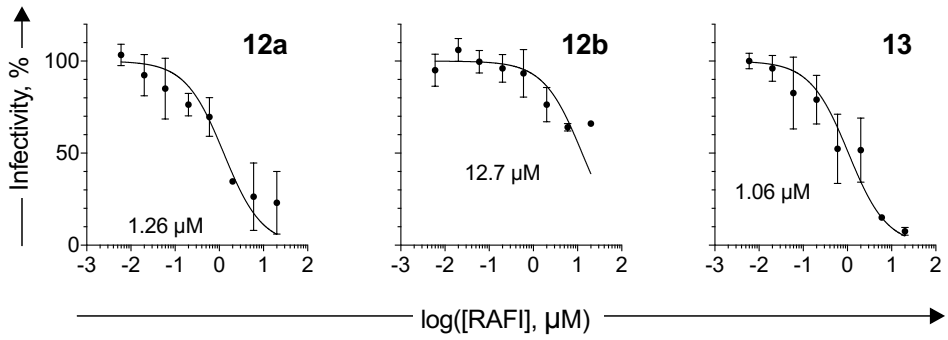

Appendix 1 Dose-response curves against HSV-1 infectivity

Cell monolayers were inoculated with virions pre-exposed to semi-logarithmic concentrations of test compound. Average ± SD (n = 3). Curves fitted by a symmetrical sigmoidal regression $Y = 1 / (1 + 10^{X - \log(IC_{50})}$ for which Y, relative infectivity; X, log [test compound]. Insets EC_{50}. $r^2 \geq 0.9$ for all compounds with $EC_{50} < 20\ \mu M$, except **1b**, **2a**, **7b**, and **12a** $0.8 \leq r^2 < 0.9$; and **11b** $r^2 = 0.53$.

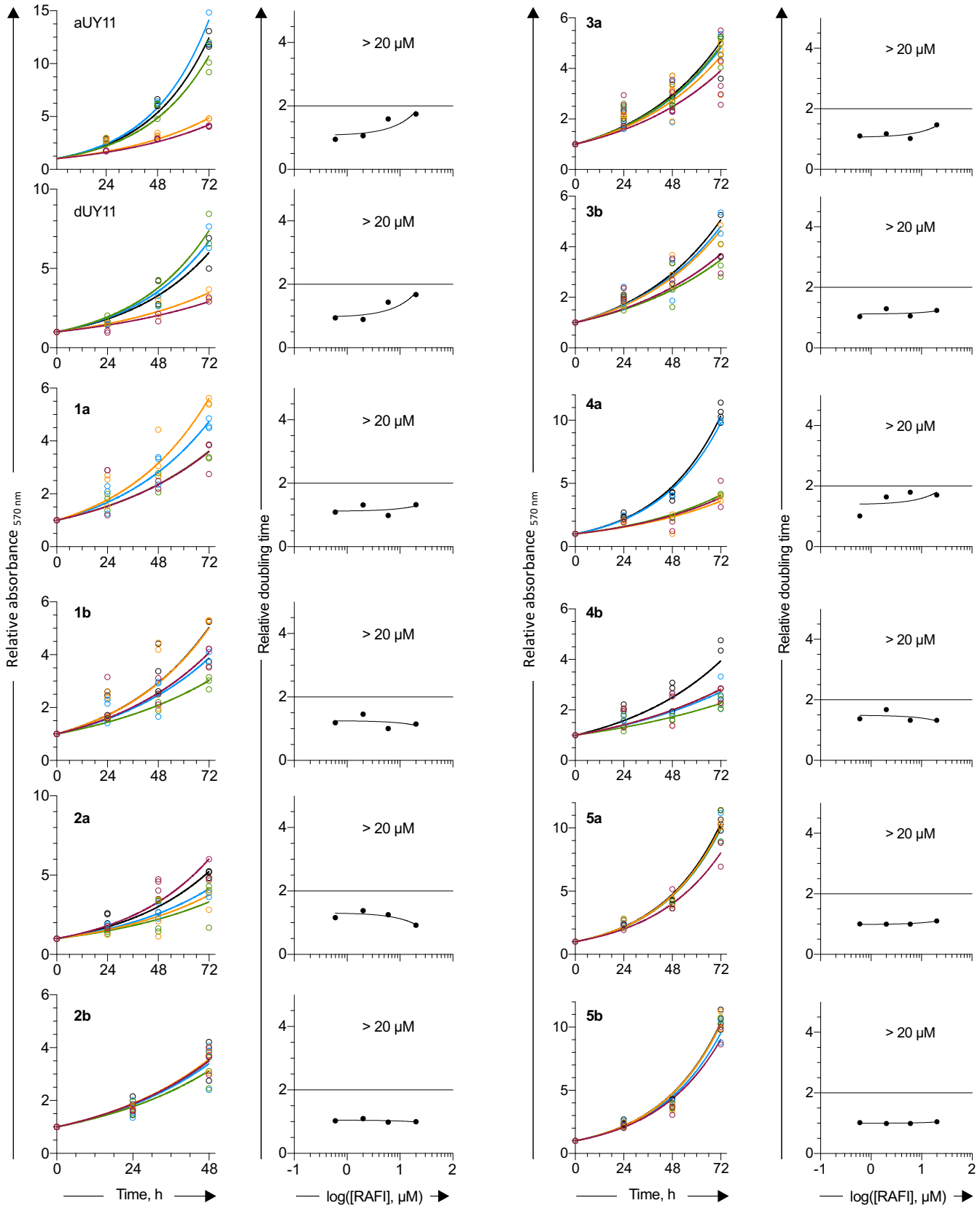
aUY11
dUY11
1a
1b
2a
2b
3a
3b
4a
4b
5a
5b
> 20 μM
Relative absorbance 570 nm
Relative doubling time
Time, h
log([RAFI], μM)

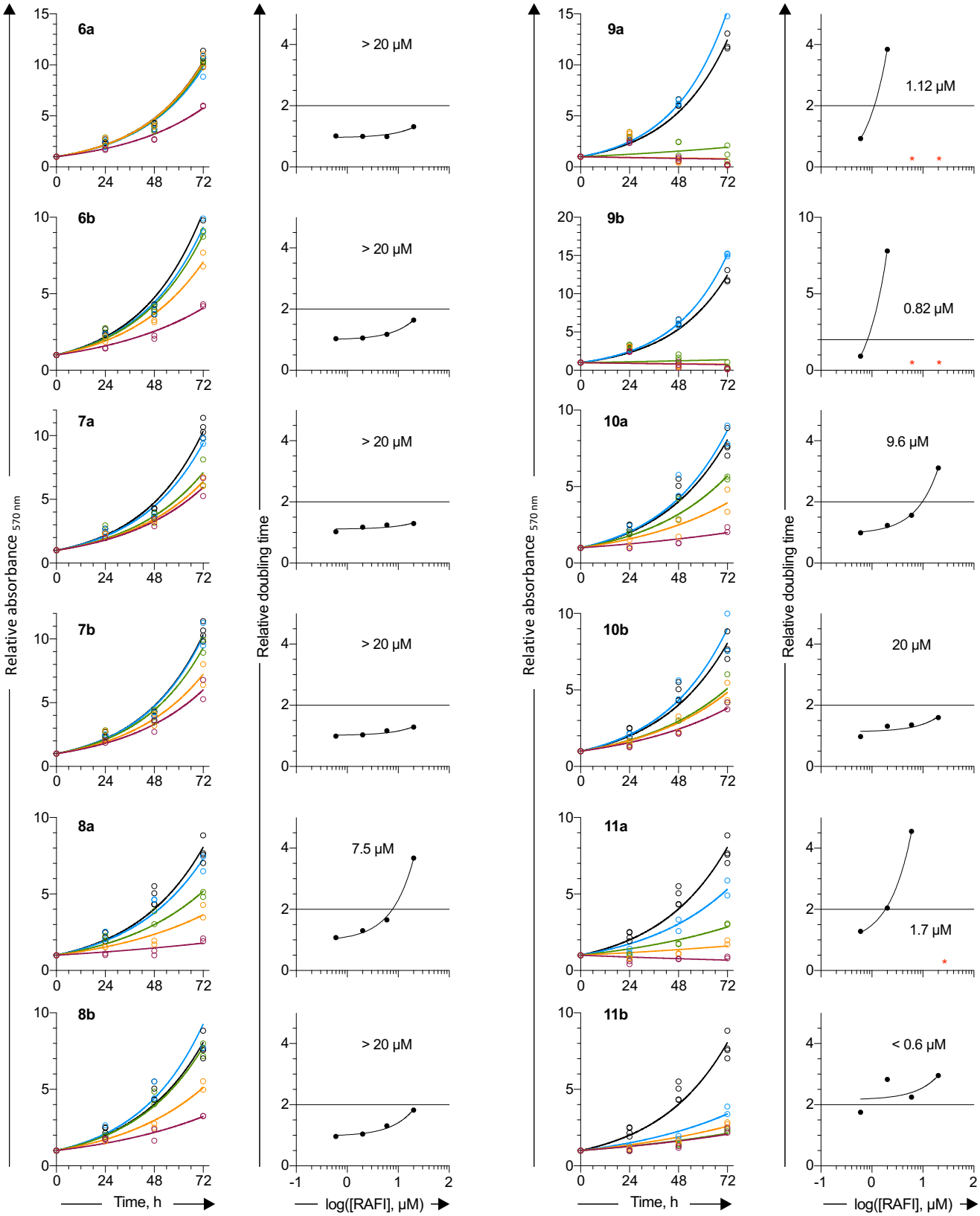
6a
> 20 μM
6b
> 20 μM
7a
> 20 μM
7b
> 20 μM
8a
7.5 μM
8b
> 20 μM
9a
1.12 μM
9b
0.82 μM
10a
9.6 μM
10b
20 μM
11a
1.7 μM
11b
< 0.6 μM
Relative absorbance 570 nm
Relative doubling time
Time, h
log([RAFI], μM)

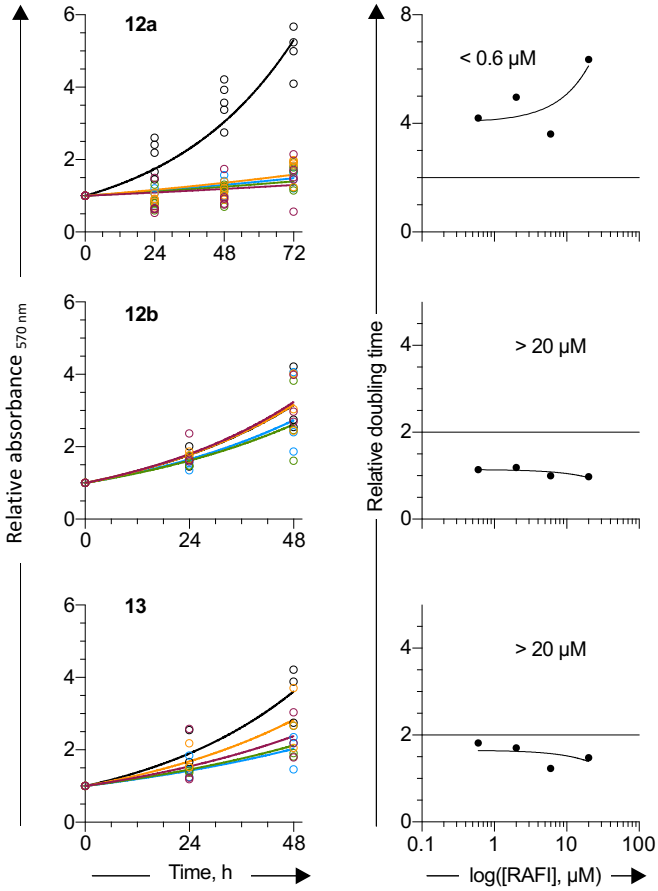
12a
12b
13
Relative absorbance 570 nm
Time, h
Relative doubling time
< 0.6 µM
> 20 µM
> 20 µM
log([RAFI], µM)

Appendix 2 Cytotoxicity dose-response curves

Left: Absorption of formazan produced by cells exposed to semi-logarithmic concentrations of test compound (20 μM, pink; 6 μM, orange; 2 μM, green; 0.6 μM, blue; DMSO, black). Individual data points (compounds aUY11, dUY11, **1a** – **3b**, **4b**, **12a**, **12b**, and **13**, *n*=3; compounds **4a**, **5a** –**11b**, *n*=2); curves fitted by the non-linear regression $Y = Y_0^{kx}$, where Y_0, initial cell number (set to 1); *k,* growth constant in reciprocal hours; *x*, time in hours. $r^2 > 0.9$ and $k \leq 0$ for all curves except: **2a (**0.59, 20 μM); **13** (0.55, 2 μM); **12a** (0.13, 20 μM; 0.52, 6 μM; 0.34, 2 μM; 0.55, 0.6 μM) and all $k \leq 0$.

Right: Doubling times in hours. *ln(2)/k* and plotted relative to DMSO vehicle (set to 1); fitted by linear regressions. The half cytostatic concentration (CC_{50}) is defined as the concentration at which doubling time doubles that of cells treated with DMSO vehicle (intercept with relative doubling time = 2; CC_{50}). Toxic concentrations ($k < 0$) indicated with a red asterisk. $r^2 \geq 0.9$ [**8a**, **8b**, **9a**, **9b**, **10a**, **11a**]; $0.8 \leq r^2 < 0.9$ [aUY11, **5a**, **7b**]; $0.7 \leq r^2 < 0.8$ [dUY11, **2a**, **3a**, **10b**]; $0.6 \leq r^2 < 0.7$ [**7a**, **12a**, **12b**]; $r^2 < 0.6$ [**1a**, **1b**, **2b**, **3b**, **4b**, **5b**, **11b**, **13**].

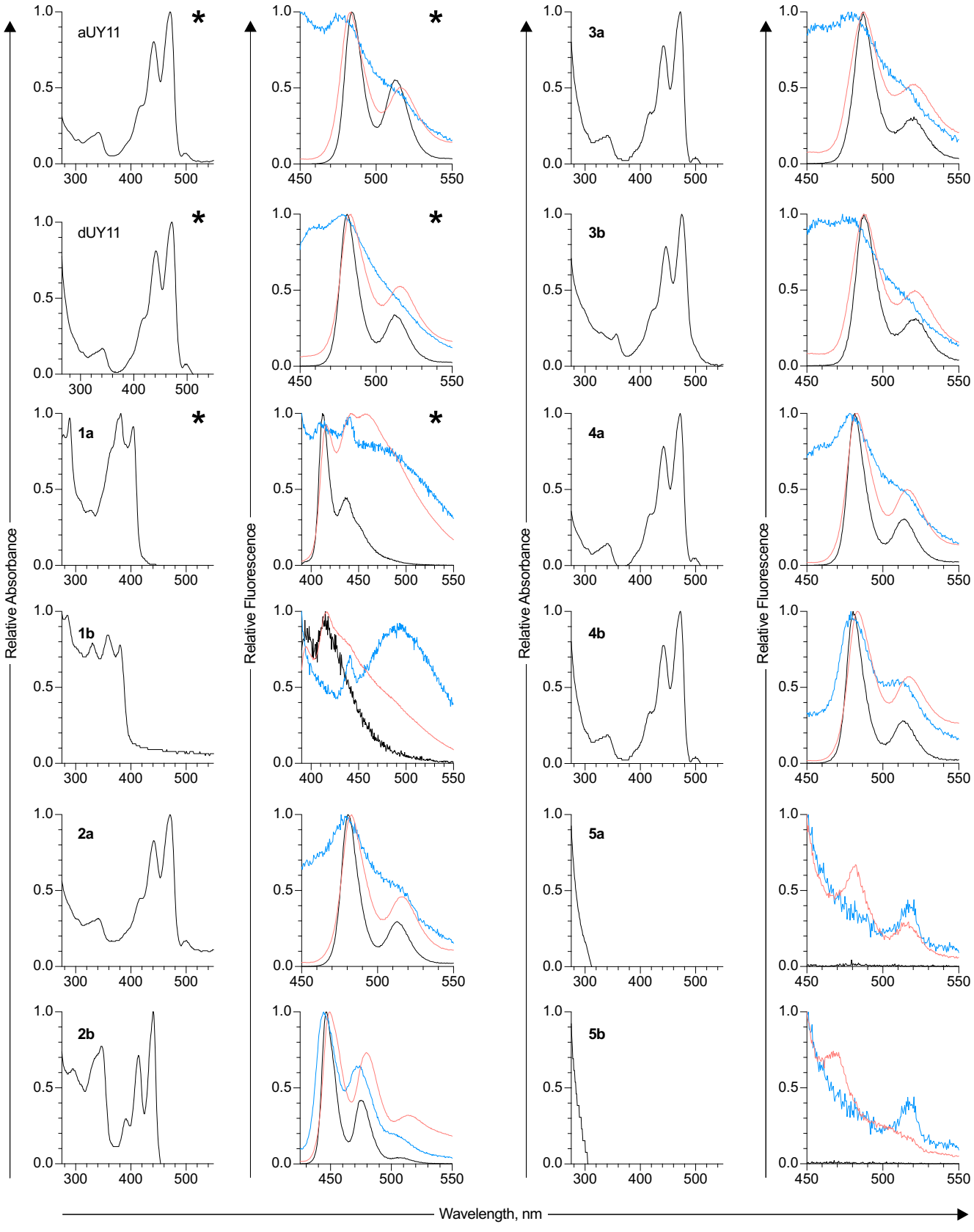
aUY11
dUY11
1a
1b
2a
2b
3a
3b
4a
4b
5a
5b
*
Relative Absorbance
Relative Fluorescence
Wavelength, nm
1.0
0.5
0.0
300
400
500
450
550

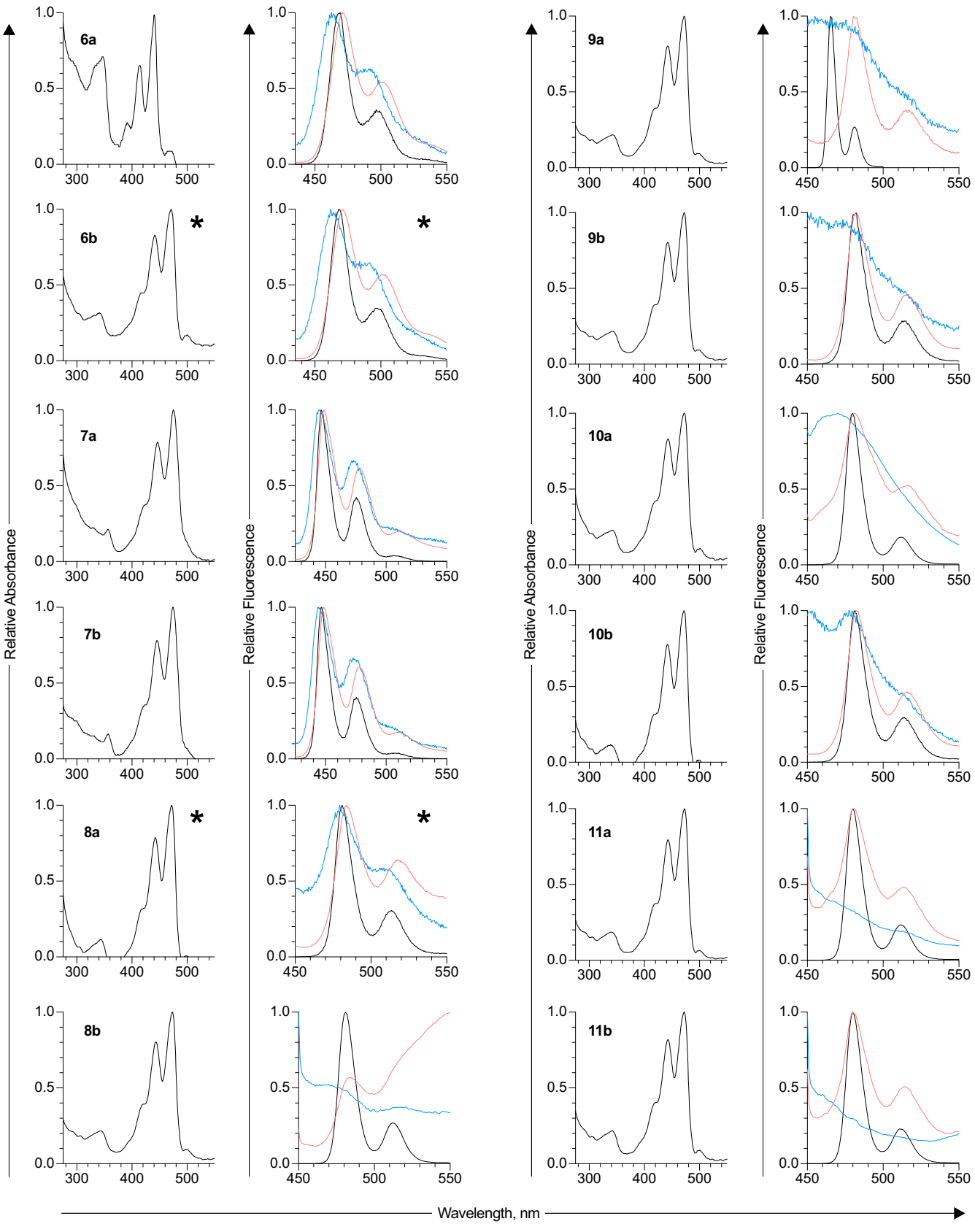
Relative Absorbance
Relative Fluorescence
Wavelength, nm
6a
6b
7a
7b
8a
8b
9a
9b
10a
10b
11a
11b
*
1.0
0.5
0.0
300
400
500
450
550

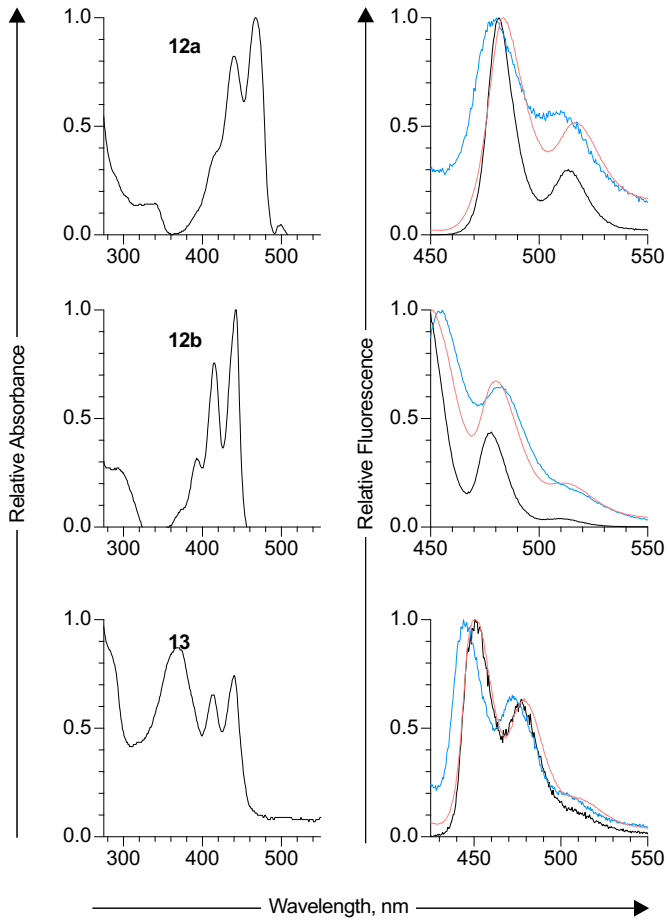

Appendix 3 Absorbance and fluorescence spectra of RAFIs

Left: Absorbance spectra of aUY11, or representative RAFIs.

Right: Emission spectra of aUY11, or representative RAFIs in aqueous (blue) or non-polar environments (octanol, black), or in aqueous environments containing liposomes (orange). * Graphs of representative RAFIs presented in **Figure 3.6** presented here again for comparison.